Charles Univerzity in Prague
Faculty of Mathematic and Physics

DOCTORAL THESIS

Lukáš Shrbený

Meteor Shower Fireballs

Astronomical Institute (v. v. i.)
Academy of Sciences of the Czech Republic
Ondřejov Observatory

Supervisor: **RNDr. Pavel Spurný, CSc.**
Adviser: **RNDr. Jiří Borovička CSc.**

I would like to thank in Czech...

Rád bych na tomto místě poděkoval všem, kteří mi buď vědomě či nevědomě pomohli, pomáhali, motivovali mě, usnadnili mi a nebo mi zpříjemnili vypracování této disertační práce. Velmi si Vašeho času a úsilí vážím a navždy zůstávám Vaším dlužníkem.

I declare that this thesis was written by my own with the use of cited resources. I agree with the borrowing of this work.

In London

Lukáš Shrbený

Acronyms and Explanations

Theory of ablation

v velocity

t time (independent variable)

m mass

h height

l distance along the trajectory

z zenith distance

ρ air density

Γ drag coefficient

Λ heat transfer coefficient

A shape factor

S head cross section

ρ_d bulk density

ξ energy necessary for ablation of a unit mass

σ ablation coefficient

K shape-density coefficient

M Mach number

Measurement of all-sky images

a azimuth

z zenith distance

u angular distance from the center of projection

b azimuth of projection

r distance of measured point from the center of projection

ϑ local sideral time (at the station) of the meteor passage

φ geographic latitude

φ' geocentric latitude

λ geographic longitude

$\mathbf{R}$ value of the geocentric radius vector at the zero height level

$\mathbf{Q}_{AB}$ convergence angel between two planes

$\mathbf{L}$ ecliptical longitude

$\mathbf{B}$ ecliptical latitude

$L_{\odot}$ solar longitude

Atmospheric trajectory

$\mathbf{N}$ number of station where the fireball was photographed

$\mathbf{h}_B$ beginning height

$\mathbf{h}_E$ terminal height

$\mathbf{L}_{obs}$ length of observed atmospheric trajectory

$\mathbf{Z}_{DE}$ zenit distance of the radiant at the end point of the atmospheric trajectory

v_{∞} initial velocity

$\mathbf{M}_{max}$ maximum absolute magnitude

$\mathbf{m}_{inf}$ initial photometric mass

m_{∞} initial mass (dynamic or photometric or an estimate for modelling)

$\mathbf{PE}$ coefficient describing the empirical end height criterion

$\mathbf{H}_{MF}$ height at maximum of the brightness

$\mathbf{H}_{TF}$ height at the terminal flare

$\mathbf{p}_{MF}$ dynamic pressure at maximum of the brightness

$\mathbf{p}_{TF}$ dynamic pressure at the terminal flare

ΔT_{mf} duration of the maximum flare

ΔT_{yf} duration of the terminal flare

Radiant and orbital elements

α_G right ascension of the geocentric radiant

δ_G declination of the geocentric radiant

$\mathbf{V}_G$ geocentric velocity (without atmospheric drag)

a semimajor axis

e eccentricity

q perihelion distance

Q aphelion distance

ω argument of perihelion

Ω longitude of the ascending node

i inclination of the orbit with respect to the ecliptic plane

π length of perihelion

P orbital period

$\lambda_\odot$ solar longitude

$\mathbf{T}_J$ Tisserand's parameter with respect to Jupiter (Jupiter's semimajor axis taken $\mathrm{a}_J = 5.204267\,\mathrm{AU}$)

Others

R coefficient of determination

deg degree

EN European Fireball Network

DN Desert Fireball Network (in Australia)

AFO Autonomous Fireball Observatory

IAU MDC International Astronomical Union Meteor Data Center

Explanations

Values of standard deviations for each entry are in the tables presented below the entry. For higher clarity and readability of the tables the standard deviations are not written in classical form but only in kind of shortcut.

An example:

entry	real meaning
15.1981 11	15.1981 ± 0.0011
2.15 2	2.15 ± 0.02
7.1 1.2	7.1 ± 1.2

Title: *Meteor Shower Fireballs*
Author: *Lukáš Shrbený*
Institute: *Astronomical Institute (v. v. i.) of the Academy of Sciences of the Czech Republic*
Supervisor: *RNDr. Pavel Spurný, CSc.*
Adviser: *RNDr. Jiří Borovička CSc.*
Study branch: *f1 – Theoretical physics, astronomy and astrophysics*
Keywords: *fireball – shower – orbits – light curves*

Abstract

Centimeter-sized meteoroids cause bright meteors, called meteoric fireballs, during their encounter with the Earth's atmosphere. These fireballs can be observed by all-sky photographic methods. In this thesis, bright meteors belonging to major meteor streams are studied. All presented fireballs were recorded during last few years by all-sky photographic cameras from the Czech part of the European Fireball Network, Spain (Leonids 1999 campaign), and from the Australian Desert Network. Physical properties in terms of different methods (end height criterion, beginning heights, apparent ablation coefficient, fragmentation, dynamic pressure at the height of fragmentation or terminal flare), very detailed light curves (periodic changes of brightness, afterglow, short-lived flares, profiles) and heliocentric orbits are studied by individual showers. Studied meteor showers are Orionids, Geminids, α-Capricornids, Southern δ-Aquariids, Leonids and Perseids and a comparison of their main properties was performed. Also comparison with meteorite dropping fireballs was performed.

Název: *Bolidy meteorických rojů*
Autor: *Lukáš Shrbený*
Instituce: *Astronomický Ústav Akademie věd České republiky (v. v. i.)*
Školitel: *RNDr. Pavel Spurný, CSc.*
Konzultant: *RNDr. Jiří Borovička CSc.*
Studijní obor: *f1 – Teoretická fyzika, astronomie a astrofyzika*
Klíčová slova: *bolid – meteorický roj – dráha – světelná křivka*

Abstrakt

Meteoroidy velikosti několika centimetrů způsobují při střetu s atmosférou Země jasné meteory, kterým se říká bolidy. Takové bolidy mohou být pozorovány pomocí celooblohových fotografických metod. V této práci jsou studovány jasné meteory příslušející k hlavním meteorickým rojům, které byly vyfotografovány během posledních několika let z české části Evropské bolidové sítě, ze Španělska při pozorování Leonid v roce 1999 a nebo v Austrálii pomocí pouštní sítě. U jednotlivých rojů jsou na základě různých metod studovány jejich fyzikální vlastnosti (koncové a počáteční výšky, zdánlivý ablační koeficient, fragmentace, dynamický tlak v místě fragmentace či v koncovém výbuchu) detailní světelné křivky (periodické změny jasnosti, dosvit meteorické stopy, krátkotrvající zjasnění, celkové profily) a heliocentrické dráhy. Zařazené meteorické roje jsou Orionidy, Geminidy, α-Capricornidy, Jižní δ-Aquaridy, Leonidy a Perseidy. Provedeno bylo srovnání jejich základních vlastností a také srovnání těchto vlastností s bolidy, u kterých je velká pravděpodobnost pádu meteoritu.

Contents

Chapter 1

Introduction

Solid particles of the solar system are large enough to produce light during their collision with the Earth's atmosphere. The phenomenon is termed a meteor and the particle a meteoroid. The smallest meteoroid size able to produce meteor depends on its velocity. Size 0.01 mm can be taken as a rough limit. The upper sizes of interplanetary bodies are offten limited to the largest meteoroids recorded by scientific instruments as meteors in the Earth's atmosphere, which is about 10-m-size bodies.

Part of the meteoroid population is linked to comets as shower meteors derived from cometary meteoroid stream. Another part is linked to asteroids and some of these bodies we can study in our laboratories as meteorites. There are only fourteen cases by now (September 24, 2009), when recovered meteorite was observed by scientific instruments (or recorded by video camera) as meteor and its heliocentric orbit was successfuly measured. Meteors not belonging to any specific shower are called sporadic. Orbital motion of a meteoroid is dominated by the gravity of the Sun perturbed by close approaches to bigger bodies.

Majority of our knowledge on meteoroids comes from an extremely short interval of their atmospheric penetration. The Earth's atmosphere is actually a large sensor of meteoroid impacts. The penetration through the atmosphere may cause, for certain sizes and velocities of meteoroids, a luminous phenomenon called a meteor, or if brighter, a meteoric fireball, eventually also a bolide, which is used for detonating fireballs. Velocities of solar-system meteoroids at their encounter with the Earth's atmosphere are within the following limits: the lower one 11.2 km/s (only gravity of the Earth), the upper one 72.8 km/s (42.5 parabolic at Earth's perihelion plus 30.3, which is the velocity of the Earth at perihelion). The direction where the meteoroid comes from is called the radiant. The ability to penetrate into the atmosphere depends strongly on the meteoroid velocity. The mass loss due to ablation causes a practical upper velocity limit of about 30 km/s (approximate value, terminal mass also depends strongly on ablation coefficient) for the occurence of a meteorite fall (the terminal mass varies as about v_∞^{-6}, where v_∞ is the initial velocity of the meteoroid before entering the atmosphere). Thus, at higher

velocities only a huge body can produce some small meteorite. The term ablation has the meaning of mass loss of a meteoroid in any form and phase: solid as fragments, fluid as droplets and loss of hot gas, which forms always the final stage and is responsible for the observed meteor phenomena.

The chapters 1 and 2 of this thesis are collected from several articles, books and papers, which are not cited directly in the text. Used sources in alphabetical order are as follows: Borovička et al. (1996); Borovička (2006); Ceplecha and McCrosky (1976); Ceplecha (1987); Ceplecha et al. (1993, 1998); Ceplecha and Revelle (2005); Jenniskens (2006); Plavec (1956)

1.1 Meteor phenomenon

The penetration of a meteoroid into the Earth's atmosphere at hypersonic velocity give rise to 4 different phenomena, depending mostly on mass and partly on velocity. In all four types of interaction, ions and free electrons are produced during the atmospheric flight, an ionized column is formed, and forwarding with the meteoroid velocity.

1.1.1 Meteors

Typical meteors seen by naked eye, recorded by television camera or by a telescope, are caused by meteoroids larger than 0.01 mm. The exact size depends on velocity. A zero magnitude meteor is caused by the body of 2-cm size at a velocity 15 km/s, of 1-cm size at 30 km/s and of 0.5-cm size at 60 km/s for vertical flight in all cases. Typical meteors are associated with meteoroid sizes between 0.05 and 20 cm. Entering the denser part of the atmosphere they are heated up very quickly and if the size is less than 0.5 mm, the body is heated throughout. If the body size is greater than 0.5 mm, only a surface layer down to a few tenths of millimeter is heated. Reaching about 2200 K, the meteoroid material starts to sublimate from the surface and fills the surroundings of the body by its hot vapors. Excited states of these vapors are gradually de-excited by radiation. Meteor light consist mostly of radiation of descrete emission spectral lines belonging to metals and mainly to iron. More than 90% of the meteor light originates from radiation of single low-excited atoms of meteoroid material (several eV, temperatures 3000 - 5000 K). After traveling a distance of several kilometers up to few tens of kilometers, the meteor terminates its light, because it has lost all of its mass. The meteoroid has not radically changed its velocity, about of the order of some percent to a few tens of percent.

1.1.2 Fireballs, Bolides, Meteorite Falls

This type of meteoroid interaction with the atmosphere happens, when the size of the body is larger than about 20 cm (for 15 km/s and vertical flight). In this case there is not enough time to ablate the entire meteoroid mass, before the body slows down to a critical limit of about 3 km/s. At such a small velocity

there is not enough energy to keep the surface temperature above 2200 K, so the luminous phenomenon disappears. However, there is still some remnant flying down with continuously lower velocity. The meteoroid starts to be cooled on its surface. The thin melted layer on the meteoroid surface solidifies and forms a crust, which is typical for meteorities. Meteoric fireball (it is fireball of -8 mag or brighter) terminates its light due to small velocity of the meteoroid remnant. The remnant (mass of about 10 g and higher) falls down to the Earth's surface in a dark flight and its velocity approaches gradually the free fall velocity, which is a velocity limit being approached by slowing down from higher velocities. The dark flight lasts typically several minutes in contrast to the luminous trajectory that lasts several seconds.

1.1.3 Explosive Impacts

The third type of meteoroid interaction with the atmosphere is a very rare phenomenon due to the small probability of Earth's encounter with a very large body. If the body is larger than several meters and sufficiently strong, the body hits the Earth's surface at hypersonic velocity of the order of several kilometers per second. The meteoroid vapors emit light down to the Earth's surface, where an explosive crater forms.

1.1.4 Meteoroid Dust Particles

The fourth type of encounter cannot be observed as a luminous phenomenon. If the size of the meteoroid is less than several hundredths of a millimeter, it is slowed down to less than a few kilometers per second very high in an extremely rare atmosphere before its temperature can rise to the evaporation point. Such a meteoroid dust particle sediments slowly and unchanged through the atmosphere to reach the surface.

1.2 Atmospheric Penetration

Preheating is the first stage of the meteoroid penetration and is caused by the impacting molecules of the individual constituents of the air gas at hights of 300 to 100 km (depending on energy of encounter that depends on v^3). The surface temperature rises by the same rate as the ambient air density, i.e., proportionally to e^t. The preheating lasts only seconds or tens of seconds. For bodies larger than 1 mm the process is governed by heat conductivity, while radiation transfer and internal compression are important for smaller bodies. When the surface tension reaches the strength of the material, spallation starts. For a homogenous solid stone of a centimeter size (or larger) coincides this with heating to about 900 K. At altitudes up to 250 km the dominant luminous mechanism is sputtering and the subsequent collision cascade of metal atoms and air molecules with the ambient environment.

(a)

v (km/s)	$\log \tau$
≤ 9.3	-12.75
9.3-12.5	$-15.60 + 2.92 \log v$
12.5-17.0	$-13.24 + 0.77 \log v$
17.0-27.0	$-12.50 + 0.17 \log v$
27.0-72.0	$-13.69 + \log v$

(b)

Type	
I	$-4.60 < PE$
II	$-5.25 < PE \leq -4.60$
IIIA	$-5.70 < PE \leq -5.25$
IIIB	$PE \leq -5.70$

Table 1.1: (a) The dependency of luminous efficiency, τ, in terms of c.g.s. units and magnitude-based intensity, on the velocity based on observations of the artificial meteors (Ayers et al., 1970). (b) The definition of the fireball groups according to the empirical end height criterion (Ceplecha and McCrosky, 1976).

The next stage of atmospheric penetration of the meteoroid is ablation. It starts as fragmentation or spallation at lower temperatures. After melting becomes evaporation from the body and from its fragments. When evaporation starts, temperatures are close to about 2500 K. Further increase in temperature is then small because most of the kinetic energy is spent in the ablation process itselves. The fragmentation process has not been well understood until recently and mostly single-body theory has been used. Modifications of the single-body theory due to gross-fragmentation process at discrete trajectory points was succesfully applied to observations. Deceleration can compete with the ablation in consuming kinetic energy only for larger bodies (the meteorite dropping) and when they move lower down in the atmosphere. Reaching about 3 km/s somewhere high above the surface and there are not enough hot gases round the body to emit visible light but there still remains significant mass, this mass continues to move without emitting light in dark flight, which is the third stage of atmospheric penetration of the meteoroid.

During a dark flight there is not enough kinetic energy to either evaporate or to provide heating. The body starts to cool exponentialy with time and the solidification of the crust takes place. The crust is a black opaque glass, which dark color is caused by sub-micrometer-sized inclusions of magnetite (Fe_3O_4). Without wind and being decelerated to several hundreds of m/s very soon, the body motion changes to vertical trajectory quite quickly and a free fall follows with velocity decreasing proportionally to square root of the air density. Different wind directions and speeds at different heights perturb the trajectory and make the solution of the dark flight more complicated. The biggest unknown in this problem is always the shape of the body, and thus also the unknown aerodinamic lift. The atmospheric penetration ends with an impact, the body has reached the surface. Impact velocities are 10 to 100 m/s for 10 g to 10 kg terminal masses, respectively. The impact forms a small pit on the surface, which is comparable to the size of the meteorite itself. If ablation continues to the Earth's surface, a much bigger impact crater is formed due to sudden explosive release of the enormous kinetic energy.

According to ablation abilities, fireballs are divided into four types. Type I

has the lowest ability to ablate, the highest bulk density, and potential meteorites belong probably to ordinary chondrites of asteroidal origin. Type II has a bit higher ability to ablate, a bit lower bulk density, and meteorites are assumed to be carbonaceous chondrites. Type II fireballs are likely both of asteroidal and of cometary origin. Type IIIA meteors are caused by fragile bodies with high ablation and bulk density lower than the water. In general, the most fragile and the weakest bodies cause type IIIB fireballs, which have the highest known ablation coefficient and the lowest bulk density. Type IIIA and IIIB are considered to be of cometary origin.

This division is based on single-body theory (only fireballs with $v_\infty < 40\,\mathrm{km/s}$ were used) with luminous efficiencies listed in Table 1.1 (a). The empirical end height criterion serves for determination of appropriate fireball type and is expressed by the value of PE

$$\mathrm{PE} = \log \rho_E + \mathrm{A} \log m_\infty + \mathrm{B} \log v_\infty + \mathrm{C} \log(\cos z), \qquad (1.1)$$

where A = -0.42 ± 0.05, B = 1.49 ± 0.31, and C = -1.29 ± 0.20. The air density at the fireball terminal height, ρ_E, is in $\mathrm{g\,cm^{-3}}$, initial mass, m_∞, in grams, initial velocity, v_∞, in km/s, and zenith distance, z, in degrees. The conversion key between the value of PE and the fireball type is in Table 1.1 (b).

1.3 Phenomena Connected with Meteors

1.3.1 Meteor Flares

The meteor flare is a sudden increase in meteor brightness usually by more than one magnitude. It is typical for high velocity meteors. A flare at the terminal point may be due to a real explosion and a terminal disintegration into many small fragments. Two usual reasons for flares are sudden gross or discrete fragmentation (in contrast to continuous fragmentation) or sudden change in physical circumstances giving rise to more evaporation, excitation and ionization.

1.3.2 Meteor Wakes

Meteor wake is a special term for radiation, which is emmited just behind the meteoroid. The radiation surrounding the body is sometimes called head radiation. Typical dimension of a wake is several hundreds of meters to several kilometers behind the body and a typical duration is of order of several tenths of second (usually less than 0.1 second). Depending on the origin we distinguish two types of wakes: gaseous and particulate.

In the upper part of meteor trajectory a wake is formed by rarified non-equilibrium gas that is quickly decelerated relatively to the meteoroid. Spectra of gaseous wakes show lines of the same elements as in the head radiation, but the excitation energy is significantly lower. Thermal equilibrium cannot be

used even as a first approximation for radiation of a gaseous wake. The dominant characteristics for wake spectrum are intercombination lines, it means the lines with low excitation and small transition probability. These include Mg I - multiplet 1, Ca I - multiplet 1 and Fe I - multiplets 1, 2, 3. Intercombination lines have the lowest decay and are visible toward the end of the wake. Besides them, low excitation lines (Na I - multiplet 1) are strong in the first part of the wake.

At lower heights a wake is formed by tiny droplets and solid fragments evaporating subsequently – the formation of fragments resembles a wake, and thus this kind of phenomenon is called a particulate wake.

1.3.3 Meteor Trains

There are three types of trains. The short-duration train is formed exclusively by a green forbidden line of neutral atmospheric oxigen at 557.7 nm, and thus it is sometimes called a green train. Green trains are typical for high-velocity meteors of medium and low brightness. The green line appears with a short delay after the passage of the meteoroid, reaches maximum intensity after about 0.1 second and than gradually becomes weak. The typical height where the line is brighest is 105 km and duration is less than 3 seconds.

Self-luminous persistent trains can be visible for tens of minutes after meteor disappearance and are produced mostly by bright fireballs of high velocity. These trains always form in the region of meteor maximum brightness (often at the position of flare). At the time of formation, the train may be very bright, but its brightness falls quickly within few seconds. In this afterglow phase, the spectrum exhibits atomic lines of low excitation and with low transition probability. Cooling of low-density non-equilibrium gas is in progress. Next stage is called recombination phase. After initial fading, the brightness of some lines stabilizes and a few even rises. This phase lasts several tens of second and its spectrum is similar to that of the afterglow phase but lines with higher excitation (up to 7 eV) are also presented. The two brightest lines are Mg I at 517 nm and Na I at 589 nm. The spectrum can be explained by atomic recombination that is more efficient at lower temperature, so the intensity of recombination lines increases after the train has cooled. The last stage is a continuum phase. It can lasts for several minutes (occasionally for hours) has wide or narrow appearance and is fed by chemiluminescence of iron oxide molecules (FeO) and sodium atoms (Na), which are catalysts in the recombination reactions of oxigen atoms and ozone molecules. In the spectrum there is line of Na I at 593 nm but most luminosity is produced by molecules. Optical luminosity is driven by exotermic chemical reactions, the emission of FeO, other metal oxides, NO_2 and OH is represented in the spectrum as well.

Reflection trains are similar in appearance to persistent trains, but they are caused by reflection or scattering of sunlight on dust particles left in the atmosphere after the meteoroid disruption. These trains are offten formed by the explosion of bright bolide during the daytime or twilight and may last for

hours.

1.3.4 Meteor Sounds

Lots of acoustic reports from the observers of large fireballs have been quoted. They are generally of two different types: hypersonic booms (heard one to several minutes after the fireball) and electrophonic sounds (heard simultaneously with the fireball).

Hypersonic booms are meteor sounds caused by meteoroid moving at a speed $v(h)$ at height h that is faster than the abiabatic phase speed of acoustical wave $c_s(h)$ and for cases where the mean free path of the neutral gas is sufficiently smaller than the size of the meteoroid. The energy of this wave propagates away from the source and is confined to a Mach cone whose half angle is $arcsin(c_s(h)/v(h))$. If terminal gross-fragmentation creates a point source-like explosion, spherical wavefronts are generated.

Electrophonic sounds are defined as sounds produced by direct conversion of electromagnetic radiation into audible sounds. If very bright fireball (say -9 mag and brighter) penetrates deeply enough to reach so called transition altitude where a continuum flow regime is commenced and turbulent plasma trail is produced, then the geomagnetic field lines are twisted. During subsequent relaxation of these field lines back to an equilibrium state Extra Low and Very Low Frequency (ELF/VLF) radio emissions are generated. These radio emissions with frequency 1 – 10 kHz propagate through the atmosphere and can be transduced into audible sounds by various electrically conducting materials (metal or paper objects).

The ELF/VLF radiation can also be produced by expanding plasma during major fragmentation or explosion that takes place above transition altitude. For a short time of the order of a tenth of a second, the effective frontal area of the fireball may fulfill continuum flow conditions and the ELF/VLF radiation may be produced and transduced into a brief burst of electrophonic sound. In general, electrophonic sounds may be produced also by events of strong lightning, very bright aurora, earthquake and nuclear explosion.

Chapter 2

Theory

2.1 Ablation

The motion, ablation, and radiation of a single non-fragmenting body through the atmosphere (gravity is neglected) can be represented by four differential equations: the drag equation (2.1), the mass-loss equation (2.2), the luminous equation (2.3), and the heigh equation (2.4), which is purely geometrical and is written here for a spherical Earth's surface. Masses determined from motion and ablation of the body are sometimes called dynamical masses to distinguish them from photometric masses, which are computed from a light curve.

$$\frac{dv}{dt} = -\Gamma A \rho_d^{-2/3} \rho m^{-1/3} v^2 \tag{2.1}$$

$$\frac{dm}{dt} = -\frac{\Lambda A}{2\xi} \rho_d^{-2/3} \rho m^{2/3} v^3 \tag{2.2}$$

$$I = -\tau \left(1 + \frac{2}{\sigma v^2}\right) \frac{v^2}{2} \frac{dm}{dt} \tag{2.3}$$

$$\frac{dh}{dt} = \frac{l - A/2}{h + B/2} v \tag{2.4}$$

$$\frac{l - A/2}{h + B/2} = -\cos z(t) \tag{2.5}$$

$$Al + Bh + C = l^2 - h^2 \tag{2.6}$$

For a meteoroid at an arbitrary point of its linear trajectory, the notation is as follows: v the velocity; t the time (independent variable); m the mass; h the height; l the distance along the trajectory; ρ the air density; z the zenith distance; Γ the drag coefficient; Λ the heat transfer coefficient; $A = Sm^{-2/3}{\rho_d}^{2/3}$ the shape factor; S the head cross section; ρ_d the bulk density; ξ the energy necessary for ablation of a unit mass; τ the luminous efficiency; and constant values A, B, C, which are given by the geometrical relation between l and h. The shape factor, A, and one constant describing the geometry have

the same notation, but in the following calculations the shape factor will be replaced by the shape-density coefficient, K.

Two independent parameters of the problem can be expressed as the ablation coefficient σ (2.7) and the shape-density coefficient K (2.8).

$$\sigma = \frac{\Lambda}{2\xi\Gamma} \tag{2.7}$$

$$K = \Gamma A \rho_d^{-2/3} \tag{2.8}$$

2.1.1 Simplified Solution

Most of the photographically recorded meteoroids behaved according to the single-body theory with constant ablation and shape-density coefficients. The solution of this simplified problem can be described by following equations. By keeping σ and K constant we can derive some integrals of equations (2.1) - (2.4):

$$m = m_\infty \exp\left(\frac{1}{2}\sigma[v^2 - v_\infty^2]\right), \tag{2.9}$$

where $m \to m_\infty$ and $v \to v_\infty$ for $t \to -\infty$ (outside the atmosphere). By substitution (2.9) into (2.1) and integrating we obtain the velocity integral:

$$Ei(\frac{1}{6}\sigma v_\infty^2) - Ei(\frac{1}{6}\sigma v^2) = \frac{2K\exp(\frac{1}{6}\sigma v_\infty^2)}{m_\infty^{1/3}} \int_h^\infty \frac{(B/2+h)\rho\, dh}{\sqrt{A^2/4 + C + h^2 + Bh}}. \tag{2.10}$$

$$t - t_0 = \int_{l_0}^{l} \frac{dl}{v} \tag{2.11}$$

$$\frac{Ei(\frac{1}{6}\sigma v_\infty^2) - Ei(\frac{1}{6}\sigma v^2)}{Ei(\frac{1}{6}\sigma v_\infty^2) - Ei(\frac{1}{6}\sigma v_0^2)} = \frac{\int_h^\infty \frac{(B/2+h)\rho\, dh}{\sqrt{A^2/4 + C + h^2 + Bh}}}{\int_{h_0}^\infty \frac{(B/2+h)\rho\, dh}{\sqrt{A^2/4 + C + h^2 + Bh}}} \tag{2.12}$$

$$h = -B/2 + \sqrt{B^2/4 - C + l^2 - Al} \tag{2.13}$$

$$Ei(x) = \int_{-\infty}^{x} \frac{e^x}{x}\, dx \tag{2.14}$$

These integrals hold for any air density profile. Equations (2.11) and (2.12) represent the complete solution of the problem of the single non-fragmenting body with constant coefficients σ and K, and express the distance along the trajectory and the height as function of time.

The problem contains four unknown parameters, l_0, v_0, v_∞, σ, to be determined from observations. We can make the problem linear by writing it

for small increments of the parameters. The partial derivatives of (2.11) and (2.12), with respect to all four unknown parameters, are explicit analitical expressions (2.16) - (2.19). This makes the computation convenient and speedy, especially if we have some good estimates of the initial values of the parameters. We proceed by writing the total differential according to changing parameters:

$$l_{obs} - l = \frac{\partial l}{\partial l_0}\Delta l_0 + \frac{\partial l}{\partial v_0}\Delta v_0 + \frac{\partial l}{\partial v_\infty}\Delta v_\infty + \frac{\partial l}{\partial \sigma}\Delta\sigma. \tag{2.15}$$

$$\frac{\partial l}{\partial l_0} = \frac{1}{v_0 D}\left\{2v\exp(\frac{1}{6}\sigma v^2)\int_{h_0}^{\infty}\frac{\rho\,dh}{\cos z} + \right.$$
$$\left. + v_0 v^2[Ei(\frac{1}{6}\sigma v_\infty^2) - Ei(\frac{1}{6}\sigma v^2)]\rho(h_0)\int_{l_0}^{l}\frac{dl}{v^2}\right\} \tag{2.16}$$

$$\frac{\partial l}{\partial v_0} = \frac{2v^2}{v_0 D}\exp(\frac{1}{6}\sigma v_0^2)\int_{h}^{\infty}\frac{\rho\,dh}{\cos z}\int_{l_0}^{l}\frac{dl}{v^2} \tag{2.17}$$

$$\frac{\partial l}{\partial v_\infty} = -\frac{2v^2}{v_\infty D}\exp(\frac{1}{6}\sigma v_\infty^2)\left[\int_{h}^{\infty}\frac{\rho\,dh}{\cos z} - \int_{h_0}^{\infty}\frac{\rho\,dh}{\cos z}\right]\int_{l_0}^{l}\frac{dl}{v^2} \tag{2.18}$$

$$\frac{\partial l}{\partial \sigma} = \frac{v^2}{\sigma D}\int_{l_0}^{l}\frac{dl}{v^2}\left[\exp(\frac{1}{6}\sigma v_0^2)\int_{h}^{\infty}\frac{\rho\,dh}{\cos z} - \right.$$
$$\left. - \exp(\frac{1}{6}\sigma v_\infty^2)\int_{h}^{h_0}\frac{\rho\,dh}{\cos z} - \exp(\frac{1}{6}\sigma v^2)\int_{h}^{\infty}\frac{\rho\,dh}{\cos z}\right] \tag{2.19}$$

The denominator D is given by

$$D = 2\exp(\frac{1}{6}\sigma v^2)\int_{h_0}^{\infty}\frac{\rho\,dh}{\cos z} + v^2[Ei(\frac{1}{6}\sigma v_\infty^2) - Ei(\frac{1}{6}\sigma v_0^2)]\rho(h)\int_{l_0}^{l}\frac{dl}{v^2}. \tag{2.20}$$

Also continuous fragmentation can be treated by this solution because of the general definition of the ablation coefficient. If the body fragments suddenly at a point, the solution is no longer valid, but we can easy generalized the solution in this respect. When we have only one point of gross-fragmentation, we integrate in two steps: before and after the fragmentation point, and thus we have two aditional parameters.

$$l_{obs} - l = \frac{\partial l}{\partial l_0}\Delta l_0 + \frac{\partial l}{\partial v_0}\Delta v_0 + \frac{\partial l}{\partial v_{\infty 1}}\Delta v_{\infty 1} + \frac{\partial l}{\partial \sigma_1}\Delta\sigma_1 + \tag{2.21}$$
$$+ \frac{\partial l}{\partial v_{\infty 2}}\Delta v_{\infty 2} + \frac{\partial l}{\partial \sigma_2}\Delta\sigma_2$$

Type	ρ_d $\mathrm{g\,cm^{-3}}$	σ $\mathrm{s^2\,km^{-2}}$	K c.g.s.
I	3.7	0.014	0.46
II	2.0	0.042	0.69
IIIA	0.75	0.10	1.33
IIIB	0.27	0.21	2.63

Table 2.1: Average values of σ and K on assumption of $\Gamma\mathrm{A} = 1.1$

Six unknown increments of parameters to be determined from observations are $\Delta v_{\infty 1}$ and $\Delta\sigma_1$ (before fragmentation), Δl_0 and Δv_0 (at fragmentation), $\Delta v_{\infty 2}$ and $\Delta\sigma_2$ (after fragmentation). Since the solution is again equivalent to keeping K constant, the relative change of mass at the fragmentation point is a part of the solution. The ratio of $Km^{-1/3}$ before and after the fragmentation point determines m_f, the ratio of mass after and before the fragmentation point, which is independent of the actual value of K. In case of more fragmentation points, the solution is not so simple. Each aditional fragmentation point adds four parameters, if the relative amount of fragmented mass and the positions of fragmentation points are taken as unknown.

We recognize two different types of the values of σ, K, and τ. If the single-body equations are solved without taken the fragmentation into account, the results are apparent values of the coefficients. On the other hand, if the fragmentation process is incuded into computation, the intrinsic values of σ, K, and τ are determined. The intrinsic values are the apparent values corrected for the effects of fragmentation (either continuous or discrete at a point).

2.1.2 General Solution

General solution of the problem of meteoroid ablation is described by the same set of equations (2.1) – (2.8) but is solved for $\sigma = \sigma(t)$ and $K = K(t)$; ablation and shape-density coefficients are functions of time to be determined from observation. In this case, very precise observation is required. Standard deviation for arbitrary measured point of the atmospheric trajectory have to be of the order of 10 m.

From equations (2.1) and (2.2) we can eliminate mass, and thus we arrive at:

$$\ln\frac{K}{K_0} = \frac{1}{3}\int_{v_0}^{v} \sigma v\, dv - \ln\frac{\rho v^2}{(-\frac{dv}{dt})} + \ln\frac{\rho_0 v_0^2}{(-\frac{dv}{dt})_0}, \tag{2.22}$$

where the term with integral is called the ablation term and the residual of natural logarithms is called the deceleration term. If these two terms are identical during the whole trajectory, then K is being constant.

Complete solution is now represented by equations (2.11) and (2.22). Similar numerical procedure as for the case with constant σ and K can be applied to fit the computed distances along the trajectory to the observed distances,

except that the partial derivatives of (2.11) and (2.22) with respect to all unknown parameters cannot be written in close form and have to be computed numerically. If (2.22) would have been solved and velocity and deceleration are known from observation, mass and ablation are given:

$$m = \frac{K^3 \rho^3 v^6}{(-\frac{dv}{dt})^3}, \tag{2.23}$$

$$\frac{dm}{dt} = \sigma m v \frac{dv}{dt}. \tag{2.24}$$

It is necessary to say that σ cannot be computed for the early part of the trajectory, where velocities and decelerations are almost independent of σ. For this part of the trajectory only an average value of σ (Table 2.1) corresponding to the meteoroid type have to be used. This limitation has not much influence on K during the early part of the trajectory, because σ and K are there almost independent. We only must assume K_0, the value of K at a point, where the integration starts. Statistical average of K (Table 2.1) for the corresponding meteoroid type is used.

2.2 Processing of all-sky images

The all-sky cameras capable of imaging the entire visible hemisphere in one photograph are commonly used in meteor astronomy. We use stars as known reference points. On each photograph we measure the rectangular coordinates x, y and convert them to the celestial coordinates azimuth, a, and zenith distance, z. The origin of the plate coordinates x, y is set near the center of projection and the definition of the rectangular coordinates is given by the x axis oriented toward the south and the y axis toward the west. On each photograph we define the angular distance from the center of projection, u, and the azimuth of projection, b. The u ranges from 0 to 90°, the b from 0 to 360° (the zero point of b is defined so that for the zenith is $b = 180°$). If the center of projection were identical with zenith, u would be identical with the zenith distance, z, and b would correspond to the astronomical azimuth, a. In reality, the camera is never oriented precisely toward the zenith, and thus the center of projection lies at a small zenith distance ε and azimuth E. The relations between the astronomical coordinates and the plate coordinates are set by these equations:

$$\cos z = \cos u \cos \varepsilon - \sin u \sin \varepsilon \cos b, \tag{2.25}$$

$$\sin (a - E) = \frac{\sin b \sin u}{\sin z}, \tag{2.26}$$

$$b = a_0 - \arctan \left(\frac{y - y_0}{x - x_0} \right). \tag{2.27}$$

The point with coordinates x_0, y_0 is the center of projection in the x, y system and a_0 is the angle between the x axis and the direction to the south.

The angular distance u can be written as a function of the distance from the point $[x_0, y_0]$. If projection would be axially symmetrical with respect to the optical axis of objective and photographical film would be identical with the focal plane of camera, then the distance r_0 from the center of projection is

$$r_0 = \sqrt{(x - x_0)^2 + (y - y_0)^2}. \tag{2.28}$$

In reality, projection is elliptical, this results to change of the scale depending on the direction from the center of projection. The distance of measured point $[x, y]$ from the center of projection $[x_0, y_0]$, r, depends on the angle between the x axis and the axis of ellipse, the important direction of the elliptical projection. This angle is denoted by α.

$$r = r_0[1 + A \sin(\alpha - F)] \tag{2.29}$$

$$\alpha = a_0 + \arctan\left(\frac{y - y_0}{x - x_0}\right) \tag{2.30}$$

A a F are reduction constants to be determined together with ε, E, x_0, y_0, a_0. Then the angular distance u is function of r (empirical formula 2.31) with reduction constants V, S, D, P, Q to be also determined.

$$u = Vr + S(e^{Dr} - 1) + P(e^{Qr^2} - 1) \tag{2.31}$$

Using additive formula to $sin(\alpha - F)$ we can exclude α from equations (2.29) and (2.30) and write the formula for r

$$\begin{aligned} r = C \Big[& \sqrt{(x - x_0)^2 + (y - y_0)^2} + \\ & + A(y - y_0)\cos(F - a_0) - A(x - x_0)\sin(F - a_o) \Big], \end{aligned} \tag{2.32}$$

where C is the global scale factor of projection.

The reduction constants can be devided into four groups according to their physical meaning.

1. x_0, y_0, a_0 - the plate constants. They define the rotation and shift of the rectangular coordinate system on the film.

2. A, F, C - the camera constants. They define the position of the film relative to the optical axis. A and F express the inclination of the film relative to the focal plane. C is equal to unity when the center of the plate lies at a standard distance from the lens (the nominal focal length). Otherwise it differs a little from unity.

3. V, S, D, P, Q - the lens constants. They define the projection of the objective in dependency on the distance from the optical axis. The influence of astronomical refraction is also included.

4. ε, E - the station constants. They define the deviation of the camera optical axis from the zenith. An apparent deviation may be also caused by an incorrect timing.

The lens constants and the constant C are not independent and cannot be computed simultaneously. This can be seen from the fact that both V and C define the scale at the center of projection in the same way. Either C is set to unity and the lens constant are computed or the lens constant are fixed an C is being determined.

2.3 Conversion of a, z to α, δ and radiant

For conversion of azimuth and zenith distance into the right ascension, α, and declination, δ, we must know the local sideral time at the station, ϑ_s, of the fireball instant, and the geographic coordinates of the station, φ_s and λ_s.

All the computations are performed in geocentric coordinates. There is need to convert geographic latitude, φ, into geocentric latitude, φ', and to determine the value of the geocentric radius vector at the zero height level, R.

$$\begin{aligned}\varphi' = \varphi - 0.1924240867^\circ \sin 2\varphi + \\ +0.000323122^\circ \sin 4\varphi - 0.0000007235^\circ \sin 6\varphi\end{aligned} \tag{2.33}$$

$$R = \left(4068669.86 \frac{1 - 0.0133439554 \sin^2 \varphi}{1 - 0.006694385096 \sin^2 \varphi}\right)^{1/2} \tag{2.34}$$

The rectangular geocentric system of coordinates is then given by the following definition

$$\begin{aligned} X &= (R + h) \cos \varphi' \cos \vartheta \\ Y &= (R + h) \cos \varphi' \sin \vartheta \\ Z &= (R + h) \sin \varphi', \end{aligned} \tag{2.35}$$

where h is height above sea level. Any unit vector in direction of α, δ in the same system of coordinates is

$$\begin{aligned} \xi &= \cos \delta \cos \alpha \\ \eta &= \cos \delta \sin \alpha \\ \zeta &= \sin \delta. \end{aligned} \tag{2.36}$$

Enough points are measured on the fireball trail to determine the straight line of the trajectory. Each point can be represented according to (2.36) as vector (ξ_i, η_i, ζ_i), $i = 1...k$, where k is total number of measured points. These vectors define the average plain Γ, which contains the average fireball trajectory and the station where the fireball was photographed. If (a, b, c) is a unit vector perpendicular to Γ, then

$$a\xi_i + b\eta_i + c\zeta_i = \Delta_i, \tag{2.37}$$

where $\Delta_i = 0$ in the ideal case of all measured points being exactly on the meteor trail. In fact, Δ_i are small values to be minimized by the choise of unknown vector (a, b, c).

$$\Sigma \Delta_i^2 = minimum \tag{2.38}$$

is the condition that gives a, b, c as

$$\begin{aligned} a' &= [\xi_i\eta_i][\eta_i\zeta_i] - [\eta_i^2][\xi_i\zeta_i] \\ b' &= [\xi_i\eta_i][\xi_i\zeta_i] - [\xi_i^2][\eta_i\zeta_i] \\ c' &= [\xi_i^2][\eta_i^2] - [\xi_i\eta_i][\xi_i\eta_i] \\ d' &= \sqrt{a'^2 + b'^2 + c'^2} \\ a &= a'/d' \\ b &= b'/d' \\ c &= c'/d', \end{aligned} \tag{2.39}$$

where symbol [ ] means Σ.

The geocentric position of the plain Γ is derived from (2.36) and from the geocentric position of the station, where the fireball was photographed, [X_s, Y_s, Z_s]:

$$a\xi + b\eta + c\zeta + d = 0 \tag{2.40}$$

$$d = -(aX_s + bY_s + cZ_s). \tag{2.41}$$

d is the distance of the plain Γ from the Earth's center.

The fireball is photographed from at least two stations, and thus we have several pairs of planes Γ. Any pair of them, for example plane Γ_A, derived from station A, and Γ_B, from station B, defines the fireball trajectory as their intersection. If Γ_A is described by a_A, b_A, c_A and Γ_B by normal unit vector a_B, b_B, c_B then a unit vector derived from the intersection of planes Γ_A and Γ_B is

$$\begin{aligned} \xi_R &= (b_A c_B - b_B c_A)/s \\ \eta_R &= (a_B c_A - a_A c_B)/s \\ \zeta_R &= (a_A b_B - a_B b_A)/s, \end{aligned} \tag{2.42}$$

where $s = [(b_A c_B - b_B c_A)^2 + (a_B c_A - a_A c_B)^2 + (a_A b_B - a_B b_A)^2]^{1/2}$. Vector ($\xi_R$, η_R, ζ_R) defines the radiant of the fireball and thanks to (2.36) we can convert it into (α_R, δ_R). If this point (α_R, δ_R) is below the horizon, then it is the antiradiant and the computation proceeds just by changing the sign of the vector (ξ_R, η_R, ζ_R).

The statistical weight of the intersection of plains Γ_A and Γ_B is proportional to the angle between these two plains, Q_{AB}, more accurately to $\sin^2 Q_{AB}$. The value of the angle Q_{AB} is given by normal unit vectors (a_A, b_A, c_A) and (a_B, b_B, c_B):

$$\cos Q_{AB} = |a_A a_B + b_A b_B + c_A c_B| \,. \tag{2.43}$$

2.4 Atmospheric Trajectory

Points of the fireball trajectory do not lie exactly in the plain Γ_A, and thus we are looking for perpendicular projection of these points onto the average fireball trajectory defined by the intersection of plains Γ_A and Γ_B.

If n is the suffix of any measured point, then (ξ_n, η_n, ζ_n) and the geocentric position of station A define a staight line deviating a bit from the plain Γ_A. We define the plain perpendicular to Γ_A containing (ξ_n, η_n, ζ_n) and [X_A, Y_A, Z_A]. This plain is described by a normal unit vector (a_n, b_n, c_n) and distance of this plain from the Earth's center, d_n:

$$\begin{aligned} a_n &= \eta_n c_A - \zeta_n b_A \\ b_n &= \zeta_n a_A - \xi_n c_A \\ c_n &= \xi_n b_A - \eta_n a_A \\ d_n &= -(a_n X_A + b_n Y_A + c_n Z_A). \end{aligned} \tag{2.44}$$

The intersection [X_n, Y_n, Z_n] of this plain and the average fireball thajectory is the point we are searching for. This point is the intersection of these three plains

$$\begin{aligned} a_A\xi + b_A\eta + c_A\zeta + d_A &= 0 \\ a_B\xi + b_B\eta + c_B\zeta + d_B &= 0 \\ a_n\xi + b_n\eta + c_n\zeta + d_n &= 0 \end{aligned} \tag{2.45}$$

and the distance of this point from station A is

$$r_n = \left[(X_n - X_A)^2 + (Y_n - Y_A)^2 + (Z_n - Z_A)^2\right]. \tag{2.46}$$

The projection of this point onto the Earth's surface can be computed by solving (2.35), which yields φ'_n, ϑ_n, $R + h_n$. Since the projection of the point [X_n, Y_n, Z_n] using (2.35) is in the direction of radius vector and not vertical, the following correction have to be done

$$\varphi_n = \varphi_{nc} + h_n \frac{(\varphi'_n - \varphi_{nc})}{(R + h_n)}, \tag{2.47}$$

where φ_{nc} is φ'_n corrected by means of (2.33).

Now we have geometry of the fireball in the atmosphere, but we are interested in dynamics as well. To determine distances along the trajectory, velocities and decelerations as functions of time, the positions of the time marks have to be measured. The time marks are given by any timed occultation of the moving fireball image by a rotating shutter. In case of all-sky camera, the rotating shutter is placed very close to the focal plain, and the progressive motion of the shutter combines with the motion of the fireball image, and thus a correction is necessary. If we define the relative time, t_n, as zero at the first measurable time mark ($t = 0$ for $l = l_1$) then

$$t_n = \frac{1}{f}\left(l_n - l_1 + \frac{n_{SR}\Delta\varphi_n}{2\pi}\right), \tag{2.48}$$

where n_{SR} is the number of rotating shutter arms, f is the number of rotations of the shutter per second, and $\Delta\varphi_n$ is an angle between the position of the

shutter at the occultation instant of time mark 1 and time mark n and is given by

$$\Delta\varphi_n = \arctan\left[\frac{(x_1 - x_c)}{(y_1 - y_c)}\right] - \arctan\left[\frac{(x_n - x_c)}{(y_n - y_c)}\right], \tag{2.49}$$

where x_c, y_c are the rectangular coordinates of the axis of the rotating shutter, x_1, y_1 are the rectangular coordinates of the time mark 1 and x_n, y_n of the time mark n.

Now we have for each l_n and h_n also corresponding t_n and we can analyze them as functions of time and determine velocities and decelerations at any point of the fireball trajectory also as functions of time.

For further computation, initial velocity is one of critical parameters. Different procedures are applied to determine this parameter depending on quality of actual data of l_n and h_n. If a meteor trajectory is not long enough (generally for fast and fragile meteors), we calculate only mean velocity along the trajectory. l_n and h_n are fitted as linear functions of time then. For longer meteors, which experience at least moderate deceleration, empirical interpolation formulae for dependency of length and height on time is used. For the length the formula has a form of $l = A + Bt + C\exp(Kt)$ and contstant values of A, B, C and K are being determined from observation. The B coefficient has meaning of initial velocity. If an atmospheric trajectory of a fireball is long enough, the deceleration is presented, and the accuracy of measurement is high (standard deviation generally less than 30 meters for arbitrary point of the trajectory), we can apply procedure described in section 2.1.1 (page 10).

The method described above is based on intersection of planes. There is another one method how to determine the atmospheric trajectory – the method of skew lines. In this method, we aim rays (from at least two stations of observation) at the measured points on the meteor atmospheric trajectory and find the line, which is closest to all rays – residua are minimized. The solution is the same as intersection of planes, but has higher accuracy for such cases, where the convergence angle between the two planes is very small (say less than 5°).

2.5 Fireball Orbit

The initial velocity, v_∞, radiant (α_r, δ_r), and time of meteor beginning define the initial velocity vector, which is important to determine the fireball heliocentric orbit. We start with the average observed values v_∞, $\bar{v}$ and (α_r, δ_r). $\bar{v}$ is observed average velocity at the average point, [$\bar{X}_n$, $\bar{Y}_n$, $\bar{Z}_n$], which lies close to a middle of the average fireball trajectory. The direction of $\bar{v}$ is same as the direction of v_∞. Time of the event is determined either from visual observation or computed from guided camera (nautical triangle) or derived from brightness detector.

First, we correct the observed velocity vector $\bar{v}$, α_r, δ_r for the Earth's rota-

tion. The Earth's rotation velocity, v_E, in km/s is given by

$$v_E = \frac{2\pi}{86164.09}(\bar{R}_n + \bar{h}_n)\cos\varphi'_n, \tag{2.50}$$

where $(\bar{R}_n + \bar{h}_n)$ is the radius vector to the average point and φ'_n its geocentric latitude. The components of $\bar{v}$ can be written in rectangular geocentric system of coordinates (2.36) as

$$\begin{aligned} \bar{v}_x &= |\bar{v}|\,\bar{\xi}_R \\ \bar{v}_y &= |\bar{v}|\,\bar{\eta}_R \\ \bar{v}_z &= |\bar{v}|\,\bar{\zeta}_R, \end{aligned} \tag{2.51}$$

and thus the corrected velocity vector $\bar{v}_c = (v_{xc}, v_{yc}, v_{zc})$ is

$$\begin{aligned} v_{xc} &= \bar{v}_x - v_E\,\cos\alpha_E \\ v_{yc} &= \bar{v}_y - v_E\,\sin\alpha_E \\ v_{zc} &= \bar{v}_z, \end{aligned} \tag{2.52}$$

where α_E is the right ascension of the east point corresponding to latitude $\bar{\rho}_n$ and longitude $\bar{\lambda}_n$ of the average point $[\bar{X}_n,\, \bar{Y}_n,\, \bar{Z}_n]$.

The next step is the correction of $\bar{v}_c$ for the no-atmosphere value by adding the difference $v_\infty - \bar{v}$. The direction of the vector is not changing. The no-atmosphere value of $\bar{v}_c$ is denoted $v_{\infty c}$ and its absolute value is

$$v_{\infty c} = \bar{v}_c + v_\infty - \bar{v} \tag{2.53}$$

and the absolute value of the geocentric velocity vector, v_G, is in km/s given by

$$v_G = \left(v_{\infty c}^2 - \frac{797201.0}{(\bar{R}_n + \bar{h}_n)}\right)^{\frac{1}{2}}. \tag{2.54}$$

The radiant $(\alpha_c,\, \delta_c)$ corrected for the Earth's rotation can be determined from the coordinates (2.52), which are transformed by (2.36). Then the zenith distance from the observed "geocentric" radiant, z_c, is computed from

$$\cos z_c = \sin\delta_c\,\sin\varphi'_n + \cos\delta_c\,\cos\varphi'_n\,\cos(\bar{\vartheta}_n - \alpha_c). \tag{2.55}$$

The observed radiant is shifted, thanks to the gravity of the Earth, a bit towards the observer's zenith with respect to the geocentric radiant of the fireball. The value of this shift, Δz_c, is always positive and is called the zenith attraction. If the geocentric trajectory of the meteoroid inside the Earth's sphere of activity (the gravity of the Earth is higher then the gravity of the Sun) is a hyperbola and the atmospheric trajectory of the meteor is approximated

by a line (a tangent of the hyperbola), then the zenith attraction, Δz_c, is due to geometrical properties of a hyperbola given by

$$(v_{\infty c} + v_G) \tan\left(\frac{\Delta z_c}{2}\right) = (v_{\infty c} - v_G) \tan\left(\frac{z_c}{2}\right) \tag{2.56}$$

and the zenith distance of the geocentric radiant, z_G, is then

$$z_G = z_c + \Delta z_c. \tag{2.57}$$

Since the gravity of the Earth does not change the plane of the hyperbola of the meteoriod trajectory, the azimuth of the geocentric radiant is not changing as well. If a_c is the azimuth of the radiant (α_c, δ_c), which is corrected for the Earth's rotation, then the azimuth, a_G, of the geocentric radiant is

$$a_G = a_c. \tag{2.58}$$

For the reduction of the photographic record the apparent coordinates of stars were used, and thus the components of the geocentric radiant (α_G, δ_G) are also given in apparent system of coordinates and it is usual to convert them into coordinates of the standard epoch J2000.0, which depends on precessional and nutational constants and the time elapsed from the standard epoch.

Having v_G, α_G, δ_G, we can compute the heliocentric velocity vector, v_H, L_H, B_H, of the meteoroid in orbit at collision with the Earth. L is the ecliptical longitude and B the ecliptical latitude. First we convert the apparent α_G, δ_G into ecliptical coordinates, L_G, B_G for the epoch of the closest beginning of the year or the middle of the year. The heliocentric ecliptical system of rectangular coordinates is defined as

$$\begin{aligned} X &= r \cos B \cos L \\ Y &= r \cos B \sin L \\ Z &= r \sin B, \end{aligned} \tag{2.59}$$

where r is the distance from the Sun. The position of the Earth in this system is given by the solar longitude, $L_\odot$. The ecliptical longitude of the Earth is $L_\odot - 180°$. The ecliptical latitude is equal to zero. To determine the heliocentric velocity of the meteoroid we have to know the velocity vector of the Earth in its orbit, which is given by the time change of the solar longitude, $L_\odot$, the time change of the Earth's radius vector, r, and the ecliptical longitude of the Earth's apex, L_{AP}. If V_{AP} is the velocity of the Earth in AU per solar day and t the time in solar days, then

$$V_{AP} = \left[\left(\frac{dr}{dt}\right)^2 + \left(r\frac{dL_\odot}{dt}\right)^2\right]^{\frac{1}{2}} \tag{2.60}$$

$$L_{AP} = L_\odot - \frac{\pi}{2} - \left(\frac{dr}{dt}\right) / \left(r\frac{dL_\odot}{dt}\right). \tag{2.61}$$

The components of the heliocentric velocity vector of the meteoroid are then

$$\begin{aligned} v_{Hx} &= -v_G \cos L_G \cos B_G + V_{AP} \cos L_{AP} \\ v_{Hy} &= -v_G \sin L_G \cos B_G + V_{AP} \sin L_{AP} \\ v_{Hx} &= -v_G \sin B_G \end{aligned} \tag{2.62}$$

and because we can write the components also in the system (2.59)

$$\begin{aligned} v_{Hx} &= v_H \cos L_H \cos B_H \\ v_{Hy} &= v_H \sin L_H \cos B_H \\ v_{Hz} &= v_H \sin B_H, \end{aligned} \tag{2.63}$$

we can determine the heliocentric radiant of the fireball, L_H, B_H, and the heliocentric velocity, v_H. Since V_{AP} is in AU per solar day and v_G in km/s, a conversion factor have to be applied.

$$v_G\,[\mathrm{km/s}] = 1731.456829\, v_G\,[\mathrm{AU/solar\ day}] \tag{2.64}$$

If we know v_H in AU/solar day, the semimajor axis a can be directly determined from low of conservation of energy

$$a = \frac{k^2 r}{2k^2 - r v_H^2}, \tag{2.65}$$

where $k = 0.01720209895$ is the Gaussian gravitational constant in AU-solar day-solar mass units. The longitude of the ascending node, Ω, depends on the sign of B_H

$$\begin{aligned} &\text{for} \quad B_H > 0\,, \quad \Omega = L_\odot \\ &\text{for} \quad B_H < 0\,, \quad \Omega = L_\odot - 180^\circ. \end{aligned} \tag{2.66}$$

The inclination of the orbit, i, is determined from low of conservation of angular momentum

$$\begin{aligned} \sqrt{p}\cos i &= \frac{1}{k}\left(r v_{Hx} \sin L_\odot - r v_{Hy} \cos L_\odot\right) \\ \sqrt{p}\sin i &= -\frac{r v_{Hz} \sin L_\odot}{k \sin\Omega} \qquad \text{or} \\ \sqrt{p}\sin i &= -\frac{r v_{Hz} \cos L_\odot}{k \cos\Omega}. \end{aligned} \tag{2.67}$$

The inclination is in the range from 0° to 180°, and thus if we determine $\tan i$ from (2.67), then i is unambiguous. From (2.67) we also obtain the parameter p. The eccentricity, e, and the true anomaly, ν, can be then obtained from

$$\begin{aligned} e\sin\nu &= -\frac{\sqrt{p}}{k}\left(v_{Hx}\cos L_\odot + v_{Hy}\sin L_\odot\right) \\ e\cos\nu &= p/r - 1. \end{aligned} \tag{2.68}$$

The argument of perihelion, ω, depends on the sign of B_H

$$\begin{aligned} &\text{for} \quad B_H > 0\,, \quad \omega = 180^\circ - \nu \\ &\text{for} \quad B_H < 0\,, \quad \omega = -\nu. \end{aligned} \tag{2.69}$$

If the semimajor axis is positive, the perihelion distance, q, and the aphelion distance, Q, can be computed from geometrical relations of an ellipse.

$$\begin{aligned} q &= a(1-e) \\ Q &= a(1+e) \end{aligned} \tag{2.70}$$

All the angular orbital elements have to be now converted into values of some standard epoch, for example the standard epoch J2000.0.

2.6 Meteor Photometry

Startrails on the all-sky image are used for determination of meteor brightness. Two different methods are used for this purpose: the width photometry and the Fishscan photometry. The biggest trouble in both methods is the fact that the fireball is often the brightest object on the image, and thus its brightness has to be extrapolated and the standard deviations of fireball brightness may exceed one stellar magnitude in some cases.

- Width Photometry
  Measured widths of startrails are used for determination of visual brightness of meteor on the basis of characteristic density curve. This curve describes dependency of width of startrail on stellar magnitude. This method gives good results for stars measured in the interval of zenith distances from 0° to 70°. The process is as follows: catalogue stellar magnitudes are transformed to panchromatic system of magnitudes (properties of used emulsion are taken into account), corrected for the zenith distance influence (extinction coefficient and lenses effect), and velocity of the image caused by daily motion (trailing velocity). The difference of occultation by the rotating shutter (star images are occulted by the shutter, but the fireball image is not) and the fireball trailing velocity (known from measurement of the time marks) are taken into account for determination of the fireball brightness.

- Fishscan Photometry
  Fishscan photometry is the name for a recently implemented method that uses the darkening of startrails on scanned negatives to determine the characteristic density curve and meteor brightness. The FishScan software, created by Dr. Jiří Borovička, serves for this purpose. Before the measurement, the image is corrected for decreasing sensitivity with the distance from the center of projection (i.e. flat-fielded) using the factory curve for the Zeiss Distagon lens. The measured darkening of a star trail

is corrected for star trailing velocity (daily motion). Stars are measured in wide interval of zenith distances and the actual extinction coefficient is determined together with the characteristic curve. When converting meteor darkening into magnitudes, the difference due to occultation by the rotating shutter (star images are occulted by the shutter, but the fireball image is not) and the fireball trailing velocity are taken into account. The Schwarzschild's coefficient of 0.80 ± 0.05 is assumed.

2.7 Dark Flight and Impact

If a fireball penetrates very deep into the apmosphere and the computed velocities and decelerations at the end of the luminous trajectory yield non-zero mass of the body, a meteorite fall follows and we are interested in predicting the impact point. A dark flight is a flight without emitting light. The last measured velocity and deceleration at the terminal point, the position of the terminal point and the direction of flight completely define the solution of this problem. Main uncertainties are the unknown shape of the body, which is assumed to be symmetrical, and the poor known wind field. The equations of motion of non-ablating body are:

$$\frac{dv_l}{dh} = -\frac{1}{v_h}\left[\Gamma S\rho v(V_l + v_l) + 2\omega(v_x \sin\varphi + v_h \cos\varphi \sin a_R)\right] \qquad (2.71)$$

$$\frac{dv_h}{dh} = -\frac{1}{v_h}\left[\Gamma S\rho v v_h + g - 2\omega\cos\varphi(v_l \sin a_R + v_x \cos a_R)\right] \qquad (2.72)$$

$$\frac{dv_x}{dh} = \frac{1}{v_h}\left[\Gamma S\rho v(V_x + v_x) + 2\omega(v_l \sin\varphi - v_h \cos\varphi \cos a_R)\right], \qquad (2.73)$$

where v, the velocity of the meteoroid is composed of three perpendicular components. The vertical plane containing the fireball trajectory contains the horizontal component of the velocity, v_l, which is higher than zero in the direction of the meteoroid flight. The vertical plane containing the fireball trajectory contains also the vertical component of the velocity, v_h, which is defined as dh/dt, and thus in the real problem of the meteoroid motion is always smaller than zero. The third component of the velocity, v_x, is horizontal and perpendicular to the vertical plane containing the fireball trajectory and is higher than zero to the right hand side viewing along the meteor motion. The other symbols are: V_l and V_x, the wind velocity components, their direction is opposite to the meteoroid velocity components; Γ the drag coefficient as function of Mach number; S the ratio of meteoroid mass, m, and meteoroid head cross section, s; ρ the air density; φ the geographic latitude; a_R the astronomical azimuth of the direction of the meteoroid flight (south $a_R = 0°$, west $a_R = 90°$); ω the angular velocity of the Earth's rotation ($2\pi/86164$) and g the acceleration of gravity. The Coriolis-force terms can be ommited because they are only small correction.

M	4	3	2	1,5	1,2	1	0,8	0,6	0,4	0,2
Γ(M)	0.580	0.618	0.632	0.596	0.552	0.504	0.441	0.389	0.351	0.328

Table 2.2: Values of Γ(M) for symetrical body

The solution of differential Equations (2.71) to (2.73) can be performed numerically starting from the terminal point and going to lower heights until the surface is reached. At each integration step (dh about 10 m is of enough precision) the velocity of the meteoroid is computed from:

$$v^2 = v_h^2 + (v_l + V_l)^2 + (v_x + V_x)^2. \tag{2.74}$$

The initial values of v_l, v_h, v_x are based on the value of the terminal velocity, v_T and zenit distance of the radiant at the terminal point, z_R:

$$v_l = v_T \sin z_R \tag{2.75}$$
$$v_h = -v_T \cos z_R \tag{2.76}$$
$$v_x = 0. \tag{2.77}$$

The initial value of ΓS is given by the drag equation written for the terminal point:

$$(\Gamma S)_T = -\frac{1}{\rho_T v_T^2} \left(\frac{dv}{dt}\right)_T, \tag{2.78}$$

where v_T and $(dv/dt)_T$ are the velocity and deceleration at the terminal point and ρ_T air density at terminal height h_T. $(\Gamma S)_T$ implicitly contains the unknown mass, shape, density and drag coefficient of the meteoroid. We change Γ as a function of Mach number for a symetrical shape (Table 2.2) and assume S constant.

The wind direction and velocity is given from aeronomic data and we usually take the closest values in location and time. From aerological measurement we can at each integration step determine:

$$\begin{aligned} T &= T(^\circ C) + 273.15 \\ \rho &= 3.483676 \times 10^{-4} P/T \\ c &= 0.0200468\sqrt{T}, \end{aligned} \tag{2.79}$$

where T is the absolute temperature, P the air pressure in hectopascals, ρ the air density in g/cm^3 and c the velocity of sound in km/s. The wind direction is given by geodetic azimuth, a_V, from where the wind blows (northern wind $a_V = 0^\circ$, eastern wind $a_V = 90^\circ$). If V is the total wind velocity we can compute its components:

$$\begin{aligned} V_l &= V \cos(a_V - a_R) \\ V_x &= V \sin(a_V - a_R). \end{aligned} \tag{2.80}$$

We are also interested in the total length of the dark flight. L denotes the component in the direction of the flight, L_x the component perpendicular to the flight (positive to the right hand side viewing along the meteor flight). Both these components are located in the zero level height of geoid. If h_T is the terminal height and h_s the height of the surface we can write:

$$\begin{aligned} L &= \int_{h_s}^{h_T} \frac{v_l}{v_h}\, dh \\ L_x &= \int_{h_s}^{h_T} \frac{v_x}{v_h}\, dh. \end{aligned} \tag{2.81}$$

If the components of the geographic coordinates along the flight are denoted by suffix l, the components perpendicular to the flight (positive to the right hand side) by suffix x, then we can for each step of the integration write:

$$\begin{aligned} a_x &= a_R + 90^\circ \\ d\varphi_l &= \left[\frac{\cos a_R}{(R+h)}\right] dL \\ d\lambda_l &= \left[\frac{\sin a_R}{(R+h)\cos\varphi}\right] dL \\ d\varphi_x &= \left[\frac{\cos a_x}{(R+h)}\right] dL_x \\ d\lambda_x &= \left[\frac{\cos a_x}{(R+h)\cos\varphi}\right] dL_x \end{aligned} \tag{2.82}$$

and the total change of geographic coordinates:

$$\begin{aligned} d\varphi &= d\varphi_l + d\varphi_x \\ d\lambda &= d\lambda_l + d\lambda_x. \end{aligned} \tag{2.83}$$

The instantenous azimuth and zenith distance of the radiant is given by:

$$\begin{aligned} a &= a_R + \arctan\left(\frac{v_x}{v_l}\right) \\ z &= \arctan\left(\frac{v_l^2 + v_x^2}{v_h^2}\right)^{1/2}. \end{aligned} \tag{2.84}$$

The numerical solution starts in the terminal height h_T above the point given by geographic coordinates φ_T and λ_T, using the terminal velocity v_T and the value of $(\Gamma S)_T$. We then proceed step by step using the aeronomical data and tabulated function $\Gamma(M)$ (Table 2.2). Thus for each height h we can compute v_l, v_h, v_x, v, L, L_x, φ, λ, a_R and z_R. We continue until the height is equal to the height of the surface, h_s. The standard deviations of all measured values yield the standard deviation of these computed quantities and define so-called impact area.

Chapter 3

Results

Very efficient and precise method how to record atmospheric interaction of larger meteoroids is the multi-station photographic observation of fireballs by fireball networks. During the short moment of ablation of meteoroids we can determine their atmospheric trajectories, orbits, light curves and basic physical properties. One of the most advanced operational fireball network is the Czech part of the European Fireball Network (EN), where each station is equipped with the newest generation camera, modern and sophisticated completely Autonomous Fireball Observatory(AFO) (Spurný et al., 2007). The AFO imaging system consists of a Zeiss Distagon fish-eye objective (f/3.5, f = 30 mm) and a large-format sheet film (9×12 cm emulsion ILFORD FP4 125 with panchromatic spectral sensitivity approximately between 360 and 650 nm). All AFOs are equipped with a rotating shutter close to the focal plane to determine fireball velocity. At present, 11 stations are operated almost uniformly deployed across the territory of the Czech Republic and 2 in cooperating countries (Austria and Slovakia). Usual precision of any individual point on the luminous atmospheric trajectory for fireballs up to approximately 200 km distance from the stations is about 10 - 15 meters. This precision is proportionally decreasing with the distance of fireball from stations. In some ideal cases it is possible to reliably determine fireballs at a distance of about 500 km from the territory. It enables us to observe fireballs over large part of Central Europe. As well as direct fireball imaging each AFO also includes an all-sky brightness sensor (radiometer) with sampling rate of 500 measurements per second. Therefore, along with the accurate time of fireball passage and its duration, we also obtain a very detailed light curve. These sensors work reliably even under a cloudy sky, so we have basic information about fireball luminosity and its very approximate location even without photographic records. Also radiometers with sampling rate of 1200 measurements per second, but with less sensitivity, are placed on two Czech stations.

Further photographic network equipped with AFOs is Australian Desert Network (DN). This network is in operation from December 2005 and at present there are four stations. Since the AFO was designed to work in conditions of central Europe few modification were performed. Resulting Desert

Fireball Observatory (DFO) is weather resistant, sealed against dust, equipped by solar shield, and designed to use minimal electrical power.

In this thesis, atmospheric, photometric and orbital results for 98 fireballs from six different meteor showers, which corresponds to six different parent objects, are presented (20 Leonids without orbital data). The fireballs were observed from Central Europe, Spain, and also from Southern Australia. All the results are based on photoghaphic observation by precise all-sky lenses and also light curves with high time resolution are available for lots of the fireballs. Appropriate visual observations are also mentioned.

The aim of the thesis is to determine main physical properties of major meteor showers in terms of different methods like end height criterion, beginning heights, apparent ablation coefficient, fragmentation, and dynamic pressure at the height of fragmentation or terminal flare. Also events like periodic changes of brightness, afterglow, short-lived flares, and general profiles are studied on the basis of very detailed light curves and heliocentric orbits for individual showers are presented.

3.1 Orionids

The Orionid meteor shower is a relatively strong and stable regular annual shower with a peak visual hourly rate of 15 – 30 meteors and broad maximum generally occurring on October 20 – 23. The parent is comet 1P/Halley, now in an orbit passing a far +0.151 AU from Earth (Jenniskens, 2006). The last return of parent comet 1P/Halley caused a renewed interest in the study of both streams originating from this comet, i.e. Orionids and η-Aquariids. Most theoretical works and modeling attempts (McIntosh and Hajduk, 1983; Hughes, 1987; McIntosh and Jones, 1988; Wu and Williams, 1993) as well as increasing number of meteor observations mostly by visual amateur observers date around this return. However no enhanced Orionid activity was observed and it was concluded that enhanced rates are not connected with the parent comet returns (Porubčan et al., 1991) but are due to isolated particle concentrations not necessarily in the comet's vicinity. The latest outbursts were observed in 1993 (Rendtel and Betlem, 1993), 2006 and 2007 (Spurný and Shrbený, 2008).

Emel'Yanenko (2001) in his theoretical work explains enhanced and short-term activity of a shower with a libration of a meteoroid stream, and for Orionids he presents three sets of parameters that describe three possible resonant zones for this shower (Table 3.1). These librating particles create a resonance substream. The 2006 Orionid activity was caused according to Sato and Watanabe (2007) by the dust trails formed by meteoroids ejected from 1P/Halley in years 1265 BC, 1197 BC and 910 BC and trapped in the 1:6 mean motion resonance with Jupiter. The exceptional activity of 2006 Orionids Rendtel (2007) is also ascribed to the meteoroids from a resonant zone with the most favorable resonance the 1:6 with Jupiter. Rendtel (2007) also mentions the decrease of the population index, r. During the maximum of the

activity the value of r was 1.6 but the long-term average is 2.3 - 2.9. This fact confirms that the meteors observed during the Orionid 2006 maximum deviated significantly from the average Orionid meteors and on average are significantly brighter. A similar effect was observed during the 1993 Orionid outburst (Jenniskens, 1995).

Majority of this section is published in Spurný and Shrbený (2008).

3.1.1 Observation

During four nights from October 20 a total of 48 bright Orionids were recorded – the 2006 Orionid enhanced activity. During this time the observation was strongly affected by unstable weather conditions. The entire data set includes multi-station photographic fireballs and those recorded photographically only from one station, some that were too short (only the brightest flare) to make it possible to compute the trajectory or to determine the velocity, and others that were recorded only by brightness sensors due to a cloudy sky. Only 10 recorded fireballs were long and bright enough to be recorded photographically from more than one station so that it was possible to determine precisely all important parameters describing their atmospheric trajectories, heliocentric orbits and basic physical properties.

Atmospheric trajectories the Orionid fireballs presented here were determined from all available images (Table 3.2). Because Orionid meteors are very fast, their atmospheric trajectories are often very short (last two columns in Table 3.2). This can decrease the precision in determination of other critical parameters. However, in all cases the fireballs listed in Table 3.2 were recorded from more than 2 stations of the Czech Fireball Network, which highly increases reliability of presented data. The only exception being ORI06 that was recorded from only 2 stations.

3.1.2 Atmospheric behavior

The results on atmospheric trajectories are collected in Tables 3.2 - 3.4. The time of meteor beginning, beginning and end heights, length and duration of observed atmospheric trajectory are presented in Table 3.2. The beginning heights range from 100 to 114 km and the terminal heights from 78 to 90 km corresponding to a range of the observed trajectory lengths from 15 to 40 km.

j':j	a [AU]	Δ a [AU]
1:6	17.19	1.0
1:5	15.22	0.9
1:4	13.12	0.8

Table 3.1: Parameters of principal resonance zone near orbit of the Orionid meteor shower (Emel'Yanenko, 2001). a is the semimajor axis at the center of the j':j resonance, Δa is the width of the resonance zone.

Table 3.2: Atmospheric trajectories of the 2006 and 2007 Orionids. H is the height above sea level, L_{obs} is the length of observed trajectory. The subscript "B" denotes values at the beginning point of the atmospheric trajectory, the subscript "E" at the end point. N is the number of stations where the fireball was photographed. The fireballs from the filament are denoted by asterisk. Standard deviations for each entry are shown below.

Meteor No.	N	Date	Time (UT)	H_B (km)	H_E (km)	L_{obs} (km)	Duration (s)
Year	2006						
ORI01*	3	21.10.	0:36:13	105.58	85.34	30.02	0.27
				1	1		
ORI02*	4	21.10.	0:50:44	104.27	90.25	20.68	0.30
				2	2		
ORI03*	8	21.10.	0:57:58	108.92	85.30	34.06	0.47
				2	2		
ORI04*	5	21.10.	1:46:13	100.74	81.97	23.71	0.33
				2	2		
ORI05*	6	21.10.	1:50:42	108.17	78.10	39.03	0.54
				1	1		
ORI06*	2	21.10.	2:01:45	101.81	89.37	15.01	0.20
				1	1		
ORI07*	4	21.10.	2:35:48	110.82	86.39	30.17	0.41
				1	1		
ORI08	3	21.10.	23:52:10	106.86	88.23	30.25	0.33
				1	1		
ORI09	3	22.10.	2:01:29	114.26	77.82	40.48	0.39
				1	1		
ORI10	4	22.10.	22:55:46	108.03	87.46	40.63	0.28
				4	2		
Year	2007						
ORI11	2	22.10.	1:23:04	98.92	80.10	24.68	0.38
				1	1		
ORI12	3	22.10.	3:04:55	104.27	87.48	19.70	0.28
				1	1		
ORI13	2	22.10.	3:29:04	106.20	85.06	25.65	0.34
				1	1		

Physical data of these fireballs are presented in Tables 3.3 and 3.4. Zenith distances for the end point, initial velocities (mean measured velocity without deceleration), maximum absolute photographic magnitudes, initial photometric masses, PE coefficients that describe the empirical end height criterion and fireball types according to the classification of Ceplecha and McCrosky (1976) are shown in Table 3.3.

The rotating shutter hides one half of the meteor trail (except for guided cameras) so in some of cases the short-term flares are not visible in the photographs at all. These flares are obvious in the light curves from the AFO brightness sensors. This is well documented in Figures 3.3 and 3.4 showing the photographic images and radiometric light curves for all 10 2006 Orionid fireballs listed in Tables. From known durations of the fireballs and their approximate light curve profile, both derived from the photographic records and from durations of the AFO's light curves, we can derive instantaneous heights of flares for each fireball in the atmosphere. Values of these quantities (if visible in the light curve) are presented in Table 3.4. Since the overlap of the light curves is approximate, the heights listed are rounded-off to kilometers. The duration of the flares varies from several tens of milliseconds (near the mid part of the trajectory) to only several milliseconds in terminal flares. A

Table 3.3: Physical data on the 2006 and 2007 Orionid fireballs. ZD_E is the zenit distance of the radiant at the end point of the atmospheric trajectory, v_∞ is the initial velocity, M_{max} is the maximum absolute magnitude, m_{inf} is the initial photometric mass, PE is the coefficient that describes the empirical end height criterion and designates the type of fireball (Ceplecha and McCrosky, 1976). The fireballs from the filament are denoted by asterisk. Standard deviations for each entry are shown below.

Meteor No.	ZD_E (deg)	v_∞ (km/s)	M_{max}	m_{inf} (g)	PE	Type
Year	2006					
ORI01*	47.7	67.6	-5.1	0.5	-5.10	II/IIIA
	4	5				
ORI02*	46.75	67.7	-8.4	6	-5.93	IIIB
	10	2				
ORI03*	45.56	67.7	-6.0	3	-5.44	IIIA
	4	3				
ORI04*	37.73	67.82	-10.0	40	-5.73	IIIB
	12	13				
ORI05*	38.68	67.80	-8.2	7	-5.13	II/IIIA
	1	11				
ORI06*	36.95	67.6	-3.0	0.1	-5.20	II/IIIA
	5	5				
ORI07*	34.85	67.63	-7.9	3	-5.61	IIIA/IIIB
	1	14				
ORI08	52.55	67.8	-6.0	2	-5.48	IIIA
	5	2				
ORI09	36.03	67.4	-8.3	10	-5.19	II/IIIA
	4	2				
ORI10	59.7	67.5	-6.9	4	-5.47	IIIA
	2	3				
Year	2007					
ORI11	40.53	67.5	-9.3	13	-5.37	IIIA
	8	6				
ORI12	34.25	67.32	-6.8	1.3	-5.55	IIIA
	3	13				
ORI13	35.0	67.31	-10.7	58	-6.05	IIIB
	2	3				

Table 3.4: Heights and durations of the flares and dynamic pressures for the 2006 and 2007 Orionids. H_{MF} is the height at maximum of the brightness and H_{TF} is the height at the terminal flare. p_{MF} is the dynamic pressure at maximum of the brightness and p_{TF} is the dynamic pressure at the terminal flare. ΔT_{mf} and ΔT_{tf} are durations of the maximum and the terminal flares. Duration of the flare presented here is the full width at half maximum. The fireballs from the filament are denoted by asterisk.

Meteor No.	H_{MF} (km)	H_{TF} (km)	p_{MF} (MPa)	p_{TF} (MPa)	ΔT_{mf} (ms)	ΔT_{tf} (ms)
Year	2006					
ORI01*	94	85	0.007	0.033	45	6
ORI02*	94	-	0.007	-	65	-
ORI03*	91	85	0.012	0.033	80	10
ORI04*	89	82	0.017	0.055	60	13
ORI05*	85	78	0.033	0.110	65	5
ORI06*	-	89	-	0.016	-	7
ORI07*	87	-	0.023	-	19	-
ORI08	-	88	-	0.020	-	8
ORI09	81	78	0.065	0.105	15	9
ORI10	90	87	0.013	0.022	40	12
Year	2007					
ORI11	-	80	-	0.074	-	5
ORI12	-	88	-	0.019	-	19
ORI13	-	88	-	0.019	-	34

typical Orionid light curve has a broader maximum and one much shorter very pronounced terminal flare. From such type of light curve we can infer that the material of the Orionid meteoroids easily disintegrates first into bigger particles which gradually ablate and create a longer middle peak and near the end of its trajectory the remaining part of the initial meteoroid completely disintegrates into a large amount of very small particles which ablate and evaporate very quickly. From the values listed in Tables 3.3 and 3.4 it is evident that all 13 presented Orionid meteoroids consist of very weak and fragile material that is usually assumed to be of cometary origin which corresponds with known parent body – comet 1P/Halley.

3.1.3 Radiant and orbit

Geocentric radiant positions and orbital elements for all 13 Orionid fireballs are tabulated in Table 3.5. All values are given in the J2000.0 equinox. The fireballs are arranged according to date and time of occurrence, which is given by increasing values of the ascending node. It is evident that the first seven fireballs which were recorded in only 2-hour interval on October 21^{st} all have very similar values. Therefore the conclusion is that these meteoroids belonged to one very compact filament which slightly differs from a regular background Orionids (Lindblad and Porubčan, 1999; de Lignie and Betlem, 1999).

The compactness of geocentric radiants of fireballs belonging to this new filament is shown in Figure 3.1 along with the mean geocentric radiant value, the 3 Orionids recorded during two following nights (ORI08 – ORI10), the 3 Orionids recorded in 2007 (ORI11 – ORI13), and the mean radiant positions determined by Lindblad and Porubčan (1999) from IAU MDC photographic data and by de Lignie and Betlem (1999) from DMS video data. Mean orbital elements for the 2006 filament, mean orbit from Lindblad and Porubčan (1999) and values of the parent comet are also listed in Table 3.5. Although the differences are not too significant in the statistical sense we can still find some distinctions. The radiant position of the 2006 filament is systematically shifted by about 0.1 or 0.6 degrees (depending on source of data) to higher right ascensions and 0.2 degrees to lower declinations. Also some orbital elements are slightly different: the filament meteoroids have about 0.01 – 0.03 AU larger perihelion distances and about 0.3 – 0.6 degrees smaller inclinations. As shown in Table 3.5 and Figure 3.1 some characteristics of the 3 Orionids recorded during the two following nights in 2006 differ from the filament. However, this difference is not so obvious as to completely exclude the possibility that these meteoroids could belong to the filament (it would need statistically larger set of data).

The mean heliocentric orbit of the Orionid 2006 filament has semimajor axis a = 14.8 AU, eccentricity e = 0.959, inclination i = 163.71°, perihelion distance q = 0.603 AU and argument of perihelion ω = 78.7°. According to Emel'Yanenko (2001) (see Table 3.1) it is probable that particles from this filament were in the 1:5 resonance with Jupiter. From detailed analysis of

Table 3.5: Radiants and orbital elements (J2000.0) of the 2006 and 2007 Orionid fireballs. (α_G, δ_G) is the geocentric radiant, V_G is geocentric mean velocity without atmospheric drag (not mesurable on our records) and T_J is Tisserand's parameter. Data for the filament and IAU MDC (Lindblad and Porubčan, 1999) are mean values. Data for the parent comet are for epoch 1986-02-19 and are taken from Jenniskens (2006). The fireballs from the filament are denoted by asterisk. Standard deviations for each entry are shown below.

Meteor No.	α_G (deg)	δ_G (deg)	V_G (km/s)	a (AU)	e	q (AU)	ω (deg)	Ω (deg)	i (deg)	T_J
Year	2006									
ORI01*	94.98	15.58	66.7	13.8	0.96	0.600	79.2	27.38605	163.8	-0.53
	2	4	6	9.4	3	10	1.9	2	2	
ORI02*	95.19	15.56	66.8	14.4	0.958	0.606	78.4	27.39710	163.87	-0.56
	16	3	3	4.8	14	6	9	2	10	
ORI03*	95.17	15.46	66.8	13.8	0.956	0.605	78.6	27.40109	163.64	-0.54
	2	5	3	4.6	14	5	9	2	11	
ORI04*	95.24	15.54	66.90	16.2	0.962	0.608	78.1	27.43440	163.9	-0.60
	25	9	13	3.8	9	6	7	2	2	
ORI05*	95.04	15.48	66.88	17.3	0.965	0.604	78.5	27.43752	163.66	-0.62
	1	1	11	2.9	6	2	4	1	3	
ORI06*	94.98	15.45	66.7	14.2	0.96	0.599	79.3	27.44516	163.54	-0.54
	6	4	5	8.6	2	9	1.6	1	14	
ORI07*	95.10	15.440	66.72	13.7	0.956	0.601	79.0	27.46867	163.56	-0.53
	2	13	15	2.5	8	3	5	1	4	
ORI08	95.84	16.25	66.9	15.7	0.962	0.595	79.6	28.35028	165.26	-0.59
	3	6	2	4.4	10	4	7	2	14	
ORI09	95.41	15.53	66.5	13.9	0.958	0.582	81.3	28.43983	163.57	-0.52
	3	4	2	3.5	10	4	7	1	9	
ORI10	96.43	15.90	66.6	14.3	0.96	0.584	81.0	29.30975	164.5	-0.54
	6	20	3	6.3	2	6	1.2	5	4	
filament	95.10	15.50	66.79	14.8	0.959	0.603	78.7	27.42	163.71	-0.57
	10	6	9	1.4	3	3	4	3	14	
IAU MDC	95.2	15.8	66.52	14.4	0.961	0.576	81.9	28.4	164.0	-0.52
	2.6	7	1.16	8.6	57	39	5.2	3.4	1.3	
Year	2007									
ORI11	95.38	15.59	66.6	13	0.96	0.589	81	28.15740	163.8	-0.45
	4	9	6	10	3	11	2	3	2	
ORI12	95.69	15.19	66.38	11	0.944	0.593	80.4	28.22783	163.0	-0.44
	3	3	13	1	6	2	5	1	7	
ORI13	95.6	15.6	66.42	11	0.947	0.588	80.9	28.24443	163.7	-0.42
	2	2	3	1	5	5	5	6	5	
1P/Halley			66.79	17.94	0.967	0.587	80.446	28.671	164.715	-0.62

visual observations of the 2006 outburst as well as another Orionid outbursts observed in 20^{th} century, Rendtel (2007) suggested that these outbursts could be caused by particles from the 1:6 resonance. Similarly Sato and Watanabe (2007) ascribe the 2006 Orionid activity to particles from the 1:6 mean motion resonance with Jupiter. However there are no arguments from the study presented here to decide which value is unambiguously correct. Although all presented values are determined with high precision and reliability, it is well known that the least-precise value is the semimajor axis (i.e. also period), which is strongly affected by the uncertainty of entry velocity that is objectively difficult to determine with sufficient precision. It is caused by the fact that Orionids are very fast meteors and their atmospheric trajectories are relatively short. Therefore it will certainly need further study to decide this discrepancy.

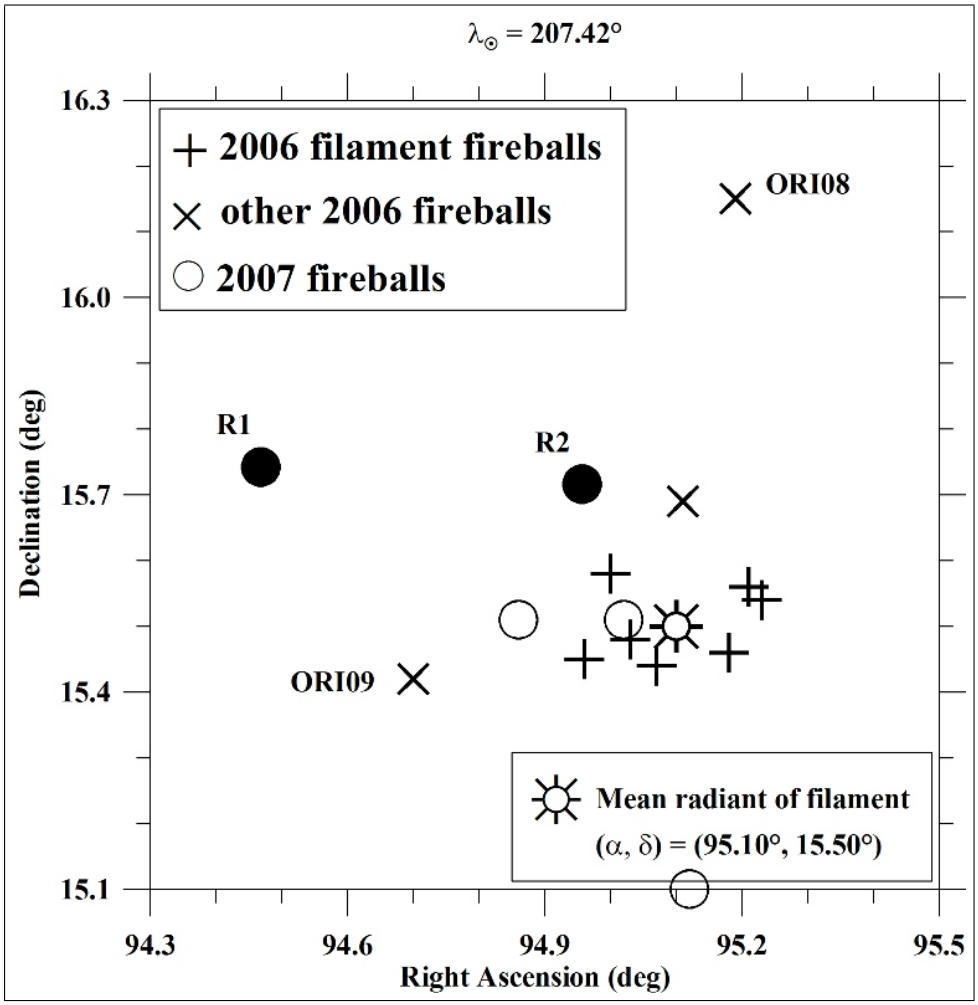

Figure 3.1: Geocentric radiants of the 2006 and 2007 Orionid fireballs (J2000.0). The radiants are normalised to the node 27.42°, with a radiant drift of 0.70 dRA/Dsol and 0.11 dDec/Dsol. Mean radiant of filament is computed from meteors ORI01 to ORI07. R1 is the radiant position according to de Lignie and Betlem (1999) and R2 according to Lindblad and Porubčan (1999), both normalised to the node 27.42°.

3.1.4 2007 Orionids

The weather conditions in 2007 were even worse than in 2006, and thus only data from the night 21/22.10. are available. It means only three multi-station Orionid fireballs. Their heliocentric orbits (Table 3.2) are similar to the 2006 filament, but with a bit smaller semimajor axis and higher argument of perihelion. These three Orionid fireballs were photographed around solar longitude 208.21° and their geocentric radiants correspond to that of the 2006 filament (Figure 3.1). Also the light curves of the 2007 Orionids agree with the 2006 Orionids and terminal flares occured in the same height range. ORI12 and ORI13 have a duration of terminal flares higher than meteors in 2006, which

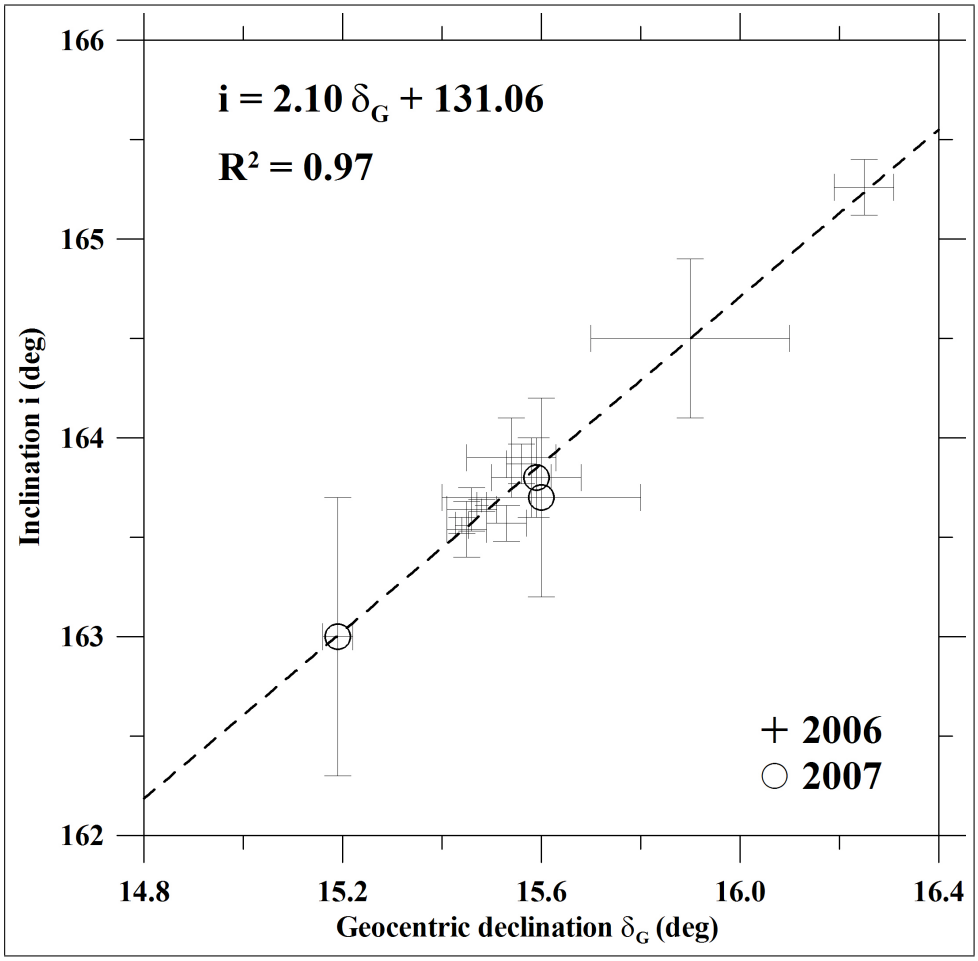

Figure 3.2: Linear dependency of inclination of heliocentric orbit on declination of geocentric radiant for the 2006 and the 2007 Orionid fireballs (J2000.0). Fireballs recorded in 2006 are denoted by crosses, the 2007 Orionids by cyrcles. R^2 is the coefficient of determination describing accuracy of the fit.

means that these meteoroids did not fragment into such small particles. Despite the differences in semimajor axis and argument of perihelion it is likely that these three Orionids also belonged to the same filament as the previous year.

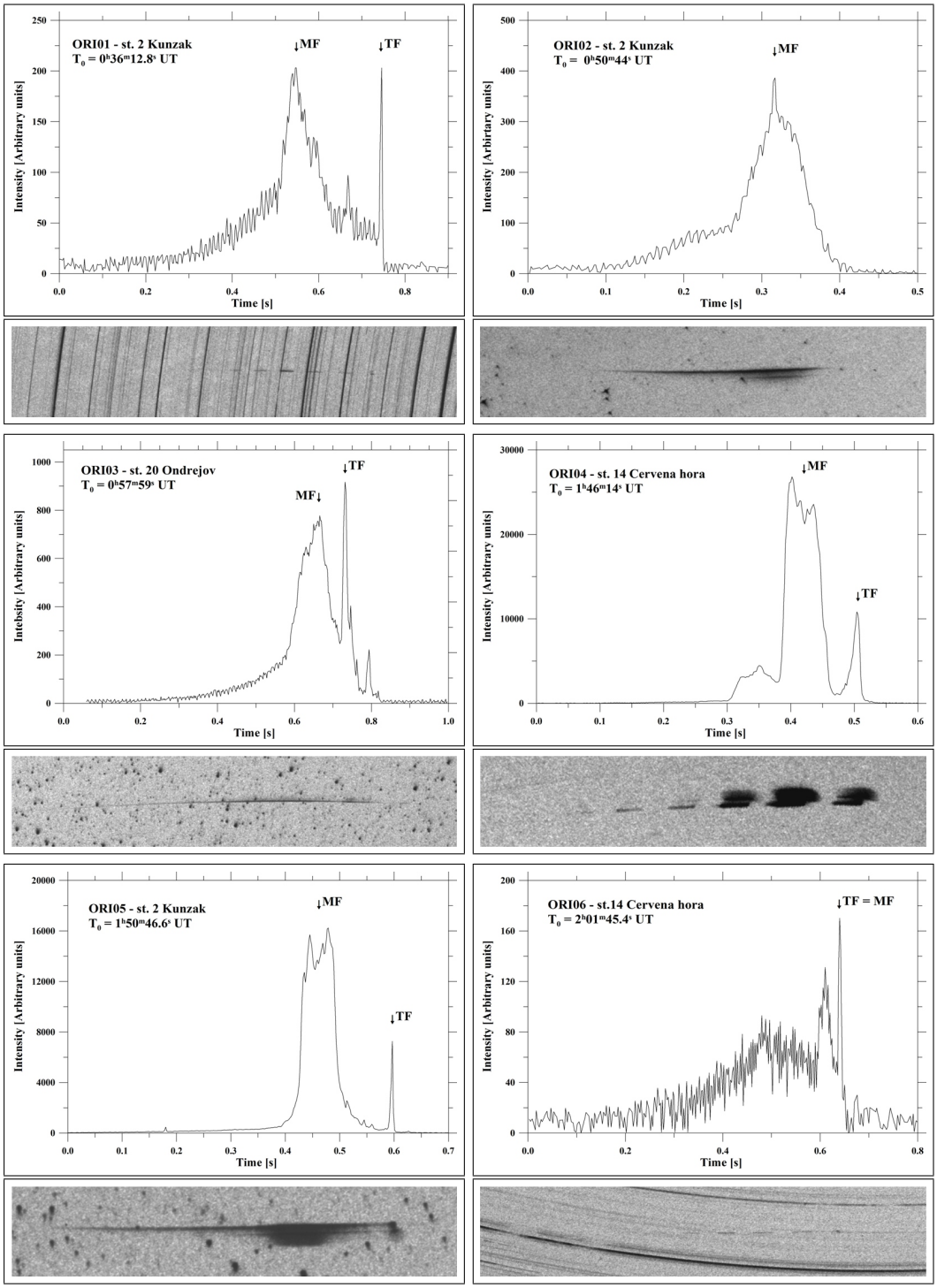

Figure 3.3: Light curves from AFO's brightness sensors and images of the 2006 Orionid fireballs from all-sky cameras. MF means the position of the maximum brightness, TF the position of the terminal flare (see Table 3.4). The images from fixed cameras display startrails and interruptions of the meteors caused by a rotating shutter (15 breaks/second). The guided images were taken by a guided all-sky camera at Ondřejov Observatory and show the entire fireball trails. All fireballs flew from left to right in the images.

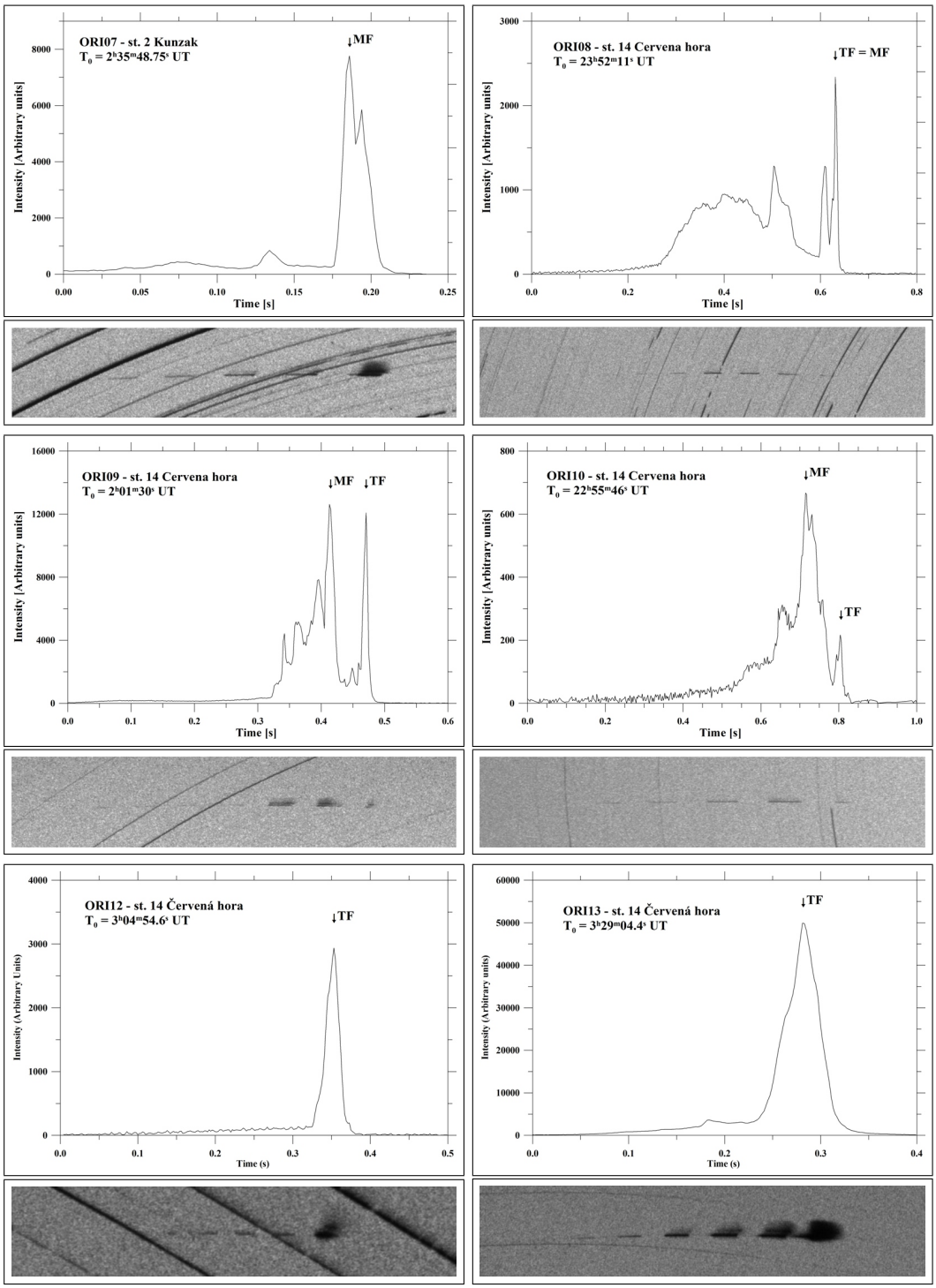

Figure 3.4: Light curves from AFO's brightness sensors and images of the 2006 and the 2007 Orionid fireballs from all-sky cameras. MF means the position of the maximum brightness, TF the position of the terminal flare (see Table 3.4). The images from fixed cameras display startrails and interruptions of the meteors caused by a rotating shutter (15 breaks/second). All fireballs flew from left to right in the images.

3.2 Geminids

The Geminids, reaching the peak activity on December 14, are one of the strongest annual meteor showers, with one of the shortest orbital period (1.6 years) and one of the shortest perihelion distance (0.14 AU). The maximum activity occurs at $\lambda_\odot = 262.16 \pm 0.04$ deg (J2000) (Rendtel, 2004). The parent body of the Geminid stream is 3200 Pheathon (Whipple, 1983; Fox et al., 1984) discovered in 1983 using Infrared Astronomy Satellite (IRAS). 3200 Pheathon is possibly degassed nucleus of responsible comet (Fox et al., 1984). Frequent exposure to the intense solar radiation near perihelion (0.14 AU) heats the Geminids to approximately 800 K and may lead to a loss of volatiles and produce materials more similar to the crust of a comet than to its interior, perhaps even more similar to asteroidal stony matter (Wetherill, 1986). This correlates well with the finding that the bulk density $\rho = 2.9 \pm 0.6\,\mathrm{g/cm^3}$, derived from photographic images of 8 Geminids using quasi-continuous fragmentation model (Babadzhanov, 2002). Also (Ceplecha and McCrosky, 1992) gives for the most suitable PN Geminid fireball the bulk density 3 - 4 $\mathrm{g/cm^3}$ (using gross-fragmentation model, at the point of fragmentation $\rho = 3.9 \pm 1.2\,\mathrm{g/cm^3}$). The bulk density of the Geminids is the highest among the other major streams.

Geminids sometimes show high-frequency (up to several hundreds Hz) pulsations of brightness. According to the data of Astapovich (1958), bright flickering Geminids were photographed at the Harward observatory (USA) in 1933 and 1934. The pulsations of brightness were observed for 6 of the 12 Geminid fireballs photographed according to the Meteoroid Observation and Recovery Program (MORP) of Canada (Halliday, 1988). Only 3 of the 11 Geminids photographed at the Institute of Astrophysics, Tajik Academy of Sciences (Dushanbe, Tajikistan) show high-frequency pulsations of brightness of more than 100 Hz. The flickering starts suddenly, approximately from the middle of a meteor trajectory and remains steady down to its end. Thus the frequency of flickering increases in the process of penetration of the meteoroid into the atmosphere, and the amplitude of flickering remains practically nearly constant during the whole visible path. The observed flickering of Geminids cannot be explained by meteoroid rotation gained in the Earth's atmosphere (Babadzhanov and Konovalova, 2004).

On the other hand, Beech (2002) presented a procedure, which enables to derive the age of the Geminid stream from rotation of Geminid meteoroids. The idea is based on non-isotropic photon scattering interaction of the meteoroids with the solar radiation field (Paddack, 1969) and for three Geminids leads to the age 2000 – 4000 years. Beech et al. (2003) published one Geminid fireball with initial rotation rate of some 6 Hz based on distinct flickering effect. From this rate he estimated that the meteoroid was ejected from the parent body 3200 Phaethon some 2500 ± 500 years ago. To first order approximation, the flickering amplitude vary as $\Delta m = 2.5\log(a/b)$ (Beech, 2001), where a and b are semi-major and semi-minor axes of assumed spinning ellipsoidal pro-

Table 3.6: Atmospheric trajectories of the 2006 Geminids. H is the height above sea level, L_{obs} is the length of observed trajectory. The subscript "B" denotes values at the beginning point of the atmospheric trajectory, the subscript "E" at the end point. N is the number of stations where the fireball was photographed. Standard deviations for each entry are shown below.

Meteor No.	N	Date	Time (UT)	H_B (km)	H_E (km)	L_{obs} (km)	Duration (s)
GEM01	5	14.12.	4:57:27	98.44	46.63	73.85	1.79
				1	1		
GEM02	6	14.12.	16:53:45	93.38	78.85	93.86	2.59
				2	1		
GEM03	2	14.12.	19:42:18	86.25	81.95	8.23	0.21
				2	2		
GEM04	2	14.12.	19:59:17	81.16	60.26	39.28	1.1
				4	4		
GEM05	2	14.12.	22:21:14	88.27	71.58	19.68	0.53
				1	1		
GEM06	2	14.12.	22:33:09	82.20	67.34	18.00	0.47
				1	2		
GEM07	2	14.12.	22:53:44	84.40	55.83	33.23	0.93
				1	1		
GEM08	7	14.12.	23:06:22	90.71	44.41	48.68	1.49
				3	3		
GEM09	2	15.12.	0:32:28	88.08	48.60	41.27	1.20
				1	1		
GEM10	2	15.12.	0:51:28	86.63	80.45	6.22	0.13
				1	1		
GEM11	3	15.12.	1:12:24	93.40	46.94	48.80	1.41
				1	1		
GEM12	3	15.12.	1:26:59	90.51	61.25	30.77	0.87
				1	1		
GEM13	3	15.12.	4:15:01	88.66	62.31	33.82	0.93
				1	2		

file. Geminid fireballs studied by Babadzhanov and Konovalova (1987) showed large 0.5 to 0.75 magnitude flickering variations (based on photographic observation) that indicate the axes ratio of the order of 1.6 to 2.0 respectively. Beech et al. (2003) interprets fireball flickering in terms of rotational modulation of the ablation process. If the Geminid meteoroids are spun-up through non-isotropic photon scattering interactions with the solar radiation field, the found age of the meteoroids is consistent with ejection times in the order of 1000 to 4000 years.

According to modelling, the Earth will continue to intersect the Geminid meteoroid stream until about AD 2100 (Hunt et al., 1985) with the peak of ZHR about 190 around AD 2050. There is no evidence that the meteoroids are trapped in an orbital resonance with the terrestrial planets, but meteoroids scatter widely and most are in between the 7:1 and 8:1 mean-motion resonance with Jupiter (Jenniskens, 2006).

3.2.1 Observation and light curves

During the night 13/14.12. 2006, one multi-station Geminid fireball was observed and in the following night another twelve. GEM01 was visually observed by P. Švadlenka (online database, 2000) who described its green colour and breakup in the end part of the trajectory. Second fireball, GEM02 was visually observed by J. Mikulecký (online database, 2000) who documented its

Table 3.7: Physical data on the 2006 Geminid fireballs. ZD_E is the zenit distance of the radiant at the end point of the atmospheric trajectory, v_∞ is the initial velocity, M_{max} is the maximum absolute magnitude, m_{inf} is the initial photometric mass, PE is the coefficient that describes the empirical end height criterion and designates the type of fireball (Ceplecha and McCrosky, 1976). Standard deviations for each entry are shown below.

Meteor No.	ZD_E (deg)	v_∞ (km/s)	M_{max}	m_{inf} (g)	PE	Type
GEM01	45.69	35.44	-8.7	490	-4.37	I
	1	2				
GEM02	81.504	35.75	-5.5	20	-4.85	II
	13	6				
GEM03	58.5	35.5	-4.3	2.2	-5.38	IIIA
	3	2				
GEM04	57.9	36.43	-9.0	420	-4.93	II
	5	22				
GEM05	32.08	36.2	-3.5	1.7	-4.89	II
	10	2				
GEM06	34.4	35.6	-4.6	4.4	-4.79	II
	4	2				
GEM07	30.81	36.15	-5.6	10	-4.27	I
	5	9				
GEM08	25.5	35.6	-12.6	11000	-4.94	II
	1	1				
GEM09	17.0	35.79	-7.6	100	-4.36	I
	2	4				
GEM10	17.08	35.7	-3.3	0.7	-5.40	IIIA
	08	1.1				
GEM11	17.89	35.84	-6.3	21	-3.98	I
	01	5				
GEM12	18.08	36.55	-5.1	7.8	-4.58	I/II
	01	6				
GEM13	38.88	36.20	-5.3	12	-4.62	II/I
	04	5				

significantly nonzero angular size. Good light curves, in respect of s/n ratio, are available for meteors 01, 02, 08, 09, 11 and 12 that were either bright enough or not so far from a station with brightness detector. Three curves present periodic changes of brightness in the first half of the meteors. No expressive terminal flares were observed, only GEM02, GEM09 and GEM13 had a small outburst at the end of the trajectory.

GEM01 shows in its light curve cyclic changes of brightness with exponentialy increasing frequency (Figure 3.5). Initial value of the frequency, it means at the point where the signal is higher enough then the noise, is approximately 26 Hz. At that time, the meteoric body was at the height of 76 km and was observed 0.8 s by this time. Cyclic change of brightness is observeable only 0.3 s, then the light curve become complicated – full of short increases and decreases of brightness. The last observed frequency at the height of 68 km is about 55 Hz. Exponential increase in frequency is function of time, $f = A(e^{Bt}\text{-}1)+f_0$ (Čapek, 2008, the thesis), where A and B are constants and f_0 is an initial frequency. For GEM01 the fit leads to A = 0.22 and B = 4.69 s^{-1}. When we extrapolate into time t = 0 we get frequency f_0 = 16.82 Hz, for t = 1.8 s (terminal point) about 1000 Hz, but these values were not observed.

The constant values of A, B and f_0 are based on the least square fit of theoretical function (Čapek, 2008, the thesis) for spinning–up of a meteoroid due to the windmill effect (Paddack, 1969). If a meteoroid is approximated by

Table 3.8: Dynamic pressures and apparent ablation coefficients of the 2006 Geminid fireballs. p_{max} and p_{tf} are dynamic pressures at maximum brightness and at terminal flare, respectively. h_{max} and h_{tf} are appropriate heights. σ are apparent ablation coefficients derived using gross-fragmentation model (Ceplecha et al., 1993). Since the listed heights are based on the light curves from AFO's, the accuracy is about 0.5 km.

Meteor No.	h_{max} (km)	h_{tf} (km)	p_{max} (MPa)	p_{tf} (MPa)	σ (s^2km^{-2})
GEM01	58		0.402		0.0102 ± 0.0008
GEM02	83	79	0.013	0.025	
GEM03	84		0.011		
GEM04	69		0.106		
GEM05	75		0.047		
GEM06	71		0.083		
GEM07	63		0.224		0.023 ± 0.002
GEM08	56		0.535		0.024 ± 0.002
GEM09	55.5	50	0.507	0.589	0.0177 ± 0.0006
GEM10	82.5		0.014		
GEM11	60.5		0.318		0.0202 ± 0.0007
GEM12	68		0.116		0.016 ± 0.003
GEM13	76	63	0.040	0.195	0.042 ± 0.002

windmill, which rotation axis is parallel to the direction of flight, the gravity is neglected, velocity, v, and zenith distance of the radiant, z, are constant and exponential low of the air density is used, then constant B is equal to b∗v∗ cos z, where b is the air density gradient. When we apply appropriate values derived for GEM01 (b = 0.14 km^{-1}), B is equal to 3.41 s^{-1}. We can then use this value of B and find only A and f_0. The initial frequency, f_0, would then be 9.68 Hz and at the terminal point about 510 Hz. A comparison of the fits is in Figure 3.6.

Next Geminids with cyclic change of brightness are GEM08 and GEM11. GEM08 have not got the change of frequency of change of brightness well defined. Only four cycles with frequencies 32, 25, 25 and 28 Hz between heights of 62 and 59 km are recognizable. In comparison to this, GEM11 have got unambiguous exponentialy increasing trend of change of frequency of change of brightness (Figure 3.6). The first observed frequency at the height of 93 km has value 14 Hz, the last one at 73 km 119 Hz. The rate of increase of frequency is similar to GEM01, the coefficient B is equal to 3.10 s^{-1}. A = 39.92 and f_0 = 0 (the best solution of the least squere fit is for f_0 = -4 Hz – an unreal solution), which would mean zero initial rotation and the terminal frequency about 3000 Hz. Nevertheless, when we apply appropriate values of b, v and cos z derived for this fireball (b = 0.16 km^{-1}), B is equal to 4.87 s^{-1}. This assumption gives rise to the initial frequency 10.18 Hz and the terminal frequency of order of 10^4 Hz. A comparison of the fits is in Figure 3.6.

According to Beech (2002) it is possible to derive the age of the Geminid stream from rotation of Geminid meteoroids. The idea is based on non-isotropic photon scattering interaction of the meteoroids with the solar radiation field (Paddack, 1969). The derived ages of the meteoroids are directly related to the albedo, A, radiation efficiency term, Q, and the meteoroid bulk density, ρ. For computation of the age of GEM01 and GEM11 by means of

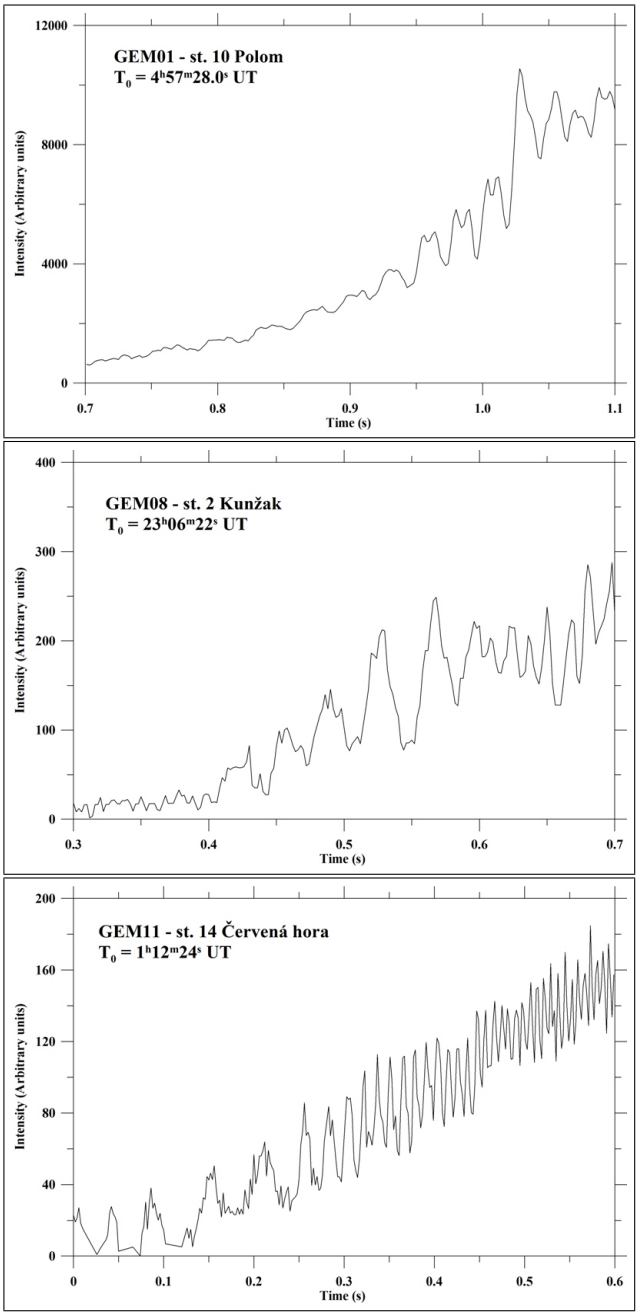

Figure 3.5: Light curves from AFO's brightness sensors that show cyclic change of brightness of the 2006 Geminids.

the windmill effect, the following values were used: A = 0.25, Q = 0.5 (Beech, 2002) and approximate average $\rho = 3500\,\mathrm{kg/m^3}$ (Ceplecha and McCrosky, 1992; Babadzhanov, 2002). By using values in Tables 3.7 and 3.9 (meteoroids approximated by homogenous square), derived age of GEM01 is 2400 years and of GEM11 650 years. If we use A = 0.5, Q = 0.5 (Misconi, 1993) and A

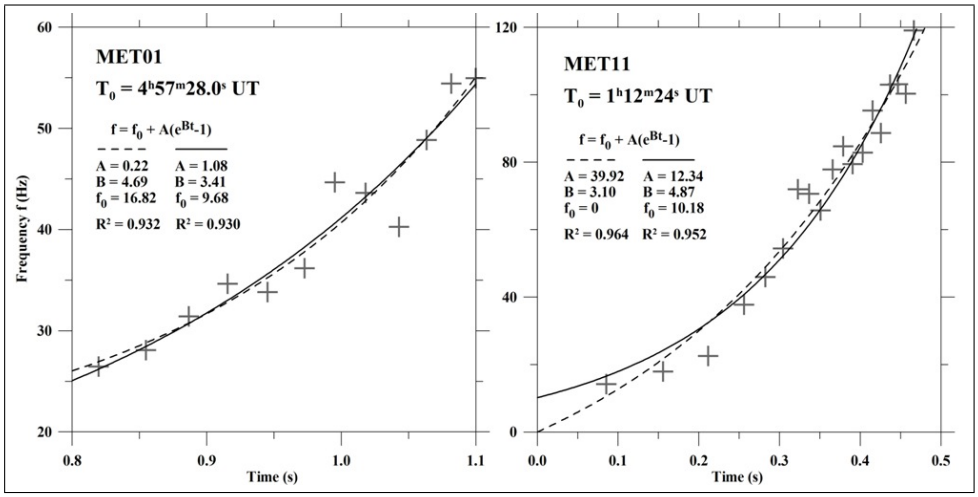

Figure 3.6: Exponential course of change of frequency of change of brightness that was observed in the light curves of the 2006 Geminids. The dashed line is the least square fit when all three parameters are fitted, the solid line is the least square fit when only A and f_0 are fitted (B derived from the observation – see text). R^2 is the coefficient of determination describing accuracy of the fit.

= 0.1, Q = 1 (Olsson-Steel, 1987) as border values, the age of GEM01 is 1200 – 3000 years and of GEM11 300 – 800 years.

3.2.2 Atmospheric behavior

Significant deceleration (example in Figure 3.7) was observed for all four type I Geminids and three type I/II or II fireballs GEM08, GEM12 and GEM13. The apparent ablation coefficient, thanks to gross-fragmentation model (Ceplecha et al., 1993), was possible to determine (Table 3.8). Its mean value for the type I is $\sigma_{type\,I} = 0.018 \pm 0.005\,\mathrm{s^2/km^2}$. GEM13, border type II/I, was decelerated not so effectively and the fit has small accuracy, nevertheless its apparent ablation coefficient was determined and its value differs significantly from that of type I Geminids. On the other side, type II meteor GEM08 and border type I/II GEM12, which experienced higher deceleration, have apparent ablation coefficient similar to that of type I. Thus the apparent ablation coefficient for all the Geminids, except GEM13, has mean value $\sigma = 0.019 \pm 0.005\,\mathrm{s^2/km^2}$.

Beginning heights for faint video Geminids are according to Koten et al. (2004) mass-independent with mean value about 101 km. At the first sight, when we plot this dependency only for Geminids, this is not evident (Table 3.7). Only when we plot the dependency for all studied showers (chapter 3.7), approximate mass-independency appeares. Mean beginning height is 88.6 ± 4.8 km. Terminal heights then decrease with increasing initial masses. No dependency between beginning height and distance from the nearest station was found for the 2006 Geminids.

An idea that Geminids changed their physical properties due to the close

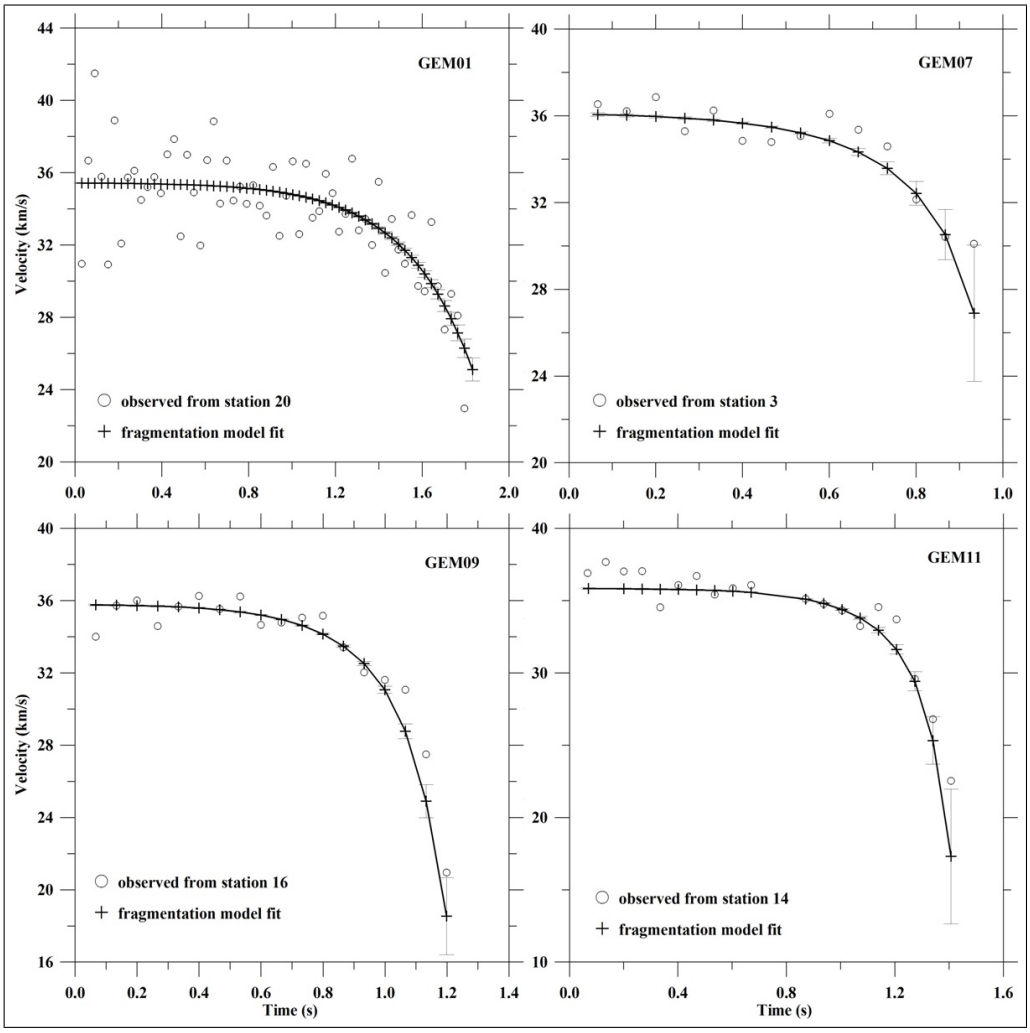

Figure 3.7: Observed deceleration and gross-fragmentation fit for the 2006 Geminids GEM01, GEM07, GEM09 and GEM11.

approach to the Sun and are similar to solid asteroidal bodies more than to weak and fragile cometary ones (Wetherill, 1986) can be, most probably, confirmed based on their atmospheric behaviour. In presented set of 13 Geminids, six are of type II, five of type I, and two of type IIIA (soft cometary material) (Table 3.7). The two IIIA meteors are GEM03 and GEM10 and have the shortest atmospheric trajectory among studied Geminids. This fact could decrease the precision in determination of their PE parameters, which are less convincing therefor.

3.2.3 Radiant and orbit

According to IAU MDC web pages the radiant position is 113.8°, 32.4°. On the basis of five of the most reliable fireballs from the second night (02, 07, 11,

Table 3.9: Radiants and orbital elements (J2000.0) of the 2006 Geminid fireballs. (α_G, δ_G) is the geocentric radiant, V_G is geocentric mean velocity without atmospheric drag (not mesurable on our records) and T_J is Tisserand's parameter. Also mean orbit from all the 13 fireballs (V_G is determined only from the most accurate fireballs – see text) and data for the parent body for epoch 2005-08-18 taken from Jenniskens (2006) are presented. Standard deviations for each entry are shown below.

Meteor No.	α_G (deg)	δ_G (deg)	V_G (km/s)	a (AU)	e	q (AU)	ω (deg)	Ω (deg)	i (deg)	T_J
GEM01	113.31	31.80	33.87	1.309	0.8909	0.1428	324.54	261.95583	21.87	4.40
	1	1	2	2	3	2	2	1	4	
GEM02	114.068	32.145	33.98	1.314	0.8908	0.1436	324.39	262.46194	22.91	4.38
	9	9	7	6	8	4	1	1	9	
GEM03	114.4	32.3	33.5	1.27	0.884	0.147	324.3	262.68099	22.8	4.52
	4	3	2	2	3	4	6	7	7	
GEM04	113.0	31.7	34.4	1.41	0.897	0.146	323.3	262.59278	21.6	4.12
	6	5	2	4	3	6	1.0	12	1.1	
GEM05	114.15	32.01	34.3	1.35	0.895	0.142	324.3	262.69330	23.0	4.27
	12	10	2	2	3	2	2	3	3	
GEM06	114.7	32.1	33.6	1.27	0.886	0.144	324.7	262.70168	22.7	4.52
	5	4	2	3	3	4	7	8	8	
GEM07	114.17	32.09	34.24	1.345	0.894	0.1428	324.21	262.71619	23.05	4.28
	6	5	9	8	1	8	10	2	15	
GEM08	114.61	31.6	33.7	1.27	0.889	0.141	325.1	262.72501	22.0	4.52
	3	2	2	1	2	2	2	4	4	
GEM09	113.4	32.2	34.01	1.37	0.8901	0.151	323.0	262.78586	22.2	4.23
	2	2	5	1	8	2	3	4	3	
GEM10	114.26	31.65	33.9	1.31	0.89	0.143	324.5	262.79925	21.9	4.40
	12	8	1.1	9	1	8	4	15	1.4	
GEM11	114.23	32.13	34.09	1.336	0.8916	0.1448	324.05	262.81415	22.90	4.32
	1	1	5	4	6	4	2	1	7	
GEM12	113.976	32.071	34.83	1.416	0.9006	0.1408	323.96	262.82451	23.50	4.09
	7	10	7	6	8	5	2	1	9	
GEM13	114.43	32.04	34.66	1.381	0.8987	0.1398	324.35	262.94322	23.55	4.18
	6	3	5	6	6	6	9	1	11	
mean orbit			34.1	1.33	0.892	0.144	324.2	262.7	22.6	4.33
			4	5	5	3	6	2	6	
3200 Phaethon			33.92	1.271	0.890	0.140	325.246	262.495	24.186	4.51

12 and 13), the radiant position is 113.5 ± 0.2 deg, 32.20 ± 0.03 deg (Figure 3.8). Values of radiant position and geocentric velocity are listed in Table 3.9 and well correspond to long-term values. Mean geocentric velocity v_G = 34.1 ± 0.4 km/s is determined from all 13 fireballs.

Orbital elements of the 2006 Geminids are listed in Table 3.9. All heliocentric orbits have semimajor axes larger or equal to that of the parent body 3200 Phaeton, but the perihelion distances and eccentricities are almost identical. It indicates that meteoroids were released from the parent body near perihelion into outer part of its orbit. The same manner of ejection of Geminids also was mentioned by Jenniskens (2006) (Figure 3.9). Mean orbit determined from all 13 fireballs has elements a = 1.33 ± 0.05 AU, e = 0.892 ± 0.005, q = 0.144 ± 0.003 AU, ω = 324.2 ± 0.6 deg, Ω = 262.7 ± 0.2 deg, i = 22.6 ± 0.6 deg. When we do not include GEM01 the resulting node remains the same (262.73 ± 0.12 deg). The mean orbit agree with mean orbit based on 38 photographic orbits from IAU MDC published by Gajdoš and Porubčan (2004).

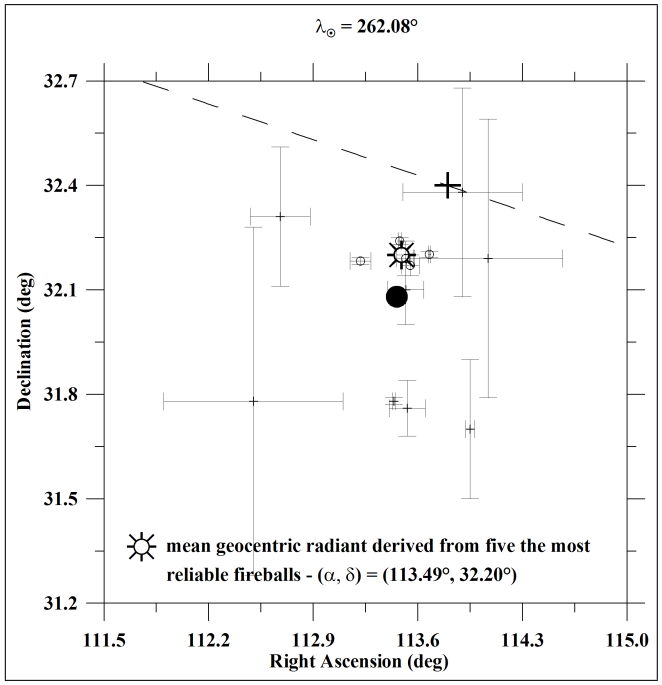

Figure 3.8: Geocentric radiants of the 2006 Geminids for solar longitude 262.08°. Mean radiant was determined from the five of the most reliable fireballs, here denoted by small cyrcles. Black dot is the mean radiant computed from all the 13 meteors and the dashed line is radiant motion according to IAU MDC web pages – radiant for $\lambda = 262.08°$ is denoted by bold cross.

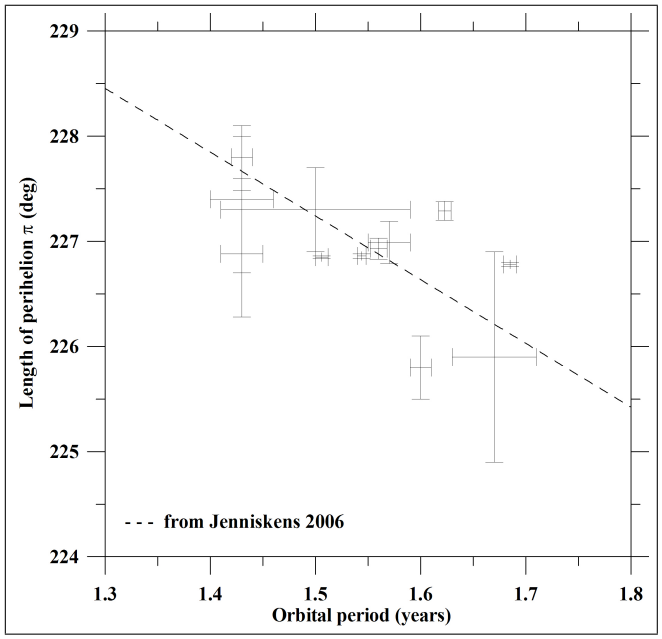

Figure 3.9: Dependency of length of perihelion on orbital period of the 2006 Geminids. The dashed line is taken from Jenniskens (2006).

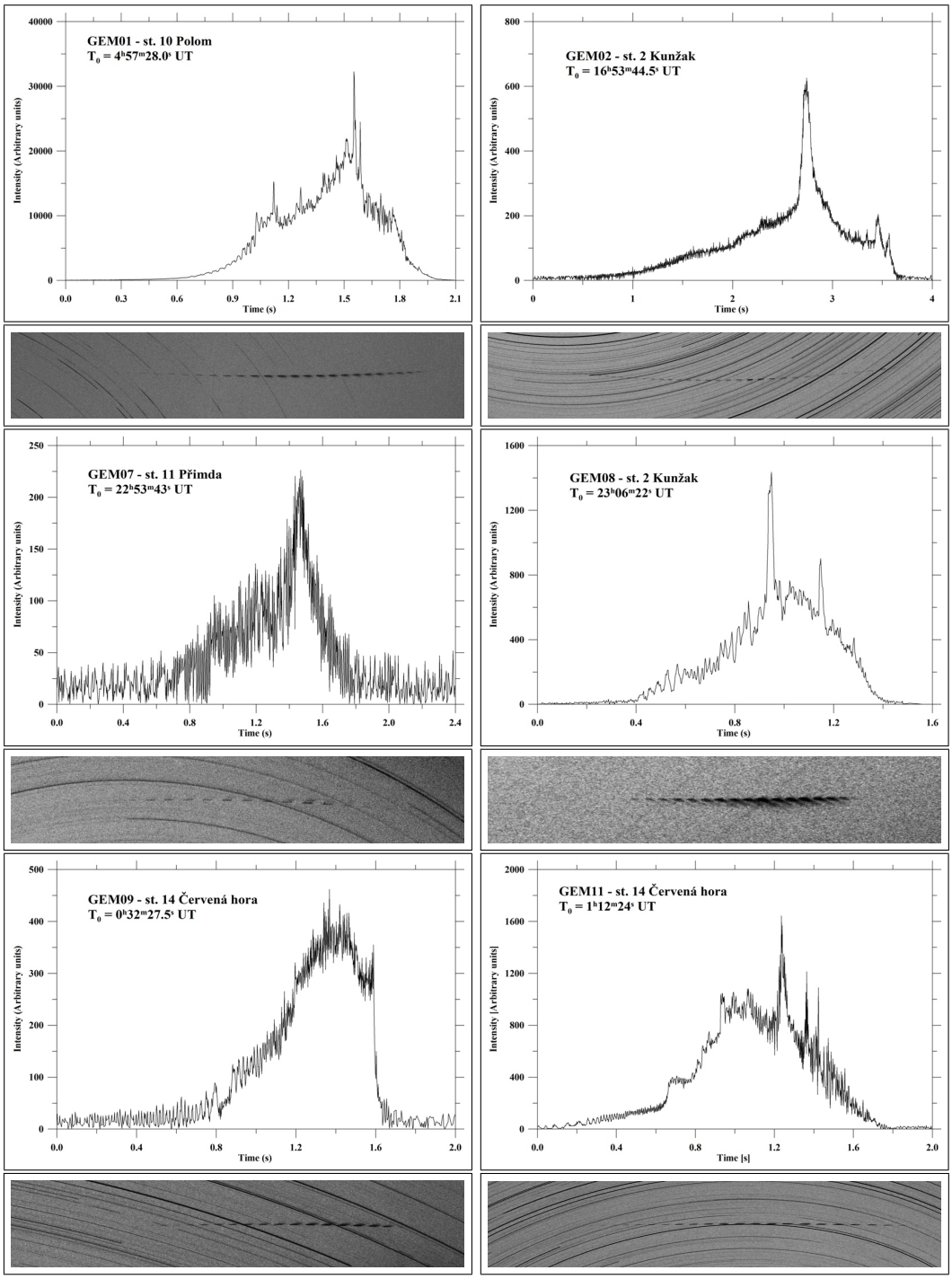

Figure 3.10: Light curves from AFO's brightness sensors and images of the 2006 Geminid fireballs from all-sky cameras. The images from fixed cameras display startrails and interruptions of the meteors caused by a rotating shutter (15 breaks/second). All fireballs flew from left to right in the images.

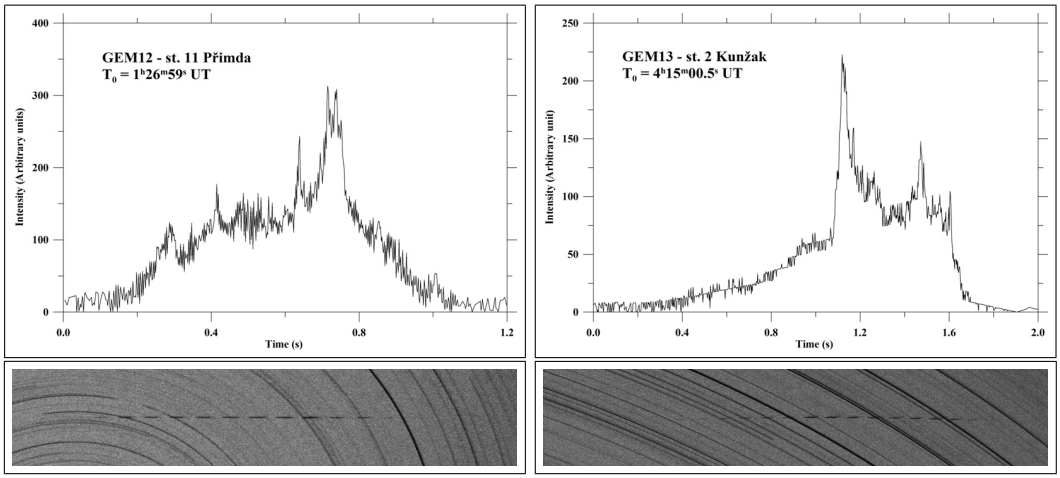

Figure 3.10 continued

3.3 α-Capricornids

The α-Capricornid meteor shower is a typical representative of ecliptical showers, being rich in bright meteors (Dubietis and Artl, 2004). For the first time, it was mentioned in 1871 by N. de Konkoly in Hungary, who determined the radiant at $\alpha = 307°$ and δ = -4° (Kronk, 1987). The α-Capricornids are active in the period July 19 until August 18 ($\lambda_\odot = 116°$–$146°$) with the maximum around August 1 (at $\lambda_\odot = 128°$). The position of the radiant is given by α = 306.2 + 0.538 ($\lambda_\odot$ - 128.0) and δ = -8.4 + 0.243 ($\lambda_\odot$ - 128.0). There is the twin shower of α-Capricornids in the daytime on January 20 ($\lambda_\odot = 299°$), it is only a few days wide with $\alpha = 306°$, δ = -30° and v_g = 22 km/s (Jenniskens, 2006).

The parent body is 169P/NEAT (Jenniskens, 2006). Next probable parent body may be 45P/Honda-Mrkos-Pajdusakova, for the first time proposed by Wright (1956), which is together with the α-Capricornids under large effects of perturbations of Jupiter. Other suggested parent objects are 72P/Denning-Fujikawa, 141P/Machholz 2, Comet 1457 L1 and minor planets (2101) Adonis and (9162) 1987 OA (Hasegawa, 2001). On the basis of study of dynamics of meteor streams (gravitational action exclusively) Neslušan (1999) proposed 14P/Wolf and D/1892 T1 as another probable parent bodies.

3.3.1 Observation and atmospheric behavior

In 2006, between July 28 and August 3 (in the period only 2 stations operated), five α-Capricornid fireballs were recorded by the Australian Desert Network. According to their atmospheric behavior, all these meteors belong to the weakest component of interplanetary matter. Based on their atmospheric trajectories and PE criterion, four of them belong to the type IIIB, CAP02 is a border type IIIA/IIIB. Except CAP05, which has flare in the middle of its trajectory, all other meteors have expressive terminal flare (Figure 3.12). Heights of these flares are in the range from 76 to 79 km for type IIIB.

Table 3.10: Atmospheric trajectories of the 2006 α-Capricornids. H is the height above sea level, L_{obs} is the length of observed trajectory. The subscript "B" denotes values at the beginning point of the atmospheric trajectory, the subscript "E" at the end point. N is the number of stations where the fireball was photographed. Standard deviations for each entry are shown below.

Meteor No.	N	Date	Time (UT)	H_B (km)	H_E (km)	L_{obs} (km)	Duration (s)
CAP01	2	28.7.	14:18:08	95.80	77.02	21.01	0.76
				10	1		
CAP02	2	28.7.	15:46:10	77.24	65.21	12.98	0.52
				2	2		
CAP03	2	29.7.	12:09:26	84.02	79.57	6.50	0.24
				2	2		
CAP04	2	29.7.	16:37:22	92.81	74.10	20.70	0.81
				1	1		
CAP05	2	3.8.	12:40:45	92.48	79.88	16.59	0.57
				1	2		

Table 3.11: Physical data on the 2006 α-Capricornid fireballs. ZD_E is the zenit distance of the radiant at the end point of the atmospheric trajectory, v_∞ is the initial velocity, M_{max} is the maximum absolute magnitude, m_{inf} is the initial photometric mass, PE is the coefficient that describes the empirical end height criterion and designates the type of fireball (Ceplecha and McCrosky, 1976). Standard deviations for each entry are shown below.

Meteor No.	ZD_E (deg)	v_∞ (km/s)	M_{max}	m_{inf} (g)	PE	Type
CAP01	26.69	24.63	-6.4	21	-5.89	IIIB
	5	8				
CAP02	22.0	24.1	-9.5	330	-5.68	IIIA/B
	7	2				
CAP03	46.8	24.69	-8.2	66	-6.14	IIIB
	4	9				
CAP04	25.38	25.39	-8.4	120	-5.99	IIIB
	3	4				
CAP05	41.0	25.2	-8.6	130	-6.34	IIIB
	3	3				

That corresponds to the range of mass from 20 to 120 g. Dynamic pressure, where the terminal explosion of the meteoroids occures, ranges from 0.013 to 0.025 MPa. The IIIA/IIIB type CAP02 has its terminal flare at 65.2 km corresponding to dynamic pressure 0.110 MPa (its first flare was at 73 km). CAP05 lost majority of its initial mass during the central flare, but as we can see at the enlargement of the all-sky image (Figure 3.12), small remnant exploded in inexpressive terminal flare at the height of 79.8 km (pressure 0.012 MPa). This results in the fact that all noted meteoroids are very similar to each other in their composition and course of ablation. No conclusive deceleration was observed among these fireballs, a suggestion of deceleration is in the end of CAP04.

3.3.2 Light curves

Some similarities also are evident in course of some light curves. CAP02 and CAP03 have almost the same course of radiation, even if they belong to different fireball types, have different initial masses and inclination to the surface. The heights of their first flares differ by 10 km and terminal flares by 15 km. For the first sight diverse light curve of CAP05 has almost the same course being compared to this pair. Heights of flares correspond to heights of flares of CAP03, both have similar inclination to the surface and first flares differ from one another by only 1 km. Very similar flares has also CAP04 - wider first one and narrow terminal - but with some bursts in addition in between of them. From the light curves we can conclude that these weak and fragile cometary meteoroids disintegrated in the Earth's atmosphere firstly into bigger pieces and in the end of their trajectory to high number of smaller pieces, which ablated and evaporated very quickly. The only one exception is CAP01, which increased its luminosity gradually without bursts until narrow terminal flare.

Table 3.12: Radiants and orbital elements (J2000.0) of the 2006 α-Capricornid fireballs. (α_G, δ_G) is the geocentric radiant, V_G is geocentric mean velocity without atmospheric drag (not mesurable on our records) and T_J is Tisserand's parameter. The mean orbit and data for the parent comet for epoch 2005-09-18 taken from Jenniskens (2006) are presented. Standard deviations for each entry are shown below.

Meteor No.	α_G (deg)	δ_G (deg)	V_G (km/s)	a (AU)	e	q (AU)	ω (deg)	Ω (deg)	i (deg)	T_J
CAP01	305.54	-8.14	21.85	2.15	0.729	0.582	270.8	125.29347	8.14	3.29
	5	5	9	2	3	1	1	3	5	
CAP02	304.4	-9.3	21.4	2.20	0.726	0.601	268	125.35248	7.2	3.25
	8	7	2	10	10	9	1	37	5	
CAP03	304.8	-8.3	22.05	2.40	0.751	0.598	267.6	126.16414	8.0	3.06
	3	6	10	6	5	4	6	26	5	
CAP04	305.48	-9.49	22.95	2.68	0.782	0.5837	268.20	126.34243	7.42	2.89
	4	4	5	2	2	7	7	2	3	
CAP05	307.8	-8.3	22.3	2.83	0.783	0.614	264.2	130.96793	7.5	2.75
	3	3	4	17	14	4	5	13	2	
mean			22.1	2.45	0.75	0.596	268	127	7.65	3.02
orbit			6	30	3	13	2	2	40	
169P/NEAT			22.21	2.603	0.768	0.605	265.952	128.784	7.622	2.90

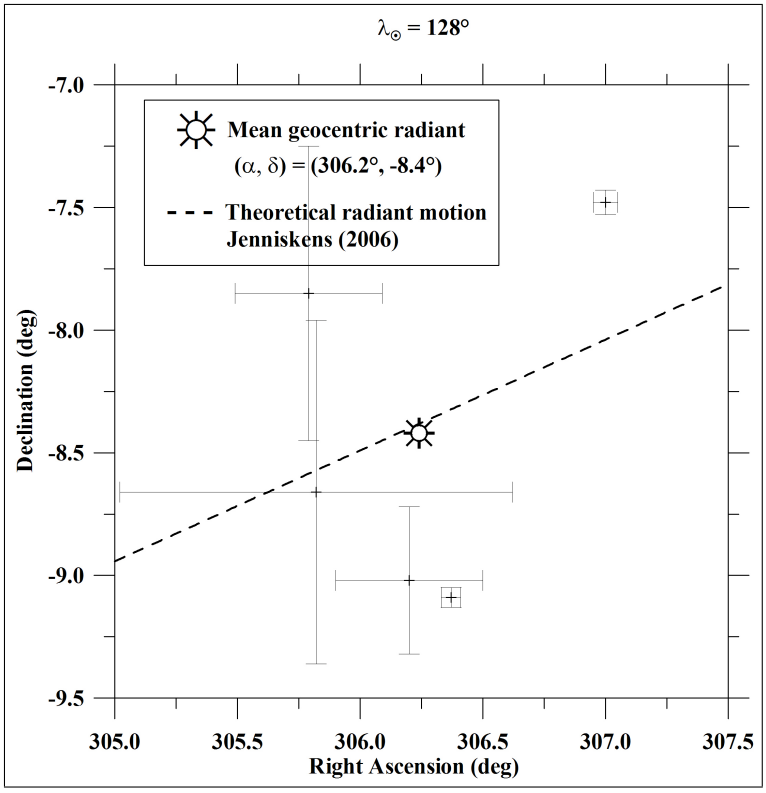

Figure 3.11: Geocentric radiants of the 2006 α-Capricornids for solar longitude 128°. The dashed line is the radiant motion according to Jenniskens (2006) – radiant for $\lambda = 128°$ is identical to the mean observed one.

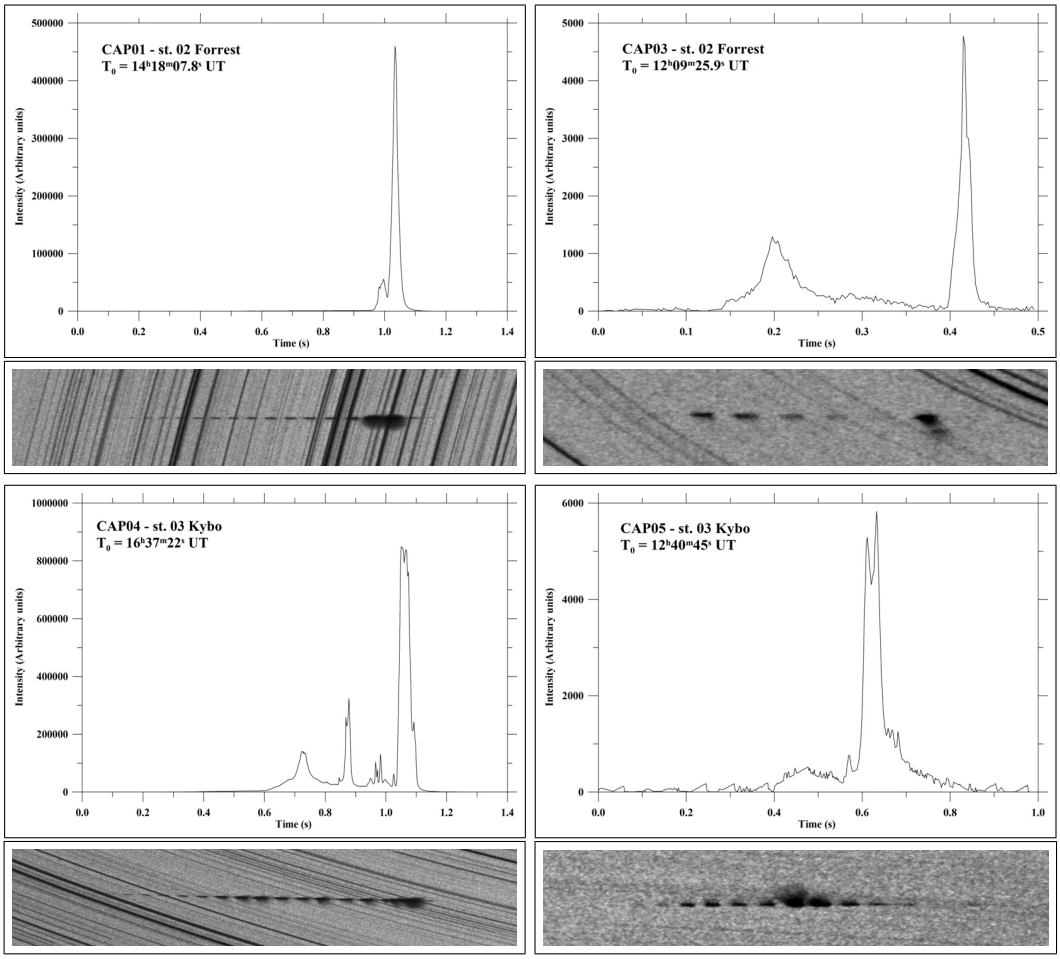

Figure 3.12: Light curves from AFO's brightness sensors and images of the 2006 α-Capricornid fireballs from all-sky cameras. The images from fixed cameras display star-trails and interruptions of the meteors caused by a rotating shutter (15 breaks/second). All fireballs flew from left to right in the images.

3.3.3 Radiant and orbit

The 2006 α-Capricornids radiated from not very compact geocentric radiant (Figure 3.11) with $\alpha = 306.2 \pm 0.5$ deg and $\delta =$ -8.4 $\pm$ 0.7 deg and with mean geocentric velocity $v_G = 22.1 \pm 0.6$ km/s. Position of the radiant is calculated for the solar longitude 128°. Heliocentric orbits have very different arguments of perihelion – the different orbital ellipses turn in the space took place, likely due to Jupiter gravitational action (mean aphelion is 4.3 AU). Different are also semimajor axes and eccentricities that increase with solar longitude. Mean orbit is a = 2.5 $\pm$ 0.3 AU, e = 0.75 $\pm$ 0.03, q = 0.60 $\pm$ 0.01 AU, $\omega = 268 \pm 2$ and i = 7.7 $\pm$ 0.4 deg (Table 3.12).

3.4 Southern δ-Aquariids

The Southern δ-Aquariid (SDA) meteor shower, member of the Machholz complex, is an annual shower with a peak visual hourly rate of 15 - 20 meteors (Zvolánková, 1992; McBeath, 2005) and a maximum generally occurring on July 28. SDA were detected for the first time as a minor shower in 1849 by Julius Schmidt (Jenniskens, 2006) and the activity of this shower was recorded first in 1870 by Captain G. L. Tupman (Tupman, 1873). From precise photographic records Jopek et al. (1999) have found 11 SDA meteors and determined elongated mean heliocentric orbit with extremely low value of perihelion distance, q = 0.08 AU (Neslušan and Welch (2001) determined q = 0.09 ± 0.02 AU), and geocentric velocity 41 km/s.

The perihelion distance increases with increasing node by +0.0041 AU/° and eccentricity decreases (-0.0017/°) for a constant semimajor axis. The argument of perihelion increases by +0.29°/° and the inclination decreases by -0.25°/°, but is less correlated. SDA have a relatively narrow dispersion in declination and a distinct decrease in speed as a function of right ascension (Jenniskens, 2006). From precisely reduced photographic meteors Jacchia et al. (1967) have found that SDA are efficiently decelerated in the Earth's atmosphere. The position of the radiant is given by α = 341.6 + 0.73 ($\lambda_\odot$ - 125.6) and δ = -15.9 + 0.26 ($\lambda_\odot$ - 125.6) (IAU MDC web pages).

3.4.1 Observation and atmospheric behavior

In 2006, between July 29 and August 4 (in the period only 2 stations operated), three Southern δ-Aquariid fireballs were recorded by the Australian Desert Network. Observed fireballs belong to bodies of probable soft asteroidal or solid cometary origin. On the basis of atmospheric trajectories and PE criterion belong SDA01 and SDA02 to type II, SDA03 is IIIA. According to definition, SDA01 is not valid fireball at all. Its absolute brightnes in the maximum is only -3 mag and photographic trajectory is only 9 km long, though all its parameters were determined reliably. SDA01 and SDA02 have the same height of the beginning 88.3 km and also "flary-like" course of light curve. That indicates

Table 3.13: Atmospheric trajectories of the 2006 Southern δ-Aquariids. H is the height above sea level, L_{obs} is the length of observed trajectory. The subscript "B" denotes values at the beginning point of the atmospheric trajectory, the subscript "E" at the end point. N is the number of stations where the fireball was photographed. Standard deviations for each entry are shown below.

Meteor No.	N	Date	Time (UT)	H_B (km)	H_E (km)	L_{obs} (km)	Duration (s)
SDA01	2	29.7.	16:23:08	88.33	79.95	8.70	0.19
				1	1		
SDA02	2	1.8.	17:23:34	88.28	62.61	26.76	0.62
				1	1		
SDA03	2	4.8.	17:38:27	84.36	56.20	29.48	0.71
				2	3		

Table 3.14: Physical data on the 2006 Southern δ-Aquariid fireballs. ZD_E is the zenit distance of the radiant at the end point of the atmospheric trajectory, v_∞ is the initial velocity, M_{max} is the maximum absolute magnitude, m_{inf} is the initial photometric mass, PE is the coefficient that describes the empirical end height criterion and designates the type of fireball (Ceplecha and McCrosky, 1976). Standard deviations for each entry are shown below.

Meteor No.	ZD_E (deg)	v_∞ (km/s)	M_{max}	m_{inf} (g)	PE	Type
SDA01	22.5 1	43.7 4	-3.0	0.25	-4.95	II
SDA02	16.39 4	42.9 2	-9.3	78	-4.93	II
SDA03	17.3 2	41.5 2	-13.3	5000	-5.37	IIIA

very similar composition of these meteoroids, which also confirms the fact that terminal heights, inclinations to the surface and initial velocities and masses differ from one another in the way, that their combination of PE criterion leads to the same result (Table 3.14).

3.4.2 Light curves

Light curves show that course of radiation differ between type II and IIIA fireballs (Figure 3.17). SDA02 (type II) has gradual increase of brightness, about maximum, some short flares occure and towards the end fades. Maximum lies approximately in 3/4 of the trajectory, which corresponds to single-body model without deceleration. Completely different is the light curve of SDA03. Its initial mass was about 5 kg and course of the light curve is something like mirrored single-body profile. Directly at the beginning of the trajectory rapid

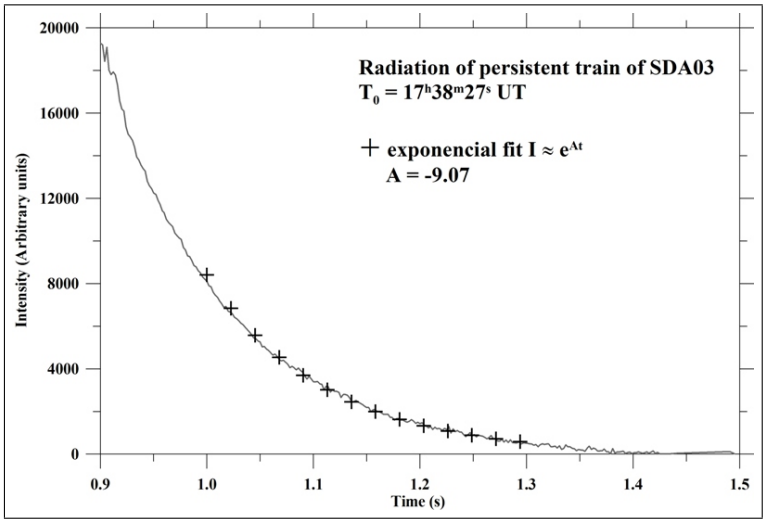

Figure 3.13: Exponential dependency of intensity on time for the 2006 Southern δ-Aquariid persistent train of SDA03. Absolute brightness of the train in time t = 1 s is -4 to -5 mag.

Table 3.15: Radiants and orbital elements (J2000.0) of the 2006 Southern δ-Aquariid fireballs. (α_G, δ_G) is the geocentric radiant, V_G is geocentric mean velocity without atmospheric drag (not mesurable on our records) and T_J is Tisserand's parameter. Also mean orbit from all the 3 fireballs and data for the Marsden Sungrazers for epoch 2004 taken from Jenniskens (2006) are presented. Standard deviations for each entry are shown below.

Meteor No.	α_G (deg)	δ_G (deg)	V_G (km/s)	a (AU)	e	q (AU)	ω (deg)	Ω (deg)	i (deg)	T_J
SDA01	339.4	-15.73	42.3	3.3	0.981	0.063	153.4	306.32687	27.7	1.85
	2	6	4	3	2	2	3	5	9	
SDA02	341.37	-16.10	41.4	3.29	0.9752	0.0816	149.61	309.23646	27.7	1.89
	6	6	2	14	14	11	14	2	4	
SDA03	343.3	-15.1	39.9	2.79	0.9661	0.095	147.7	312.11714	24.0	2.21
	2	2	2	11	16	2	4	4	6	
mean			41.2	3.1	0.974	0.08	150	309	26	1.99
orbit			1.2	3	8	2	3	3	2	
Marsden Sungrazers			43.00	3.265	0.985	0.048	156.881	303.268	26.94	1.84

increase of brightness takes place and after reaching the maximum fades out very slowly. The maximum is at the height of 76 km and in the light curve occures in 1/5 but on the image in 1/3 of the trajectory, which means that after the meteor disappearance, fading train stayed for about 0.3 s. According to the height, which it appeared in, likely it was an afterglow phase of persistent train. The decrease of its brightness can be described as exponential dependency of intensity on time $I \approx e^{At}$, where A = -9.07 (Figure 3.13). After the meteor disappearance the absolute brightness of the train was -4 to -5 mag, its total observed duration was 0.8 s and maximum absolute brightness about -10.7 mag (when we extrapolate into the time of the maximum of the light curve). The break-up of the meteoroid started at the height of 79 km, which corresponds to dynamic pressure 0.040 MPa and the beginning of the train, in the maximum of brightness at 76 km the pressure was 0.065 MPa. These two values of pressure define the strenght of the material. Total length of the train (from photograph) was about 20 km and bottom limit of the train was at about 65 km. Very probably this fireball produced also particulate wake, which consisted of small particles released from the meteoroid during the fragmentation in the beginning of its atmospheric trajectory. Maybe the observed length of the train (here ascribed to the persistent train) was partly caused by the wake.

SDA02 has in the part of maximum of its light curve very similar train – wide and diffuse. A wake or train were likely presented here, but the train disappeared (became faint) before the end of the fireball, and thus course of its brightness can not be determined from the AFO's light curve. On the basis of photograph from station Kybo, where three breaks are merged, this train was at heights from 72 to 68 km and its length was about 5 km.

3.4.3 Radiant and orbit

Elements of heliocentric orbits of Southern δ-Aquariids are dependent on each other. It is necessary to say that all presented dependencies are based only on

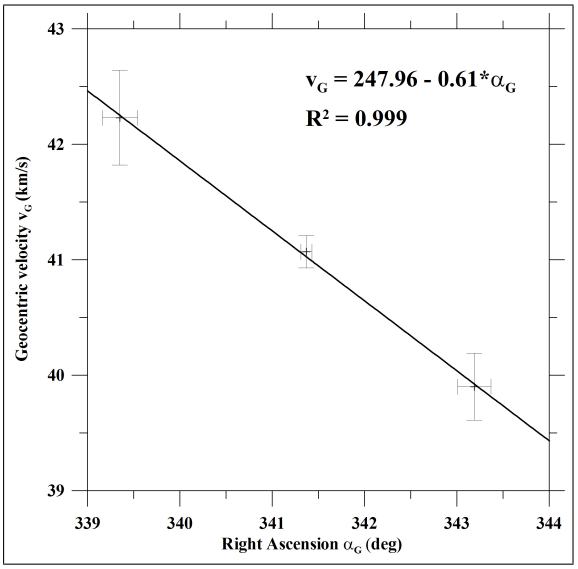

Figure 3.14: Linear dependency of geocentric velocity on right ascension of geocentric radiant for the 2006 Southern δ-Aquariids. R^2 is the coefficient of determination describing accuracy of the fit.

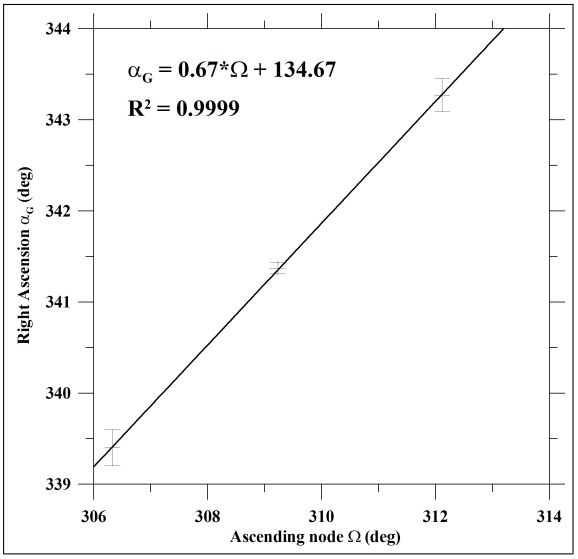

Figure 3.15: Linear dependency of right ascension of geocentric radiant on ascending node for the 2006 Southern δ-Aquariids. R^2 is the coefficient of determination describing accuracy of the fit.

three orbits, nevertheless, all the fits are very accurate (see individual Figures). The argument of perihelion decreases (-1.04 °/°) as a linear function of node, contrary to the dependency presented by Jenniskens (2006). Other dependencys agree. The perihelion distance increas with increasing node by 0.0057 AU/° and eccentricity changes by -0.0026 /°. Next dependency expreses geocentric velocity that decrease with increasing right ascension of geocentric radiant by

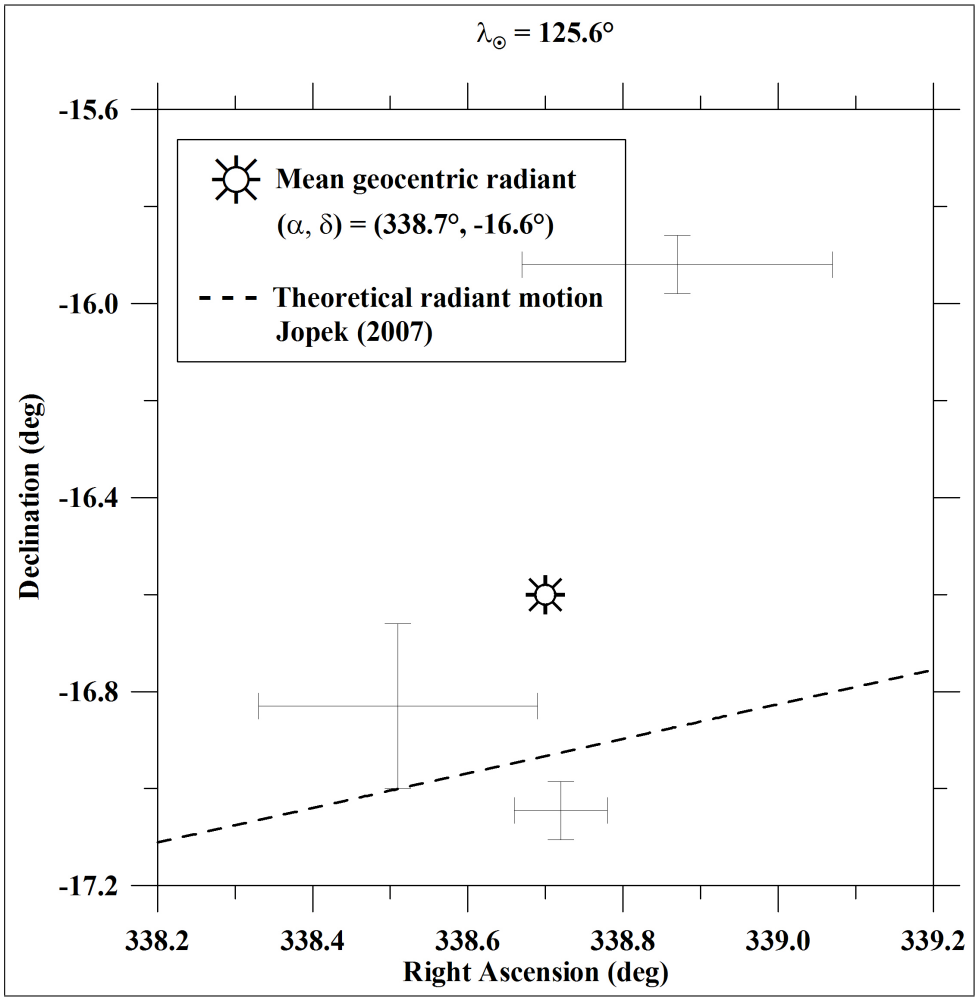

Figure 3.16: Geocentric radiants of the 2006 Southern δ-Aquariids for solar longitude 125.6°. The dashed line is radiant motion according to the IAU MDC web pages. Radiant for λ = 125.6° is outside the limits of the graph and its position is α = 341.6°, δ = -15.9°.

0.61 km s^{-1}/° (Figure 3.14). Change of declination of the radiant with ascending node is not evident but linear progress of right ascension is (Figure 3.15) and differs from that presented on the IAU MDC web pages. From measurements of these three fireballs holds α_G = 339.42 + 0.67($\lambda_\odot$ – 125.6), while the IAU MDC web pages give α_G = 341.60 + 0.73($\lambda_\odot$ - 125.6) and δ_G = -15.90 + 0.26($\lambda_\odot$ - 125.6), which corresponds to the radiant α = 341.6°, δ = -15.9° for solar longitude 125.6°. Mean value of the observed geocentric radiant (Figure 3.16) is α = 338.7 ± 0.2 deg, δ = -16.6 ± 0.6 deg (radiant motion taken from IAU MDC web pages) and geocentric velocity is function of node. Mean values of both radiants differ by 3°.

Mean values of individual elements give the mean orbit with a = 3.1 ± 0.3 AU, e = 0.974 ± 0.008, q = 0.08 ± 0.02 AU, ω = 150 ± 3 deg and i = 26 ± 2 deg. Due to time dependency it seems to be better to present equations of

individual elements as functions of solar longitude or longitude of the ascending node.

$\mathrm{e} = 0.975 - 0.0026(\Omega - 305.6)$
$\mathrm{q} = 0.062 + 0.0057(\Omega - 305.6)$ it corresponds to a $= \frac{q}{1-e} = 2.5\,\mathrm{AU}$
$\omega = 152.9 - 1.04(\Omega - 305.6)$
$\mathrm{v}_G = 41.89 - 0.41(\Omega - 305.6)$
$\alpha_G = 339.42 + 0.67(\Omega - 305.6)$

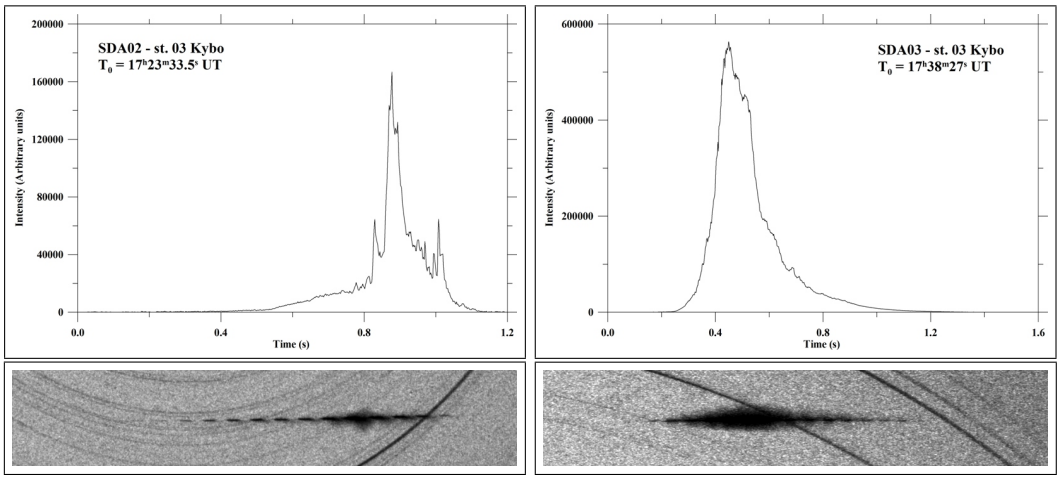

Figure 3.17: Light curves from AFO's brightness sensors and images of the 2006 Southern δ-Aquariid fireballs from all-sky cameras. The images from fixed cameras display startrails and interruptions of the meteors caused by a rotating shutter (15 breaks/second). Both fireballs flew from left to right in the images.

3.5 Leonids

Leonids have one of the most variable activities among major meteor showers. The maximum of their activity occurs around November 18. Their activity increases approximately every 33 years with the return of their parent comet 55 P/Tempel-Tuttle to perihelion. The stream consist of a ribbon-like cloud of particles spread along the comet's orbit, which is called the Leonid Filament, and of smaller dust trails released from the comet in past returns. The Filament is the result of accumulation of debris in orbital resonances over the past 1000 years (Asher et al., 1999; Jenniskens and Betlem, 2000); dust trails are responsible for occasional meteor storms. The last return of the comet to perihelion occurred in February 1998, and in the following several years, meteor outbursts with a Zenithal Hourly Rate (ZHR) of hundreds to thousands of meteors were observed (annual Leonids have ZHR about 13). Over the last decade or so, the Earth encountered the following dust trails: in 1998 the 1333 dust trail (the Fireball Night on November 16/17 was according to Asher et al. (1999) caused by the 1333 dust trail, according to Jenniskens (2006) rather by the Filament); in 1999 the 1899 and 1866 trails; in 2000 the 1932, 1733 and 1866 trails; in 2001 the 1767 and 1699 trails; in 2002 the 1767 and 1866 trails; and in 2006 the 1932 trail (McNaught and Asher, 1999a).

Bright Leonid fireballs often leave persistent trains visible few minutes after the fireball passage (Jenniskens, 2006).

Majority of this section is published in Shrbený and Spurný (2009).

3.5.1 Observation and light curves

In 1999, 2000, 2001, 2002, and 2006 the Earth's orbit intersected a few young dust trails, and the Leonid Filament. Multi-station fireballs were photographed in 1999 during two nights (15/16 and 18/19) in the Czech part of the EN, and two nights (17/18 and 18/19) in Spain (stations Punto Alto and Casa Nueva) by the same imaging system during the Dutch-Czech Leonid expedition. 13 double-station Leonids were photographed during the night of November 17/18, which covered the encounter with the 1899 dust trail. The year 2000 was adversely affected by weather, which resulted in no multi-station fireballs from the Czech part of the EN. In 2001, fireballs were photographed over two nights (14/15 and 17/18) in the Czech part of the EN. Two multi-station Leonids were recorded during the first night, and 20 fireballs during the second night. 2002 also was affected by bad weather conditions, and 10 multi-station fireballs were recorded above a small part of the Czech network during the night of November 18/19. Five multi-station Leonids were photographed in 2006 on November 15/16, 17/18 and 18/19.

Altogether, 54 fireballs were long and bright enough to be recorded photographically from more than one station, so that we can precisely determine all important parameters describing their atmospheric trajectories and basic physical properties. Unfortunately, only 34 fireballs have a precise time of passage,

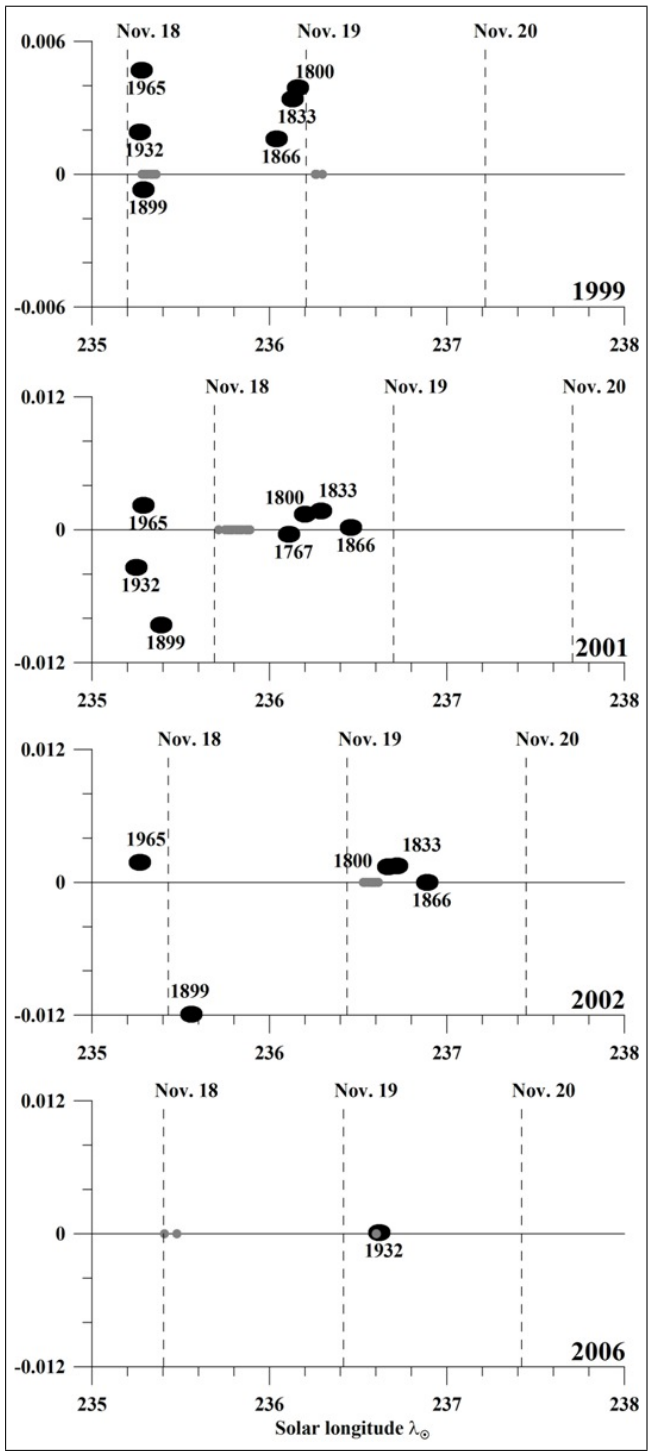

Figure 3.18: Positions of individual dust trails (black ellipses – not real sizes) in years as presented by McNaught and Asher (1999a). Vertical axes express distance $r_D - r_E$, where r_D is heliocentric distance of the dust trail's descending node and r_E heliocentric distance of the Earth at the same longitude, both in AU. Solar longitudes are expressed in J2000.0. Gray dots are positions of observed fireballs.

and thus only 34 heliocentric orbits could be reliably computed. All presented Leonid fireballs were measured and processed using our standard procedures (Borovička et al., 1996; Ceplecha, 1987). The Fishscan software, created by Dr. Jiří Borovička, serves for positional and photometric measuring of fireballs on scanned copies of films. Therefore, all presented Leonid fireballs, besides precise atmospheric trajectories, also have precise Fishscan photometry.

3.5.2 Dust trails or Filament

Positions of dust trails (black ellipses – not real sizes), as published by McNaught and Asher (1999a), and positions of observed fireballs (gray dots, solar longitude corresponding to the time of the fireball passage) are plotted in Figure 3.18. The vertical axes express the distance $r_D - r_E$, where r_D is the heliocentric distance of the dust trail's descending node, and r_E is the heliocentric distance of the Earth at the same longitude, both in AU. Solar longitudes are expressed in J2000.0.

According to positions of dust trails in 1999, observed meteor rates (Jenniskens, 2006), and times of individual meteors (Tables 3.16, 3.17 and 3.18), LEO02 to LEO14 most likely belong to the 1899 dust trail, and LEO15 to LEO17 probably belong to the 1866 trail, where activity lasted until a solar longitude of 236.4°, when the Filament began to be more dominant (Jenniskens, 2006). LEO01 belongs to the Filament. In 2001 it is hard to decide between trail or Filament. Meteors recorded on November 18 can belong to the 1767 dust trail, but its activity started approximately at $\lambda_\odot = 235.9°$ (de la Peña et al., 2008; Gural et al., 2004; Jenniskens, 2006) and observed fireballs LEO20 to LEO39 correspond to $\lambda_\odot$ between 235.71° and 235.89°. LEO18 and LEO19 most likely belong to the Filament. Leonids recorded in 2002 most likely belong (according to Figure 3.18 and observed meteor rates (Jenniskens, 2006)) to the 1800 or 1833 dust trails, however, this year was also affected by bad weather and only atmospheric trajectories are known. LEO54, photographed in 2006, probably belongs to the 1932 dust trail; the others most likely belong to the Filament.

3.5.3 Heights of atmospheric trajectories

All important parameters describing atmospheric trajectories are presented in Tables 3.16, 3.17, 3.18, 3.19 and 3.20. A very interesting result is the non-dependence of beginning heights on the initial photometric mass (Figure 3.19). The observed Leonid fireballs fulfill the same condition: beginning height, h_B, is equal to 111 ± 5 km for the range of photometric masses from 0.5×10^{-1} to 2.1×10^{3} g . The determination of the photometric masses depends very strongly on the luminous efficiency, τ, which is very difficult to derive for such fast meteors like the Leonids. For a mean initial velocity of 71.2 km/s a value for log τ = -11.84 (c.g.s. units with I = 1 for 0 stellar magnitude) was used (Ceplecha and McCrosky, 1976), which corresponds to 2.2% of the total kinetic

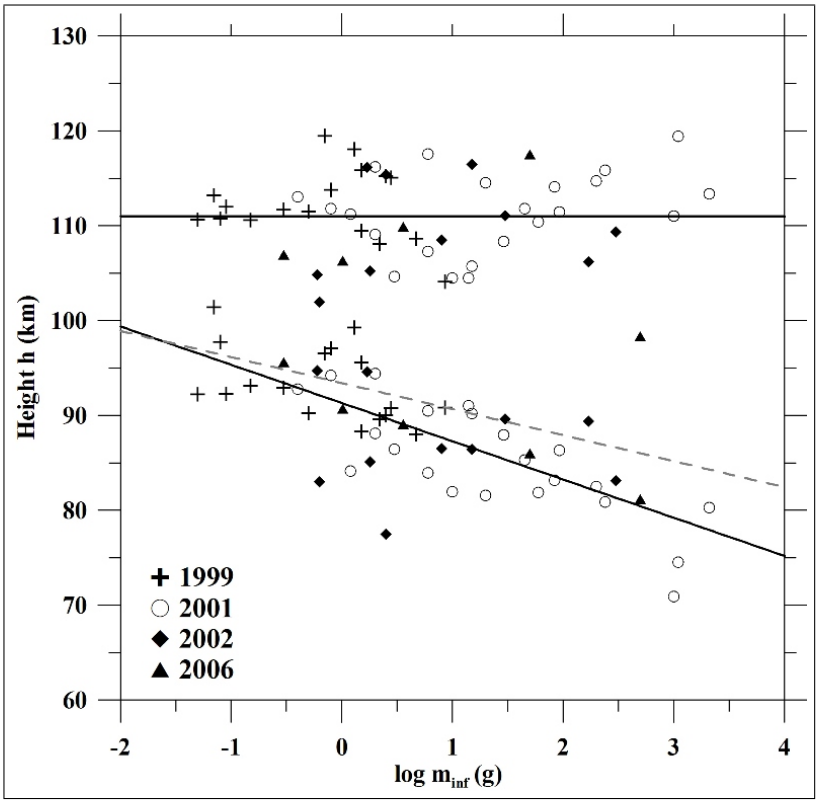

Figure 3.19: Dependencies of beginning and terminal height on initial photometric mass. The gray dashed line is the dependency for heights corresponding to the maximum dynamic pressure that was reached without fragmentation (more details in section 3.5.4).

energy of mass loss. If we used an alternative value for τ from ReVelle and Ceplecha (2001), which is dependent not only on velocity but also on mass, initial velocity, and bolide type (according to PE), we would derive an average value of 0.2%. This would lead to higher initial masses for the presented fireballs, but for consistency of the determination of the PE coefficient for all the fireballs in this paper we decided to keep the value of 2.2%. Other authors show an increasing dependency of beginning height on initial mass, but data are based on video observations (Jenniskens et al., 2008; Koten et al., 2004), or small cameras (Betlem et al., 2000), covering only a part of the sky and capable of detecting fainter meteors.

In our case the dependency is caused by the equipment used. The limiting apparent visual magnitude, which the meteor has to reach to be recorded on film by our all-sky camera, is about 0^m to -2^m (depends on angular velocity and observing conditions), and thus lower than the brightness of the actual beginning of the event. If we assume that all Leonids reach this limiting magnitude at some specific height, h_{lim}, then the fact that they are observed from different distances and with different slopes to the vertical would result in the spread of observed beginning heights around h_{lim}. This is exactly the

Table 3.16: Atmospheric trajectories of the 1999 Leonid fireballs with known time of meteor passage. H is the height above sea level, L_{obs} is the length of observed trajectory. The subscript "B" denotes values at the beginning of the atmospheric trajectory, the subscript "E" at the end point. N is the number of stations where the fireball was photographed. Values of individual entries are given with an accuracy of one or two last digits.

Meteor No.	N	Date	Time (UT)	H_B (km)	H_E (km)	L_{obs} (km)	Duration (s)
Year	1999						
LEO01	4	16.11.	4:46:23	111.50 1	90.26 2	24.16	0.34
LEO02	2	18.11.	1:54:18	118.07 1	99.28 2	36.81	0.52
LEO03	2	18.11.	2:08:14	110.76 5	97.75 3	25.95	0.37
LEO04	2	18.11.	2:19:27	115.84 1	95.58 1	37.51	0.53
LEO05	2	18.11.	2:22:13	113.78 5	97.11 5	31.07	0.44
LEO06	2	18.11.	2:22:48	113.19 2	101.40 4	21.20	0.30
LEO07	2	18.11.	2:37:29	115.24 2	90.00 2	42.92	0.61
LEO08	2	18.11.	2:39:30	119.46 3	96.54 3	38.12	0.54
LEO09	2	18.11.	3:04:35	110.64 6	92.24 3	28.02	0.40
LEO10	2	18.11.	3:07:30	108.64 6	88.02 6	31.67	0.46
LEO11	2	18.11.	3:09:55	112.01 2	92.26 2	29.48	0.42
LEO12	2	18.11.	3:25:27	109.47 1	88.32 1	29.55	0.42
LEO13	2	18.11.	3:46:48	108.06 3	89.59 3	24.84	0.35
LEO14	2	18.11.	3:48:51	110.61 1	93.12 1	22.62	0.32
LEO15	2	19.11.	1:09:55	104.09 3	90.82 3	41.38	0.59
LEO16	3	19.11.	1:20:22	115.07 2	90.81 2	41.65	0.58
LEO17	2	19.11.	2:07:32	111.71 4	92.92 2	27.14	0.38

observed dependency (Figure 3.19). It means that there exists a height h_{lim} (equal to 111 ± 5 km), where all Leonids reach an absolute magnitude of approximately -2^m.

Dependencies among initial photometric mass and the terminal height (black line), and the height of the maximum dynamic pressure (see explanation in section 3.5.4) (dashed gray line), are plotted in Figure 3.19. Both dependencies are decreasing functions of mass, which means that real terminal heights were not observed, but heights close to them. These fast cometary meteors often fragment at the end of the atmospheric trajectory into small particles that ablate very quickly, so the decrease of brightness is then faster than at the beginning of the meteor (this also holds for single-body solutions without fragmentation). The dependency of the maximum dynamic pressure shows that small meteoroids probably do not fragment and reach maximum dynamic pressure at their terminal height.

Table 3.17: Atmospheric trajectories of the 2001, and 2006 Leonid fireballs with known time of meteor passage. H is the height above sea level, L_{obs} is the length of observed trajectory. The subscript "B" denotes values at the beginning of the atmospheric trajectory, the subscript "E" at the end point. N is the number of stations where the fireball was photographed. Values of individual entries are given with an accuracy of one or two last digits.

Meteor No.	N	Date	Time (UT)	H_B (km)	H_E (km)	L_{obs} (km)	Duration (s)
Year	2001						
LEO18	3	15.11.	1:32:30	115.86 1	80.86 3	59.69	0.76
LEO19	5	15.11.	2:46:30	114.72 2	82.50 2	42.20	0.60
LEO20	3	18.11.	0:29:37	111.22 2	84.15 2	58.58	0.57
LEO21	4	18.11.	1:20:37	114.12 2	83.15 1	54.88	0.60
LEO22	5	18.11.	1:42:32	111.47 4	86.33 4	38.78	0.32
LEO23	4	18.11.	1:58:23	117.55 2	83.93 1	49.86	0.47
LEO24	2	18.11.	1:59:34	108.35 4	87.96 4	30.06	0.28
LEO25	5	18.11.	2:04:16	111.04 5	70.92 5	58.00	0.56
LEO26	4	18.11.	2:58:18	111.79 3	85.32 3	34.59	0.27
LEO27	3	18.11.	3:19:00	119.44 2	74.54 2	56.31	0.67
LEO28	2	18.11.	3:33:28	109.07 5	88.09 3	26.02	0.35
LEO29	4	18.11.	4:09:27	111.79 1	94.20 1	20.61	0.27
Year	2006						
LEO50	7	16.11.	0:56:07	117.52 2	85.99 1	58.05	0.81
LEO51	5	16.11.	3:46:21	98.35 5	81.18 5	19.52	0.25
LEO52	3	17.11.	23:58:30	106.33 1	90.71 1	41.59	0.57
LEO53	2	18.11.	1:40:00	106.94 1	95.63 1	17.82	0.24
LEO54	2	19.11.	4:23:34	109.91 2	89.06 2	24.38	0.33

3.5.4 Dynamic pressures and PE coefficients

The dependency of dynamic pressure ($p = \rho v^2$) on initial photometric mass is shown in Figure 3.20. The dynamic pressures are determined at heights corresponding either to maximum pressure along the atmospheric trajectory (meteors with smooth light curves without flares) or at the first flare (often corresponds to the terminal flare). These flares likely correspond to a fragmentation and thus to the approximate strength of the material. The values of these dynamic pressures are listed in Tables 3.19 and 3.20. Initial velocities were used to determine the dynamic pressures because the presented Leonids did not decelerate. There are only two exceptions – LEO02 and LEO04. These two Leonids, with a small inclination to the Earth's surface, likely experienced moderate deceleration, unfortunately not enough to determine a solution for the atmospheric motion (among others the ablation coefficient) using the gross-

Table 3.18: Atmospheric trajectories of the 2001 and 2002 Leonid fireballs with unknown time of meteor passage. Given time is an estimate based on approximate radiant position. H is the height above sea level, L_{obs} is the length of observed trajectory. The subscript "B" denotes values at the beginning of the atmospheric trajectory, the subscript "E" at the end point. N is the number of stations where the fireball was photographed. Values of individual entries are given with an accuracy of one or two last digits.

Meteor No.	N	Date	Time (UT)	H_B (km)	H_E (km)	L_{obs} (km)	Duration (s)	δ_G (deg)	V_G (km/s)
Year	2001								
LEO30	3	18.11.	2:08	107.27	90.47	23.90	0.27	21.62	70.62
				2	2			10	16
LEO31	4	18.11.	2:21	113.37	80.29	50.09	0.40	20.4	69.2
				8	8			7	3
LEO32	3	18.11.	2:49	105.74	90.19	20.60	0.27	21.6	67.4
				2	3			2	5
LEO33	3	18.11.	3:17	113.05	92.80	25.44	0.33	21.83	69.8
				1	1			5	2
LEO34	2	18.11.	3:37	104.64	86.5	21.98	0.27	21.5	66.5
				12	3			9	6
LEO35	2	18.11.	4:09	116.22	94.39	25.78	0.29	21.68	70.2
				2	2			9	7
LEO36	3	18.11.	4:22	110.39	81.88	32.18	0.33	21.9	73.0
				3	3			5	5
LEO37	3	18.11.	4:26	104.48	81.95	25.96	0.33	21.03	70.23
				1	1			4	12
LEO38	2	18.11.	4:34	104.49	91.04	15.37	0.11	21.75	70.4
				3	3			13	3
LEO39	4	18.11.	4:40	114.52	81.57	37.60	0.33	21.5	71.4
				4	4			1.3	6
Year	2002								
LEO40	2	19.11.	2:02	106.2	89.39	23.40	0.13	25	69.4
				1.1	6			5	2
LEO41	2	19.11.	2:17	116.16	94.61	30.34	0.20	21.71	70.43
				3	2			16	14
LEO42	2	19.11.	2:42	115.41	77.46	49.33	0.61	21.57	70.62
				1	1			2	8
LEO43	2	19.11.	2:46	108.50	86.52	28.23	0.41	21.51	70.63
				2	1			6	4
LEO44	2	19.11.	3:07	111.07	89.62	27.00	0.20	22.3	70.6
				5	4			2	3
LEO45	2	19.11.	3:14	105.23	85.09	25.07	0.22	20.6	70.2
				6	10			4	2
LEO46	2	19.11.	3:18	101.97	83.00	23.49	0.20	21.2	73.8
				10	10			4	8
LEO47	3	19.11.	3:25	109.34	83.12	32.28	0.29	21.9	70.3
				3	3			4	2
LEO48	2	19.11.	3:43	104.84	94.71	11.96	0.17	20.62	69.4
				1	1			14	5
LEO49	2	19.11.	4:03	116.49	86.45	35.18	0.29	21.1	70.93
				7	4			2	13

fragmentation model of Ceplecha et al. (1993). The model requires precisely measured values of heights and lengths for as many points as possible along the trajectory and a deceleration within the precision of these data. In the case of the fireballs described here, only a few final velocity points with deceleration were available. Spurný et al. (2000) published one Leonid fireball recorded in 1998, which fulfilled these conditions. The fireball was more than 150 km long and with a small inclination to the Earth's surface.

The approximate increase of dynamic pressure with mass is the result of the dependency of the dashed line in Figure 3.19 (increasing mass means decreasing height and thus also increasing dynamic pressure). Most of the Leonids did not

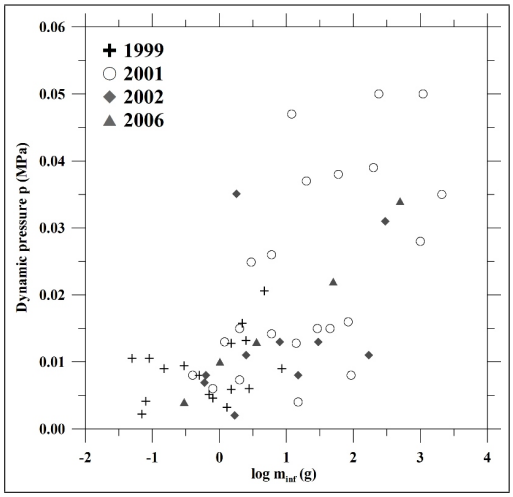

Figure 3.20: Dependency of dynamic pressure (explanation in section 3.5.4), p, on initial photometric mass, m_{inf}, for the 1999, 2001, 2002, and 2006 Leonids.

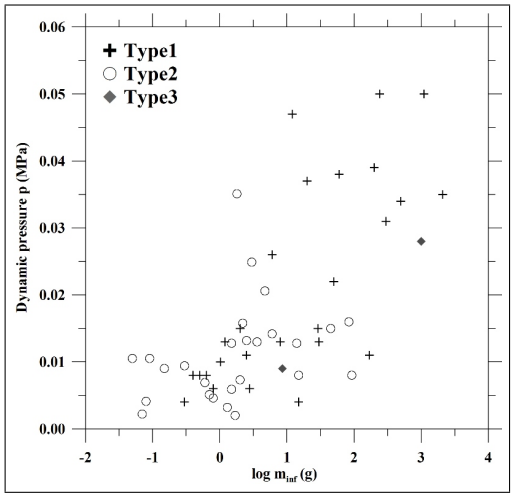

Figure 3.21: Dependency of dynamic pressure (explanation in section 3.5.4), p, on initial photometric mass, m_{inf}, for individual types of the light curve (explanation in section 3.3.2).

survive pressures higher than 0.02 MPa, which corresponds to their assumed cometary origin and fragility. The dependency of dynamic pressure on initial photometric mass, according to the type of the light curve (more details in the next section), is shown in Figure 3.21. The fact that Leonids are fragile cometary meteors is confirmed also by their PE coefficients (Tables 3.19 and 3.20). PE coefficients describe the empirical end height criterion that divides fireballs into four groups according to ablation abilities. The value of PE is a function of air density at the fireball terminal height, ρ_E, initial photometric mass, m_{inf} (with luminous efficiency according to Ceplecha and McCrosky (1976)), initial velocity, v_∞, and zenith distance of the radiant at the fireball beginning, z ($PE = \log(\rho_E) + A\ \log(m_\infty) + B\ \log(v_\infty) + C\ \log(\cos\ z)$). On the basis of values of the PE coefficients (Ceplecha and McCrosky, 1976), more than one half of the Leonids discussed in the present work belong to the weakest type IIIB of the interplanetary matter; more than one third to type IIIA, and only less than 10% to type II (only LEO20 and LEO42 were long and bright enough to safely say that they are type II; no type II fireball had a terminal flare).

3.5.5 Light curves

In general, there are three types of light curves observed for the Leonids. The first type shows only one dominant flare near the end of a visual trajectory (from 3/4 to 9/10), after which the final fading portion of the light curve is very steep. This sudden end of the luminous trajectory is typical for bright fireballs of the PE type IIIB (the same type of light curve was observed for the

1998 Leonids (Spurný et al., 2000)). The second type shows quite symmetric shape, smooth course of brightness without flares, and looks like a light curve of a single-body model of a meteor. This light curve is typical for faint Leonid meteors and was observed for all the Leonids of November 17/18 in 1999, which belonged most likely to the 1899 dust trail. The third type, observed only for two Leonids, shows two humps of comparable brightness and duration. Members of this group are LEO15 (probably belongs to the 1866 dust trail) and LEO25 (maybe the 1767 dust trail), whose terminal flare corresponds to the highest observed dynamic pressure for the presented Leonids (0.194 MPa). An assignment of the presented Leonids to appropriate types of light curves is shown in the last column of Tabels 3.19 and 3.20.

Two Leonids of the first type of the light curve, LEO42 and LEO43, did not terminate their luminous trajectory right after the dominant flare, but continued down to lower heights and their end is similar to that of the second type. Also few Leonids of the second type exhibited additional events in their light curves. Five of them (LEO07, LEO12, LEO17, LEO21, LEO54) had a significant terminal flare (for example LEO21, Figure 3.26); and four of them (LEO22, LEO26, LEO41, LEO49) had the flare at the maximum of the theoretical single-body light curve profile. LEO15, belonging to the third type, had a flare only at the second hump, while LEO25 had a flare at the first hump and showed a significant terminal flare. The first and the second type have the same relative frequency among observed light curves, approximately 48%, the rest of the Leonids, approximately 4%, belong to the third type.

Bright Leonid fireballs often leave persistent trains visible for several minutes after the passage of the fireball (Jenniskens, 2006). For two of the presented fireballs, documented visual observations are available, both connected to observation of a persistent train. On November 18 2001, LEO27 was observed by M. Kročil (online database, 2000), who described it as a blue-white event that left a train visible by the naked eye for 5 to 10 minutes. This fireball was also recorded by Ondřejov's radiometer, with a time resolution of 1200 Hz (Spurný et al., 2001). According to photographic records, the fireball lasted for about 0.7 s but the radiometric data show an event lasting for 1.1 s, suggesting a decrease in brightness consistent with a persistent train. As we can see in Figure 3.22, the decrease of intensity is an exponential function of time $I \approx e^{At}$, where A = -4.69. After the disappearance of the meteor, the absolute brightness of the train was about -8.5 mag, lasting for 0.5 s, and disappearing when it reached -6 mag (the limiting sensitivity of the detector). Most likely this was an afterglow phase of the persistent train, which was formed during expressive outburst at the end of the atmospheric trajectory, where the body fragmented into a large number of small particles that gradually ablated. Intensive increasing of the brightness started after 0.25 s of the trajectory, at a height of about 100 km (and a dynamic pressure of 0.003 MPa). The second visual fireball designated LEO54 on November 19 2006 was observed by M. Gembec (online database, 2000). He described a long-lasting train left by the fireball.

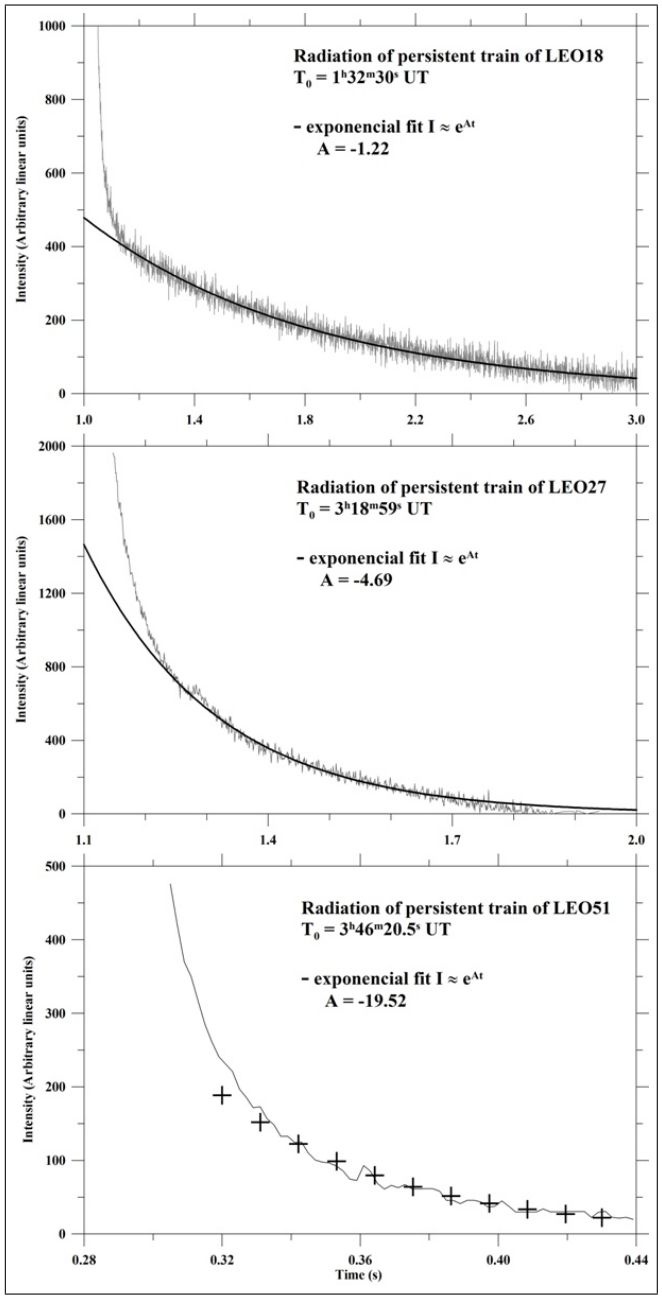

Figure 3.22: Exponential courses of decrease of brightness of the Leonids LEO18, LEO27 and LEO51. LEO18 and LEO27 were recorded by Ondřejov's radiometer with a time resolution of 1200 Hz; and LEO51 by AFO's brightness sensor with a sampling rate of 500 measurements per second.

The persistant train had a slightly ciliated appearance, and described a shape similar to a capital letter V. This fireball was not bright enough (-7.4 mag) to cause a wake, or a train observable either on images or by radiometers. However, an having initial mass of 3.6 g and speed of 71.4 km/s (E_k = 9 MJ),

Table 3.19: Physical data on the 1999 and 2006 Leonid fireballs. ZD_E is the zenith distance of the radiant at the end point of the atmospheric trajectory, v_∞ is the initial velocity, M_{max} is the maximum absolute magnitude, m_{inf} is the initial photometric mass, PE is the coefficient that describes the empirical end height criterion and designates the type of fireball (Ceplecha and McCrosky, 1976). p is the dynamic pressure (see explanation in section 3.5.4) and LC is the type of light curve (more details in section 3.5.5). Values of individual entries are given with an accuracy of one or two last digits.

Meteor No.	ZD_E (deg)	v_∞ (km/s)	M_{max}	m_{inf} (g)	PE	Type	p (MPa)	LC
Year	1999							
LEO01	28.5 3	72.2 3	-6.0	0.5	-5.57	IIIA	0.008	1
LEO02	63.29 5	71.22 10	-6.2	1.3	-6.04	IIIB	0.003	2
LEO03	60.0 2	70.89 8	-2.9	0.08	-5.48	IIIA	0.004	2
LEO04	57.26 3	71.07 5	-6.1	1.5	-5.90	IIIB	0.006	2
LEO05	57.68 17	71.31 9	-5.5	0.8	-5.89	IIIB	0.005	2
LEO06	56.3 2	71.3 3	-3.5	0.07	-5.78	IIIB/A	0.002	2
LEO07	54.1 4	72.02 11	-7.5	2.5	-5.62	IIIA/B	0.013	2
LEO08	53.16 10	71.13 17	-5.4	0.7	-5.89	IIIB	0.005	2
LEO09	49.03 15	71.13 24	-2.6	0.05	-5.14	II/IIIA	0.011	2
LEO10	49.5 2	70.03 20	-7.5	4.7	-5.67	IIIA/B	0.021	2
LEO11	48.03 7	71.32 11	-3.0	0.09	-5.26	IIIA/II	0.011	2
LEO12	44.43 4	71.01 9	-7.8	1.5	-5.53	IIIA	0.013	2
LEO13	42.0 4	70.06 30	-6.7	2.2	-5.72	IIIA/B	0.016	2
LEO14	39.40 10	70.90 20	-4.7	0.15	-5.50	IIIA	0.009	2
LEO15	71.5 4	71.28 13	-9.2	8.6	-5.57	IIIA	0.009	3
LEO16	54.52 5	72.18 11	-8.0	2.8	-5.69	IIIA/B	0.006	1
LEO17	46.27 13	71.8 3	-5.0	0.3	-5.54	IIIA	0.009	2
Year	2006							
LEO50	57.31 3	71.66 6	-10.1	50	-5.83	IIIB	0.022	1
LEO51	30.7 2	70.0 5	-12.9	500	-6.18	IIIB	0.034	1
LEO52	68.09 4	71.15 5	-7.4	5.6	-5.57	IIIA	0.010	1
LEO53	50.66 9	71.3 2	-4.7	0.3	-5.70	IIIA/B	0.004	1
LEO54	31.27 12	71.4 2	-7.4	3.6	-5.83	IIIB	0.013	2

it caused a persistent train.

For two fireballs we can see in the light curve a decrease in brightness of the persistant train - LEO18 and LEO51. According to photographic records, LEO18 lasted less than 0.8 s, but the light curve lasted for 2.6 s. In Figure 3.22 there is a 1.8 s long exponential dependency of the train's brightness on time $I \approx e^{At}$, where A = -1.22. After the disappearance of the meteor, the absolute brightness of the train was about -7.5 mag, and lasted 1.8 s. It disap-

Table 3.20: Physical data on the 2001 and 2002 Leonid fireballs. ZD_E is the zenith distance of the radiant at the end point of the atmospheric trajectory, v_∞ is the initial velocity, M_{max} is the maximum absolute magnitude, m_{inf} is the initial photometric mass, PE is the coefficient that describes the empirical end height criterion and designates the type of fireball (Ceplecha and McCrosky, 1976). p is the dynamic pressure (see explanation in section 3.5.4) and LC is the type of light curve (more details in section 3.5.5). Values of individual entries are given with an accuracy of one or two last digits.

Meteor No.	ZD_E (deg)	v_∞ (km/s)	M_{max}	m_{inf} (g)	PE	Type	p (MPa)	LC
Year	2001							
LEO18	54.31 4	71.30 11	-11.9	240	-5.79	IIIB	0.050	1
LEO19	40.35 7	71.63 12	-11.8	200	-6.02	IIIB	0.039	1
LEO20	62.7 1	71.44 7	-6.0	1.2	-4.93	II	0.013	1
LEO21	55.81 2	71.45 14	-11.5	84	-5.74	IIIB/A	0.016	2
LEO22	49.74 14	71.40 11	-11.5	93	-6.07	IIIB	0.008	2
LEO23	47.76 4	71.45 13	-7.7	6	-5.42	IIIA	0.026	1
LEO24	50.6 9	70.6 1	-9.8	29	-5.98	IIIB	0.015	1
LEO25	47.3 2	71.25 15	-13.0	1000	-5.41	IIIA	0.028	3
LEO26	40.19 10	71.1 3	-10.0	45	-5.96	IIIB	0.015	2
LEO27	37.27 4	71.59 12	-13.8	1100	-5.78	IIIB	0.050	1
LEO28	36.3 2	71.3 3	-7.0	2	-5.63	IIIA/B	0.015	1
LEO29	31.46 4	71.5 4	-5.8	0.8	-5.94	IIIB	0.006	1
LEO30	45.44 10	71.49 15	-7.8	6	-5.92	IIIB	0.014	2
LEO31	49 2	70.1 3	-14.3	2100	-6.22	IIIB	0.035	1
LEO32	41.0 2	68.3 5	-9.0	15	-6.14	IIIB	0.004	1
LEO33	37.33 5	70.6 2	-5.2	0.4	-5.68	IIIA/B	0.008	1
LEO34	34 1	67.4 6	-7.0	3	-5.63	IIIA/B	0.025	2
LEO35	32.18 8	71.1 7	-6.5	2	-6.12	IIIB	0.007	2
LEO36	27.7 6	73.8 5	-11.0	60	-5.82	IIIB	0.038	1
LEO37	29.85 5	71.10 12	-8.5	12	-5.55	IIIA	0.047	1
LEO38	28.9 1	71.2 3	-9.0	14	-6.24	IIIB	0.013	2
LEO39	29 2	72.3 6	-10.0	20	-5.61	IIIA	0.037	1
Year	2002							
LEO40	44 4	71.7 2	-12.5	170	-6.46	IIIB	0.011	1
LEO41	49.43 14	72.45 11	-6.7	1.7	-5.94	IIIB	0.002	2
LEO42	39.84 2	72.46 8	-6.9	2.5	-4.85	II	0.011	1
LEO43	38.95 6	71.64 4	-8.8	8	-5.74	IIIB/A	0.013	1
LEO44	37.5 2	71.9 3	-10.6	30	-6.22	IIIB	0.013	1
LEO45	36.6 4	71.4 2	-7.1	1.8	-5.38	IIIA	0.035	2
LEO46	36.2 6	71.0 7	-6.6	0.63	-5.05	II	0.008	1
LEO47	35.7 4	71.8 2	-12.7	300	-6.18	IIIB	0.031	1
LEO48	32.09 12	70.9 5	-5.7	0.6	-5.92	IIIB	0.007	2
LEO49	32.2 2	72.31 13	-9.1	15	-5.89	IIIB	0.008	2

Table 3.21: Radiants and orbital elements (J2000.0) of the 1999 Leonid fireballs with known time of meteor passage. (α_G, δ_G) is the geocentric radiant, V_G is geocentric mean velocity without atmospheric drag (not mesurable on our records) and T_J is Tisserand's parameter. Values of individual entries are given with an accuracy of one or two last digits or with one standard deviation.

Meteor No.	α_G (deg)	δ_G (deg)	V_G (km/s)	a (AU)	e	q (AU)	ω (deg)	Ω (deg)	i (deg)	T_J
Year	1999									
LEO01	152.82	23.05	71.3	64	0.98	0.9824	170.6	233.38595	161.0	-1.08
	17	16	3	112	3	8	6	6	4	
LEO02	153.83	21.47	70.36	8.1	0.878	0.9833	171.36	235.28120	162.75	-0.55
	5	6	10	6	9	2	18	1	10	
LEO03	154.6	21.65	70.02	6.8	0.856	0.9804	169.2	235.29096	162.0	-0.43
	2	10	8	4	8	12	8	1	2	
LEO04	153.69	21.68	70.20	7.3	0.866	0.98422	172.09	235.29881	162.48	-0.49
	4	3	5	2	4	14	13	1	5	
LEO05	153.81	21.1	70.44	8.2	0.881	0.9828	170.9	235.30074	163.4	-0.57
	9	28	10	6	9	6	5	1	4	
LEO06	153.3	22.08	70.4	8.7	0.887	0.9861	174.1	235.30116	162.1	-0.60
	24	14	32	2.2	29	7	8	1	3	
LEO07	153.47	21.6	70.15	6.9	0.858	0.9848	172.6	235.31143	162.8	-0.45
	12	6	11	6	12	10	1.0	2	1.0	
LEO08	153.42	21.83	70.26	7.6	0.871	0.9854	173.2	235.31285	162.42	-0.52
	12	5	17	9	15	4	4	1	11	
LEO09	153.65	21.65	70.3	7.6	0.87	0.9844	172.3	235.33041	162.6	-0.51
	15	17	24	1.3	2	6	5	1	3	
LEO10	154.36	22.7	69.15	4.7	0.790	0.9832	171.0	235.332	160.3	-0.07
	6	3	20	4	18	7	6	4	5	
LEO11	153.66	21.57	70.45	8.7	0.887	0.9843	172.3	235.33414	162.71	-0.60
	8	6	11	8	10	3	3	1	11	
LEO12	153.83	21.68	70.14	7.1	0.861	0.9859	171.79	235.34502	162.38	-0.46
	6	2	9	4	8	2	13	1	5	
LEO13	152.6	22.1	70.2	7.2	0.86	0.9876	176.2	235.35985	162.5	-0.46
	48	4	3	1.4	3	9	1.6	1	7	
LEO14	153.70	21.48	70.02	6.4	0.847	0.9840	171.9	235.36128	162.8	-0.39
	9	13	20	8	18	4	4	1	2	
LEO15	154.9	21.63	70.41	8.9	0.889	0.9837	171.9	236.25849	161.9	-0.61
	5	15	13	1.0	13	18	1.6	1	4	
LEO16	154.29	21.56	71.32	30	0.967	0.9856	173.91	236.26581	162.53	-1.03
	6	3	11	10	11	2	19	1	7	
LEO17	153.98	21.72	71.0	15	0.93	0.9866	175.0	236.29885	162.4	-0.83
	16	12	29	6	3	4	5	1	2	

peared when it reached about -5 magnitude. An intensive increase in brightness started after 0.5 s of the atmospheric trajectory, at a height of about 90 km (and a dynamic pressure of 0.015 MPa). In the light curve of LEO51 the train is visible for only about 0.1 s after the meteor disappeared, when its brightness was about -8 magnitude. It disappeared when it reached -5 magnitude (the sensitivity of the detector).

These three fireballs reached a maximum absolute brightness (corresponding to flares) at a height of 83 km, which corresponds to a dynamic pressure of 0.048 to 0.050 MPa (differing initial velocities). They all belong to the IIIB type and the heights of their persistent trains (assumed from merged breaks) correspond to values of the central altitude of trains published by Yamamoto et al. (2004). Nevertheless, no dependency on the rate of decrease of brightness (decay coefficient A), meteoroid initial mass, initial kinetic energy or duration of the train was observed. Perhaps a higher number of observations of this type of event are required, and/or more sensitive radiometers. According to Borovička and Jenniskens (2000) the decay of line intensity depends on exci-

Table 3.22: Radiants and orbital elements (J2000.0) of the 2001, and 2006 Leonid fireballs with known time of meteor passage. (α_G, δ_G) is the geocentric radiant, V_G is geocentric mean velocity without atmospheric drag (not mesurable on our records) and T_J is Tisserand's parameter. Values of individual entries are given with an accuracy of one or two last digits or with one standard deviation.

Meteor No.	α_G (deg)	δ_G (deg)	V_G (km/s)	a (AU)	e	q (AU)	ω (deg)	Ω (deg)	i (deg)	T_J
Year	2001									
LEO18	152.30	23.30	70.18	8.4	0.883	0.9815	169.55	232.73396	160.68	-0.56
	3	4	11	7	10	2	14	1	7	
LEO19	152.54	23.19	70.57	12.0	0.919	0.9807	169.1	232.78574	160.78	-0.76
	8	6	12	1.7	11	4	3	1	11	
LEO20	154.25	21.82	70.50	9.5	0.896	0.9842	172.1	235.71460	161.98	-0.64
		6	7							
LEO21	153.95	22.05	70.32	8.3	0.881	0.98551	173.44	235.75032	161.77	-0.56
	2	2	15	9	13	6	9	1	4	
LEO22	153.47	21.97	70.53	9.4	0.895	0.9867	175.0	235.76569	162.2	-0.64
	17	11	11	9	10	4	6	1	2	
LEO23	153.96	21.72	70.58	8.2	0.899	0.9852	173.2	235.77680	162.32	-0.66
	5	2	13	1.2	12	2	2	1	5	
LEO24	155	21.73	69.73	5.9	0.833	0.980	169	235.77759	161.4	-0.30
		7	1							
LEO25	152.2	20.92	70.38	7.1	0.861	0.9881	177.5	235.78100	164.6	-0.48
	26	12	15	7	14	3	9	1	2	
LEO26	153.91	22.19	70.2	7.5	0.87	0.9860	173.96	235.81875	161.5	-0.50
	4	13	3	1.5	3	2	25	1	2	
LEO27	154.05	21.70	70.72	11	0.913	0.9851	173.12	235.83328	162.33	-0.74
	2	5	12	1	11	1	11	1	8	
LEO28	154.33	21.4	70.4	8.2	0.88	0.9836	171.6	235.84343	162.6	-0.56
	6	6	12							
LEO29	154.13	21.80	70.7	10.7	0.91	0.9851	173.1	235.86862	162.11	-0.72
	2	4	4	4.3	4	1	2	1	9	
Year	2006									
LEO50	152.751	22.90	70.80	15.1	0.935	0.98230	170.39	233.43156	161.18	-0.85
	14	3	6	1.2	5	9	7	1	5	
LEO51	152.59	22.47	69.1	4.5	0.78	0.9819	169.6	233.55075	161.6	-0.02
	13	17	5	8	4	8	6	4	3	
LEO52	153.76	21.82	70.28	7.8	0.873	0.9846	172.4	235.40783	162.22	-0.52
	5	3	5	3	5	2	2	1	5	
LEO53	154.13	22.90	70.5	9.8	0.90	0.9844	172.3	235.47881	161.3	-0.66
	7	10	2	1.7	2	3	3	2	2	
LEO54	154.71	21.37	70.5	9.0	0.89	0.9851	173.2	236.60258	162.4	-0.62
	5	13	2	1.7	2	2	3	3	2	

tation potential, not on transition probability. This means that the decay is due to a decrease in temperature (not density), and thus we can say that there were different courses of temperature (across the cross-section) in the trains of these three fireballs.

3.5.6 Radiants and orbits

Radiant positions, geocentric velocity and orbital elements for all 34 Leonid fireballs with known time of passage are presented in Tables 3.21 and 3.22. Mean orbits of the 1999, 2001, and 2006 fireballs and data for the parent comet are presented in Table 3.23. The positions of all the observed Leonid geocentric radiants, normalized to solar longitude 235.1° (maximum of annual activity), are plotted in Figure 3.23. The radiant motion used is according to IAU MDC web pages for a right ascension of 0.66° per degree of solar longitude, and for a declination of -0.33° per degree of solar longitude. The mean radiant

Table 3.23: Mean orbits of the 1999, 2001, and 2006 fireballs and data for the parent comet for epoch 1998-08-15 taken from Jenniskens (2006) are presented. Mean orbit of the 1999 Leonids is based only on the 1899 dust trail meteoroids (LEO02 – LEO14) and mean orbit of the 2001 Leonids is based only on meteoroids recorded on November 18 (LEO23 was not taken into account). Standard deviations for each entry are shown below.

Year	V_G (km/s)	a (AU)	e	q (AU)	ω (deg)	Ω (deg)	i (deg)	T_J
1999	70.24	7.6	0.869	0.9844	172.3	235.32	162.6	-0.50
	15	7	13	18	1.7	3	4	
2001	70.5	9.2	0.895	0.9856	173.6	235.80	162.0	-0.64
	2	1.4	17	6	7	5	3	
2006	70.4	9.2	0.88	0.9837	171.6	234.9	161.7	-0.56
	4	3.8	6	15	1.5	1.4	5	
55P/Tempel-Tuttel	70.63	10.338	0.905	0.984	172.229	235.021	162.482	-0.64

is also plotted and is derived from all radiants except LEO25. Mean radiant values are $\alpha = 153.6 \pm 0.4$ deg, $\delta = 22.0 \pm 0.4$ deg, which corresponds to the radiant position of the Leonid Fireball Night in 1998 ($\alpha = 153.63°$, $\delta = 22.04°$ for $\lambda_\odot = 235.1°$) (Betlem et al., 1999). Mean radiants in individual years and for individual dust trails differ from each other but merge in the range of one standard deviation. Radiant of the 1899 dust trail in 1999 has values $\alpha = 153.5 \pm 0.5$ deg, $\delta = 21.8 \pm 0.4$ deg and its position and halo-like structure corresponds to results published by Betlem et al. (2000) and Trigo-Rodríguez et al. (2002). The radiant of the 1866 dust trail in 1999 has a position $\alpha = 153.6 \pm 0.5$ deg, $\delta = 22.02 \pm 0.09$ deg. The radiant of Leonid fireballs on November 18, 2001 is $\alpha = 153.7 \pm 0.4$ deg, $\delta = 22.1 \pm 0.3$ deg (LEO25 not taken into account).

The dependency of orbital elements on the longitude of the ascending node and right ascension of the geocentric radiant on the node are presented in Figures 3.24 and 3.25. Linear dependencies are fitted only for meteors belonging to the Filament (LEO01, LEO18, LEO19, LEO50 to LEO53). The gray dependency in Figure 3.24 is a linear fit for theoretical radiant motion of 0.66° in right ascension per degree of solar longitude. Trigo-Rodríguez et al. (2002) presented values for orbital elements of the 1899 dust trail meteoroids observed in 1999 which are very similar to each other, but as we can see in Figures 3.24 and 3.25, a large spread of individual elements appears for fireballs recorded during a short period of activity (and so likely belonging to one dust trail). The same observation holds also for Leonids from the 1866 dust trail in the same year, and for Leonids in 2001 (which likely belong to the Filament, but according to this spread of elements rather to the 1767 dust trail). The observed spread in individual elements corresponding to individual years (dust trails) is much larger than the accuracy of the elements.

Four Leonids (LEO10, LEO32, LEO34, LEO51) have initial velocities much lower than that of the mean (71.2 km/s), which results in orbits with semimajor axes significantly smaller than the mean of all orbits. This was observed previously by Betlem et al. (1999) and Trigo-Rodríguez et al. (2002). Betlem

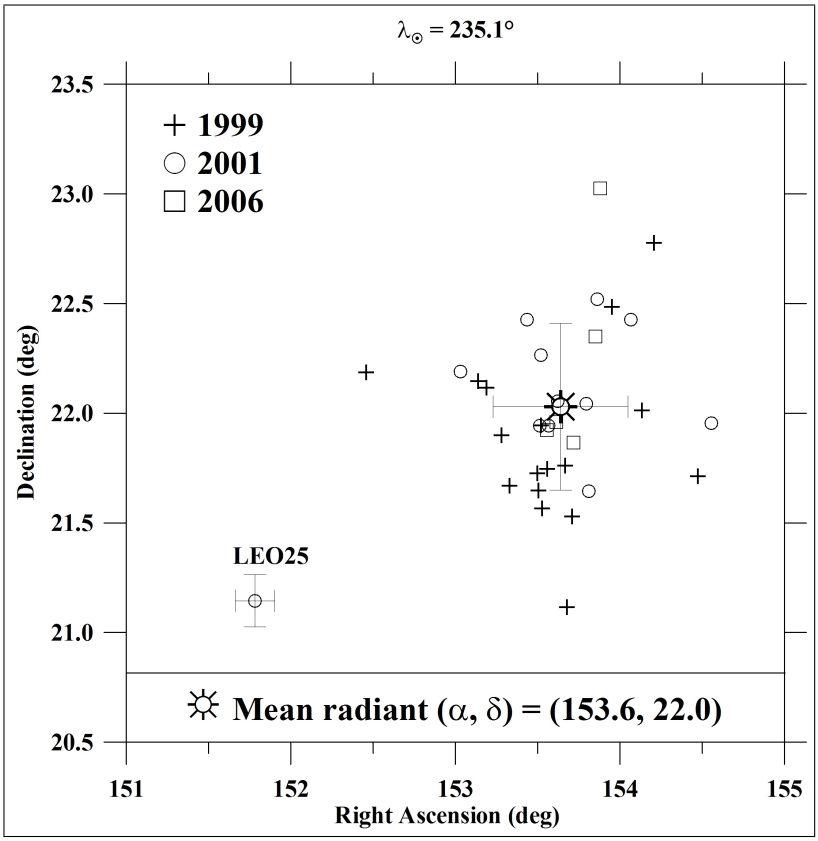

Figure 3.23: Geocentric radiants of the 1999, 2001, and 2006 Leonids for solar longitude 235.1°. Mean radiant position is determined from 30 Leonid fireballs (LEO25 was not taken into account).

et al. (1999) concluded that this can only occur after a close encounter with Earth, and that in order to detect a significant number of such meteoroids, the Earth would have had to cross appropriate dust trails numerous times in the past. Since the Leonids are very fast and their atmospheric trajectories are short, one of the less accurate observed parameter is velocity. Due to this fact, only one meteor with a known time of passage, LEO10, is determined with sufficient accuracy that we can be confident that it could have experienced a previous close encounter with the Earth. LEO32 and LEO34, with unknown times of passage, may have experienced close encounters with the Earth (their semimajor axes determined from approximate radiant position have values of 2.6 and 2.2 AU, respectively).

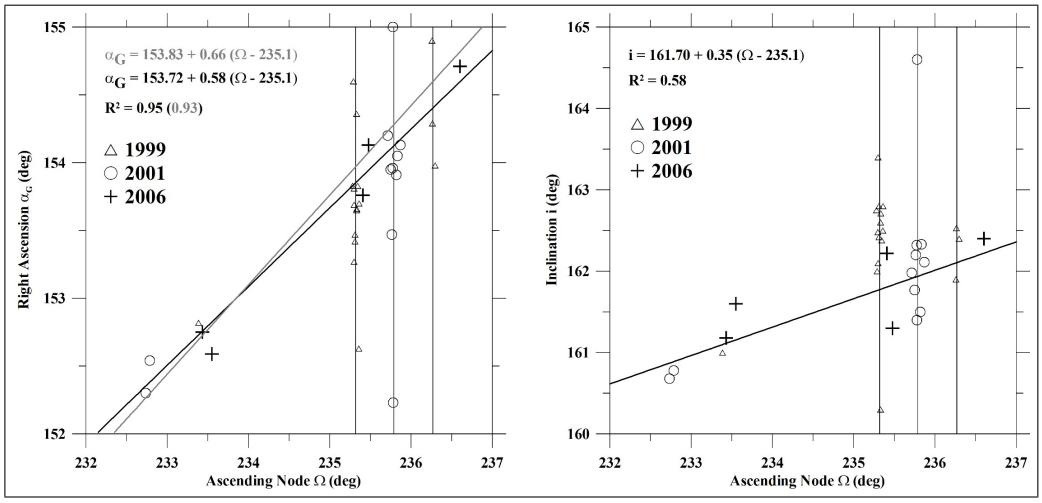

Figure 3.24: Dependencies of right ascension of observed geocentric radiants and inclination on the longitude of the ascending node for the 1999, 2001, and 2006 Leonids. Vertical lines denote ascending nodes 235.32°, 235.80°, and 236.28° corresponding to storm fireballs. Black linear fit corresponds to likely Filament no-storm Leonids. The gray linear fit describes theoretical radiant motion $+0.66°/°$ in R.A. R^2 is the coefficient of determination describing the accuracy of the fit.

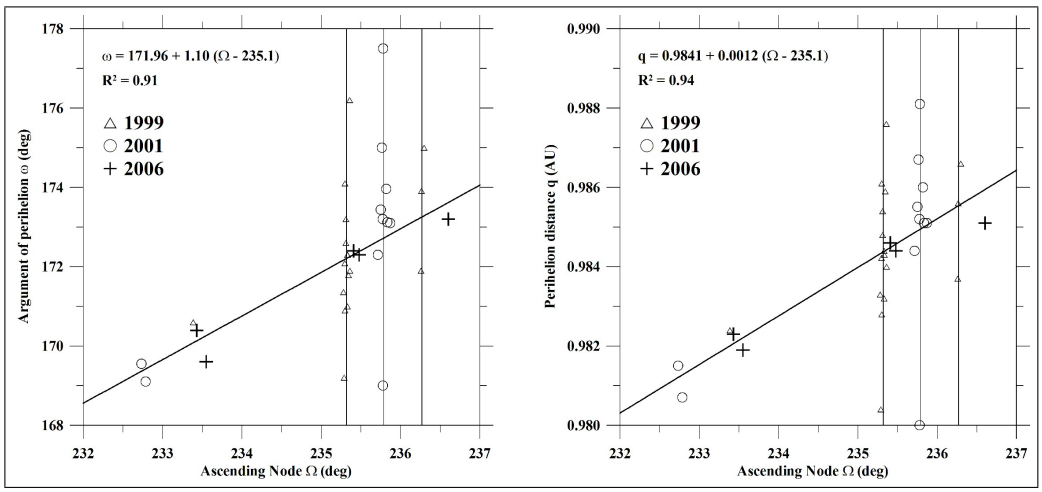

Figure 3.25: Dependencies of the argument of perihelion and perihelion distances on the longitude of the ascending node for the 1999, 2001, and 2006 Leonids. Vertical lines denote ascending nodes 235.32°, 235.80°, and 236.28° corresponding to storm fireballs. Black linear fit corresponds to likely Filament no-storm Leonids. R^2 is the coefficient of determination describing the accuracy of the fit.

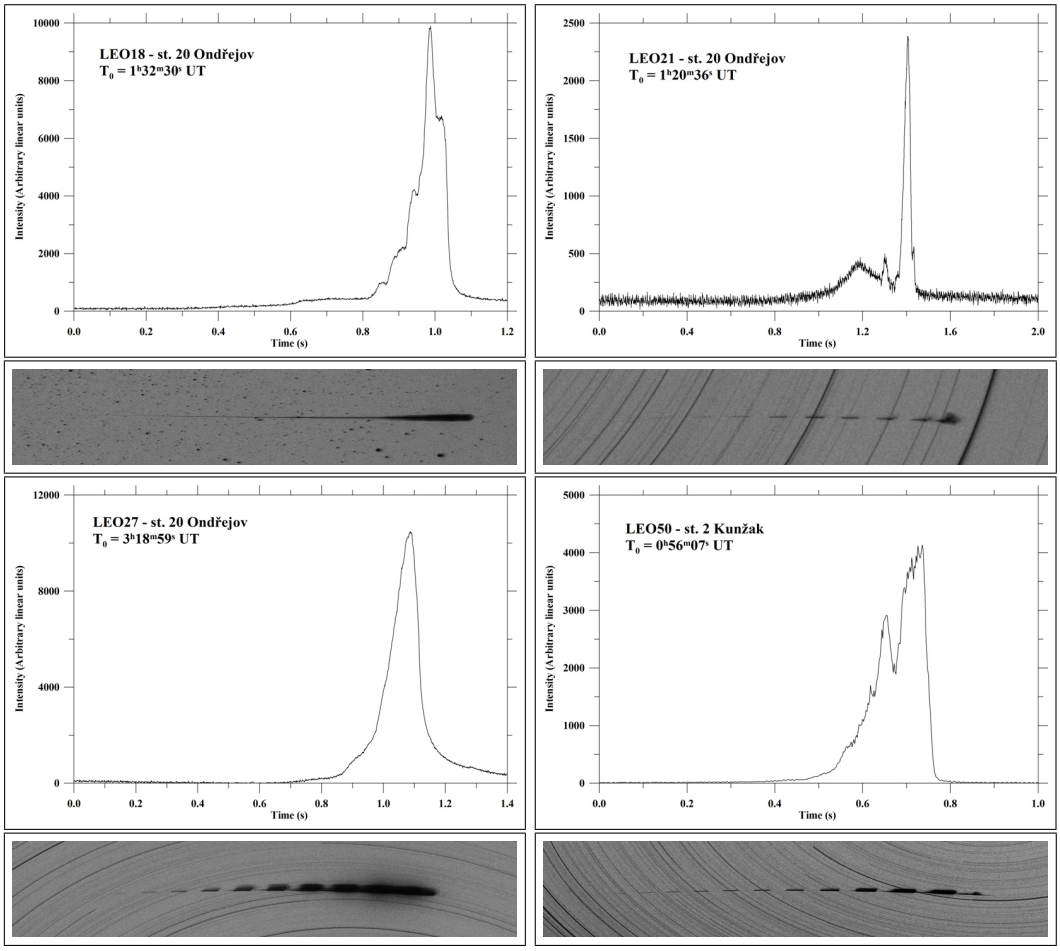

Figure 3.26: Light curves from AFO's brightness sensors and images of the 2001 and 2006 Leonid fireballs from all-sky cameras. The images from fixed cameras display startrails and interruptions of the meteors caused by a rotating shutter (15 breaks/second). The guided image was taken by a guided all-sky camera at Ondřejov Observatory and shows the entire fireball trail. The 2001 Leonids were recorded by Ondřejov's radiometer with a time resolution of 1200 Hz; and the 2006 Leonids by AFO's brightness sensor with sampling rate of 500 measurements per second. All fireballs flew from left to right in the images.

3.6 Perseids

Perseids are one of the strongest annual showers with one maximum near August 12 with ZHR slightly varying between 70 and 85 ((Cook, 1973; Hughes, 1990). Perseids are one of the most observed and studied showers, almost 20% of all photographic orbits in IAU MDC belong to them (Svoreň and Kaňuchová, 2005). The parent comet is 109P/Swift-Tuttle that returned to perihelion in December 1992.

In 1991 - 1994 the observed ZHR increased to about 200 - 500 meteors (Jenniskens et al., 1998) and two separate peaks were observed. Two different dust components were distinguished in 1993 - a Nodal Blanket (Jenniskens et al., 1998) in the present node of the comet and a Perseid Filament (Lindblad and Porubčan, 1994), a ribbon-like structure of dust along the path of the comet. The Nodal Blanket meteors have very small dispersion in radiant and speed, on the other hand, filament meteors have significant dispersion, and thus the Perseid Filament is not caused by particles released during this or the last return of the comet because planetary perturbations must have had time to disperse the stream significantly. The Nodal Blanket consists of relatively old ejecta and its particles are librating around the 1:11 mean motion resonance with Jupiter, which protected the dust from close encounters with the planet.

Mean radiant position, according to the IAU MDC web pages, is $\alpha = 48.3°$, $\delta = 58.0°$ for solar longitude $\lambda = 140.19°$ and its motion is dRA = 1.38°, dDE = 0.18°. Geocentric velocity of annual Perseids is 59.4 km/s. Kaňuchová et al. (2005) sorted 560 photographic orbits into 17 filaments with different sets of orbital elements. These filaments are not distributed in space accidentally

Table 3.24: Atmospheric trajectories of the 2007 Perseids. H is the height above sea level, L_{obs} is the length of observed trajectory. The subscript "B" denotes values at the beginning point of the atmospheric trajectory, the subscript "E" at the end point. N is the number of stations where the fireball was photographed. Standard deviations for each entry are shown below.

Meteor No.	N	Date	Time (UT)	H_B (km)	H_E (km)	L_{obs} (km)	Duration (s)
PER01	2	12.8.	20:37:44	106.4	77.94	60.07	1.00
				2	11		
PER02	4	12.8.	21:31:20	104.11	79.38	43.23	0.74
				1	1		
PER03	2	13.8.	1:15:10	100.28	81.99	21.24	0.33
				2	2		
PER04	3	13.8.	1:48:05	104.10	81.54	25.45	0.41
				1	3		
PER05	2	13.8.	22:13:15	101.46	85.03	26.32	0.44
				1	1		
PER06	4	13.8.	22:38:43	103.68	84.75	28.89	0.46
				1	1		
PER07	2	13.8.	23:35:58	103.13	82.00	28.22	0.47
				1	1		
PER08	2	13.8.	23:41:11	101.34	85.45	21.49	0.33
				1	1		
PER09	2	14.8.	0:34:47	104.98	90.01	18.65	0.27
				1	1		
PER10	6	14.8.	2:02:40	113.64	76.23	40.50	0.67
				3	2		

Table 3.25: Physical data on the 2007 Perseid fireballs. ZD_E is the zenit distance of the radiant at the end point of the atmospheric trajectory, v_∞ is the initial velocity, M_{max} is the maximum absolute magnitude, m_{inf} is the initial photometric mass, PE is the coefficient that describes the empirical end height criterion and designates the type of fireball (Ceplecha and McCrosky, 1976). Standard deviations for each entry are shown below.

Meteor No.	ZD_E (deg)	v_∞ (km/s)	M_{max}	m_{inf} (g)	PE	Type
PER01	61.9	59.75	-8.9	37	-5.15	II
	9	4				
PER02	55.27	59.01	-6.6	2.5	-4.87	II
	1	10				
PER03	30.6	60.1	-6.0	1.4	-5.18	II/IIIA
	2	3				
PER04	27.58	60.24	-7.0	2.4	-5.26	II/IIIA
	1	15				
PER05	51.46	59.78	-4.1	0.6	-5.09	II
	4	21				
PER06	49.16	59.84	-5.3	1.1	-5.20	II/IIIA
	3	13				
PER07	41.59	61.15	-4.6	0.6	-4.94	II
	7	13				
PER08	42.36	59.94	-5.2	0.8	-5.27	II/IIIA
	5	17				
PER09	36.65	60.1	-4.0	0.3	-5.52	IIIA
	2	6				
PER10	22.61	59.99	-8.0	15	-5.24	II/IIIA
	6	10				

but form higher structures.

3.6.1 Observation

Four multi-station Perseid fireballs were in 2007 observed during the night 12/13.8. and in the following night another 7. Results of only ten of them are presented because the brightest and the longest one (also an infrasound record available) deserves an individual processing and in this work will not be mention anymore. Two fireballs observed visually by K. Hornoch (online database, 2000) left about 20 seconds lasting train visible by naked eye - probably an afterglow phase of persistent train. The observer mentioned blue color of both fireballs.

3.6.2 Light curves

Light curves of the 2007 Perseids are similar to each other. Slow increase of brightness accompanied by several short bursts and an intensive flare (maximum brightness of the meteor) in 7/8 of the trajectory. Also an inexpressive or faint terminal flare occurs very often. PER01 and PER10 images show wakes (merged breaks in the photographs). According to the photograph of PER01 the wake is visible from the height of about 84 km (dynamic pressure 0.035 MPa) to 80 km (0.070 MPa) and its total length is approximately 8.5 km. PER01 reached the maximum of the brightness at the height of 82 km, which corresponds to the pressure of 0.050 MPa.

The wake of PER10 is, according to the images, about 6 km long from the

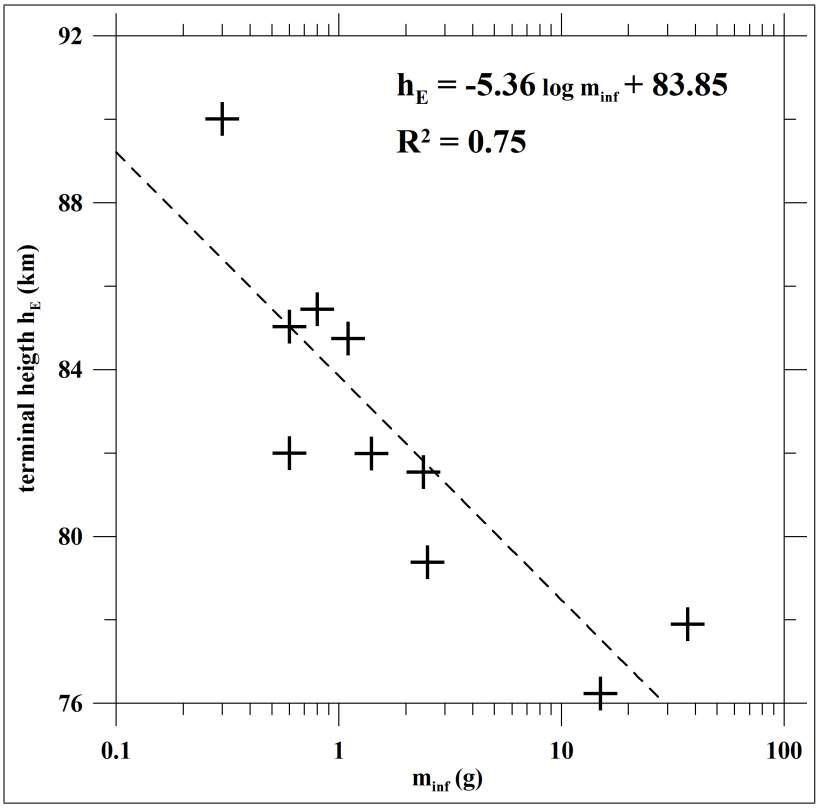

Figure 3.27: Linear dependency of terminal height on initial photometric mass for the 2007 Perseids. R^2 is the coefficient of determination describing accuracy of the fit.

height of 87 (0.020 MPa) to 82 km, where it reached its maximum brightness similar as PER01 (dynamic pressure also 0.050 MPa).

3.6.3 Atmospheric behavior

On the basis of atmospheric behavior of the 2007 Perseids we can conclude that the parent comet 109P/Swift-Tuttle consists of material of similar composition and strength. According to PE criterion, four meteors belong to type II, five to border type II/IIIA and one to IIIA, whereas the scatter of the PE values is less than 0.2 and mean value is -5.2. It means that the 109P is composed rather of hard cometary material. The beginning heights of the meteors, with initial masses under 3 g, range from 100 to 105 km, heavier meteoroids have their beginning higher. The highest observed fireball was PER10 (113 km), which was caused by the geometry with respect to the nearest station, where appeared near radiant, and thus had small angular velocity. Because of this fact, it was recorded as meteor of - 2 mag of absolute brightness. From other stations, it was recorded as -4 mag meteor at the height of about 105 km. The terminal heights, h_E, are approximately a linear function of initial mass, m_{inf}, - with increasing m_{inf} h_E decreases (Figure 3.27). It is necessary to mention PER01

Table 3.26: Radiants and orbital elements (J2000.0) of the 2007 Perseid fireballs. (α_G, δ_G) is the geocentric radiant, V_G is geocentric mean velocity without atmospheric drag (not mesurable on our records) and T_J is Tisserand's parameter. Also mean elliptical orbit from the 7 fireballs (PER01, PER07 and PER10 were not included) and data for the parent comet for epoch 1995-10-10 taken from Jenniskens (2006) are presented. Standard deviations for each entry are shown below.

Meteor No.	α_G (deg)	δ_G (deg)	V_G (km/s)	a (AU)	e	q (AU)	ω (deg)	Ω (deg)	i (deg)	T_J
PER01	46.0	58	58.71	12.8	0.93	0.958	152.5	139.65781	112.4	-0.03
	6	1	4	8.4	5	4	1.0	2	1.5	
PER02	46.47	59.804	57.96	14.8	0.936	0.9535	151.38	139.69357	109.87	-0.05
	3	11	10	1.9	8	4	15	1	7	
PER03	46.3	58.09	59.0	17.8	0.95	0.959	152.7	139.84279	112.8	-0.16
	4	15	3	7.7	2	2	7	1	3	
PER04	47.65	57.89	59.21	18.9	0.950	0.9510	150.9	139.86473	113.30	-0.20
	3	3	15	4.5	12	5	2	1	11	
PER05	47.07	58.03	58.74	10.6	0.909	0.9603	152.9	140.68178	112.94	0.03
	9	3	21	1.9	17	8	3	1	14	
PER06	47.06	58.69	58.80	16.5	0.942	0.9606	153.3	140.69877	112.13	-0.13
	6	2	13	2.9	10	5	2	2	9	
PER07	46.30	57.75	60.13	-	1.009	0.9688	155.9	140.73694	114.13	0
	13	3	13		11	8	3	2	9	
PER08	46.94	58.53	58.90	16.9	0.943	0.9620	153.6	140.74043	112.39	-0.15
	9	3	17	4.1	14	7	3	2	12	
PER09	49.96	58.196	59.1	16	0.94	0.943	149	140.77618	113.2	-0.15
	4	14	6	14	5	2	1	2	4	
PER10	47.32	59.87	58.96	-	1.004	0.9605	153.7	140.83482	110.77	0
	12	7	10		9	7	2	1	11	
mean orbit			58.8	15.9	0.939	0.956	152.0	140.3	112.4	-0.13
			4	2.7	14	7	1.6	5	1.2	
109P/Swift-Tuttle			59.41	26.092	0.963	0.959	152.989	139.384	113.454	-0.28

Table 3.27: Dynamic pressures of the 2007 Perseid fireballs. p_{max} and p_{tf} are dynamic pressures at maximum brightness and at terminal flare, respectively. h_{max} and h_{tf} are appropriate heights. Since the listed heights are based on the light curves from AFO's, the accuracy is about 0.5 km.

Meteor No.	h_{max} (km)	h_{tf} (km)	p_{max} (MPa)	p_{tf} (MPa)
PER01	82	82	0.050	0.050
PER02	82	80	0.049	0.069
PER03	85		0.029	
PER04	84.5	83	0.032	0.042
PER05	90		0.011	
PER06	91		0.009	
PER07	86	86	0.025	0.025
PER08	92	85.5	0.007	0.027
PER09	95		0.004	
PER10	81.5	78	0.055	0.098

that was photographed from two stations with convergence angle between the two planes beeing only 1.2°. Despite it, this fireball was determined relatively accurately using the method of skew lines and the results of its atmospheric behavior agree with other Perseids.

3.6.4 Radiant and orbit

Positions of geocentric radiants calculated for solar longitude 140.19° have got high dispersion in space of variables α, δ - right ascension and declination.

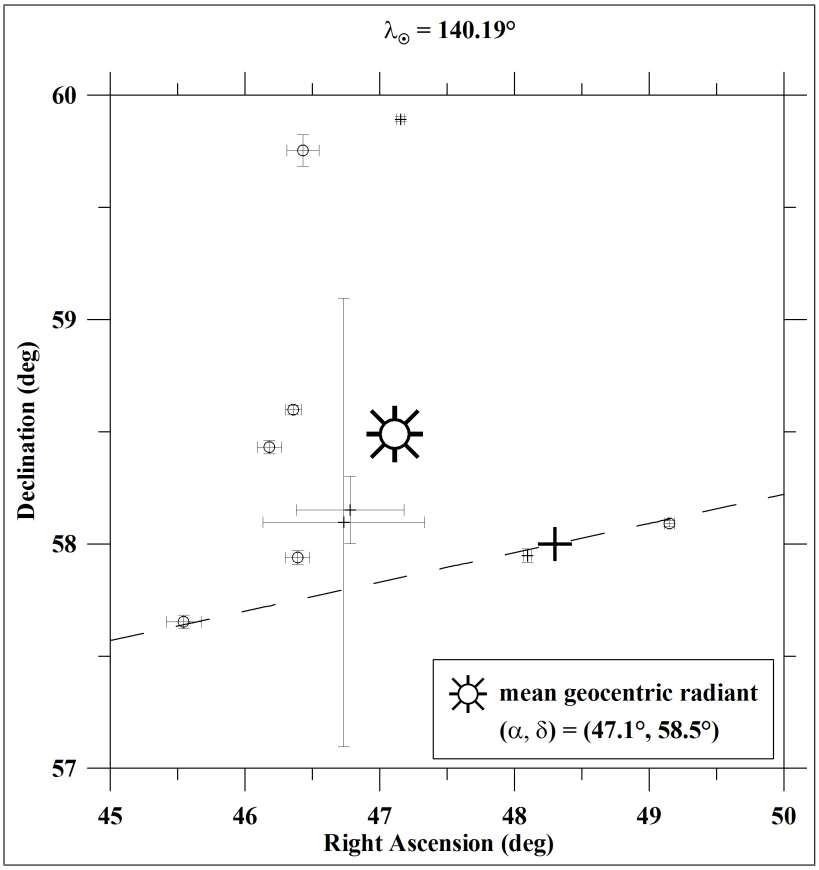

Figure 3.28: Geocentric radiants of the 2007 Perseids for solar longitude 140.19°. The dashed line is radiant motion according to IAU MDC web pages - radiant for $\lambda = 140.19°$ is denoted by bold cross.

Mean radiant determined from all ten fireballs have $\alpha = 47.1 \pm 1.1$ deg, $\delta = 58.5 \pm 0.8$ deg and the value of mean geocentric velocity is $v_G = 59.0 \pm 0.5$ km/s. If PER01, which have large error of radiant, is not included, then mean position of radiant remains the same. Also the mean geocentric velocity remains the same when PER07 and PER10 (parabolic orbits, see Table 3.24) are not taken into account for its mean value.

Mean heliocentric elliptical orbit (PER01, PER07 and PER10 are not included) has elements a = 16 ± 3 AU, e = 0.94 ± 0.01, q = 0.956 ± 0.007 AU, $\omega = 152 \pm 2$ deg, $\Omega = 140.3 \pm 0.5$ deg, i = 112.4 ± 1.2 deg. Kaňuchová et al. (2005) studied 560 Perseid orbits from the IAU MDC catalogue of photographic orbits and recognized 17 individual groups, whose members have identical orbits. The most numerous filament has 242 members with $v_G = 59.32$ km/s and q = 0.956 AU . Perseids PER03 and PER04 have similar orbits and probably belong to this filament. The second most numerous filament has 52 members among IAU MDC photographic orbits and from the 2007 Perseids only PER09 resembles. Other 2007 Perseids do not resemble any filament proposed

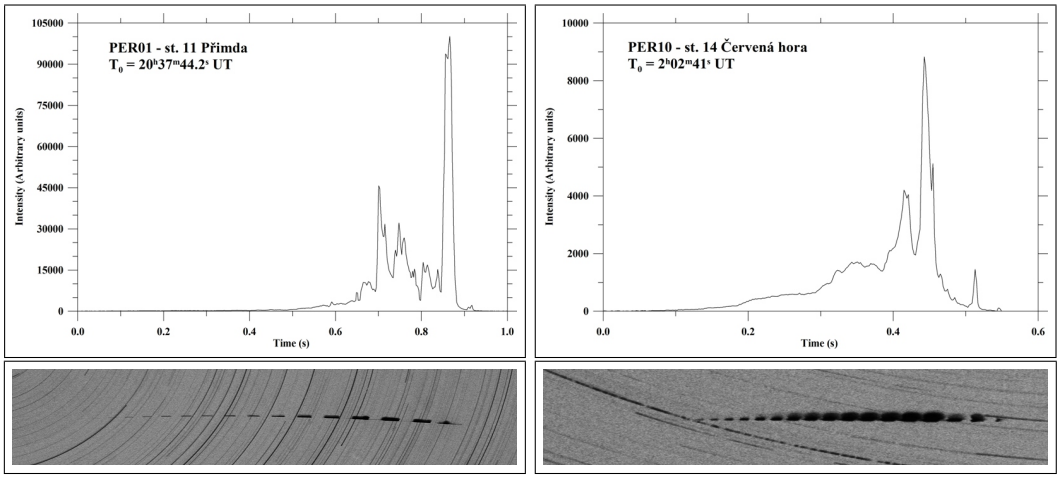

Figure 3.29: Light curves from AFO's brightness sensors and images of the 2007 Perseid fireballs from all-sky cameras. The images from fixed cameras display startrails and interruptions of the meteors caused by a rotating shutter (PER01 – 15 breaks/second, PER10 – 30 breaks/second). Both fireballs flew from left to right in the images.

by Kaňuchová et al. (2005). PER07 and PER10, both probably on parabolic orbit (both have acurate radiant and velocity, nevertheless, in the range of one standard deviation of eccentricity can be both orbits elliptical), have elements very diverse to each other, therefore there is no point in determining their mean orbit. High dispersion of values of orbital elements, positions of geocentric radiants and geocentric velocities of the 2007 Perseids indicates big age and spatial dimension of dust cloud of the shower.

3.7 Comparison

Mutual comparison of individual showers is done here on the basis of their brightness, atmospheric behavior and heliocentric orbits and dependencies between the elements.

3.7.1 Maximum brightness

Dependency of maximum absolute brightness on initial mass given by Pogson's equation (slope of the linear dependency is -2.5) is very well fulfilled for the Leonids, Perseids, α-Capricornids and Southern δ-Aquariids. It is worse fulfilled for Orionids, where the slope is -2.74 and does not agree for Geminids, where the slope is -2.14. It is evident from Figure 3.30 that meteoroid with a specific weight causes the brightest meteor, when it has composition and orbit as Leonids. After that, Orionids, Perseids and Southern δ-Aquariids follow, which corresponds to the sequence of decreasing geocentric velocity.

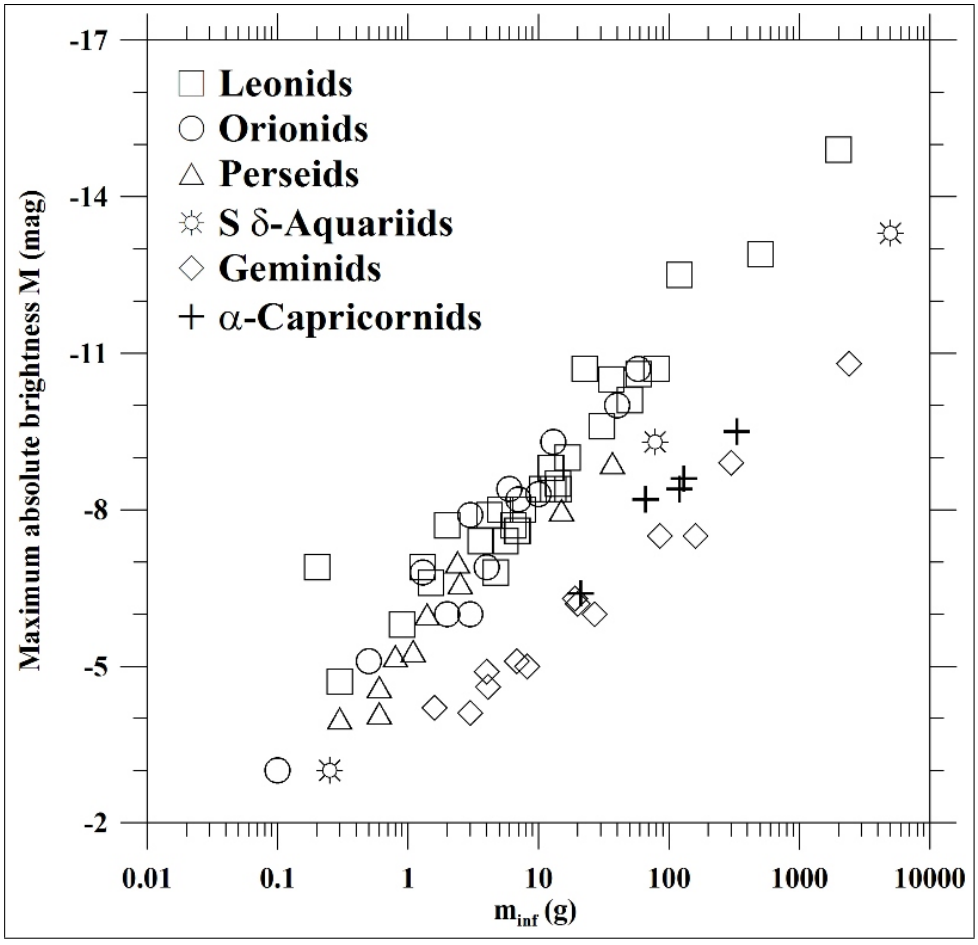

Figure 3.30: Dependency of absolute maximum brightness on initial photometric mass as a result of Pogson's equation.

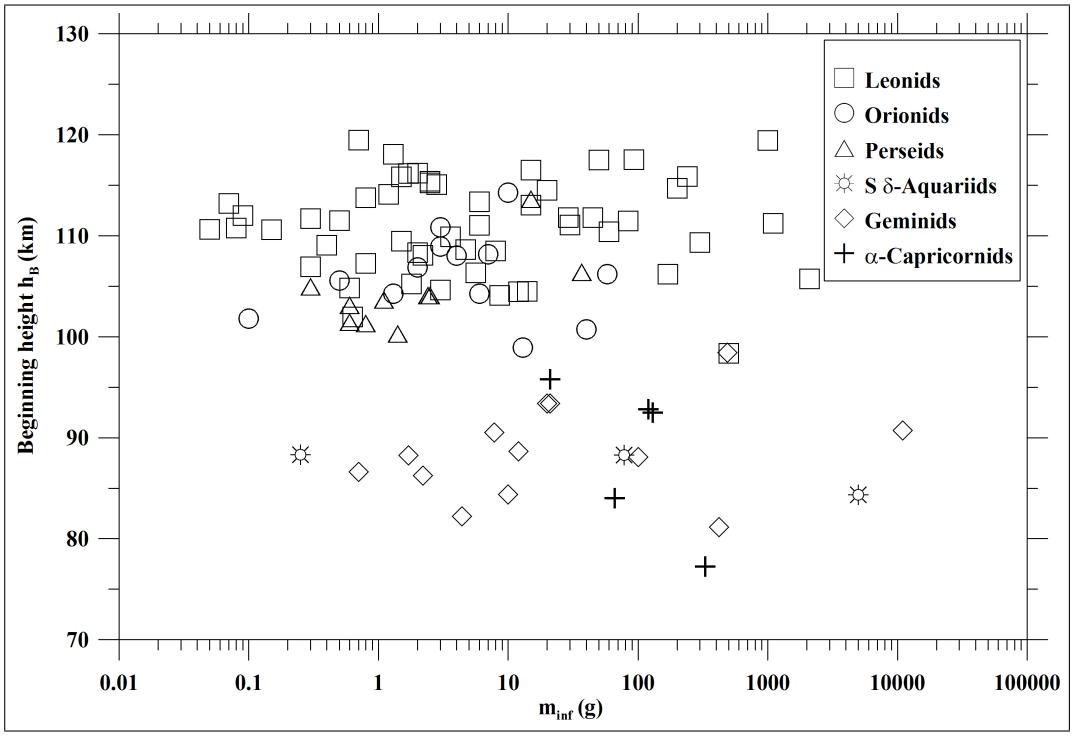

Figure 3.31: Dependency of beginning heights on initial photometric mass for all the studied showers.

This sequence also is valid due to the fact that differences in composition of individual meteoroids are not so high for these four showers. In all four cases, the meteoroids belong, according to the PE criterion, more or less to a soft cometary material. According to mutual velocities, Geminids should be on the next place, but in comparison to α-Capricornids, which are the most fragile type IIIB, the Geminids are compact bodies. That is the reason, why the sequence changes at this point and brighter meteor is produced by slower and more fragile α-Capricornid (for meteoroids with the same weight).

3.7.2 Beginning and terminal heights

Dependencies of beginning and terminal heights on initial mass are usualy expected to produce higher beginning and lower terminal heights for meteoroids with higher initial masses. This, according to Koten et al. (2004), holds for faint video Leonids, Orionids and Perseids, while Geminids, having approximately constant beginning height for whole range of studied masses (10^{-3} to 10^{-1} g), are mass-independent. The same results also hold for the fireballs in this work, only beginning heights are systematicaly shifted lower by 5 to 10 km depending on shower membership (Figure 3.31), which is caused by sensitivity of detectors used (photographic meteors from 10^{-1} to 10^{3} g). For photographic Geminid fireballs there is, in the range from 10^{0} to 10^{3} g, ap-

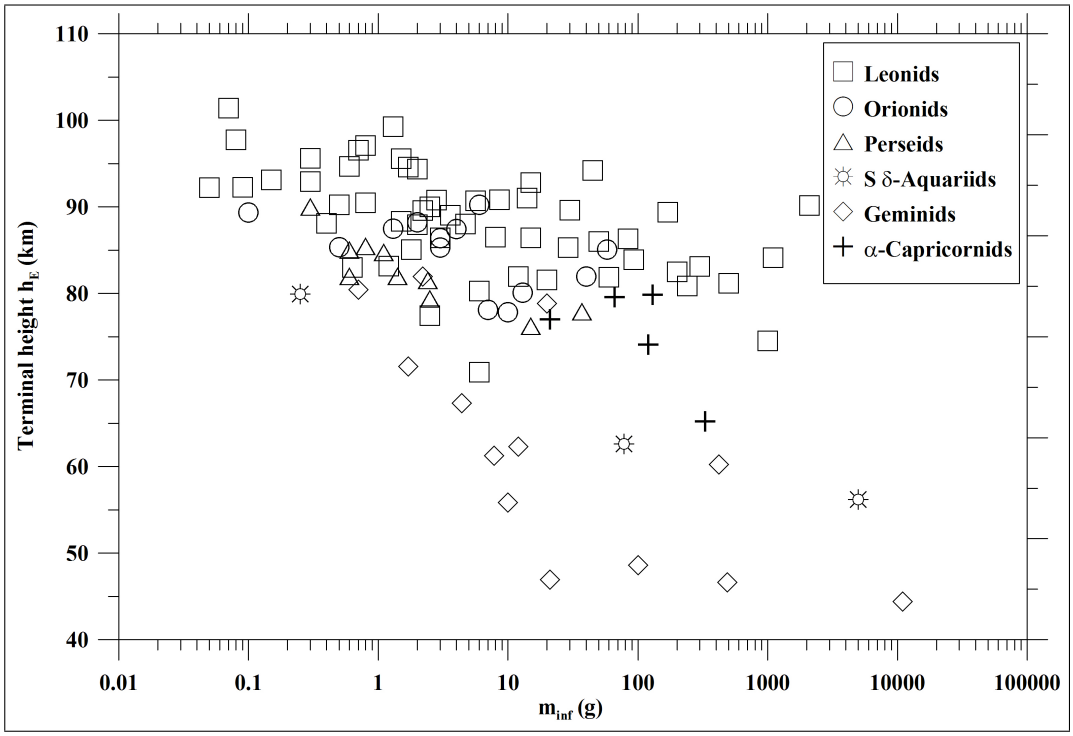

Figure 3.32: Dependency of terminal heights on initial photometric mass for all the studied showers.

proximately constant beginning height of 89 km and for Southern δ-Aquariids, in the range from 10^{-1} to 10^{3} g, approximately at the height of 87 km. Both of these showers have substantially lower perihelion distance, in comparison to other showers, which can be related to this. Around the same height also beginnings of α-Capricornids were observed (approximately 88 km). Unfortunately, from only five meteors, it is ambiguous to say if the beginning heights are mass-independent. Possible mass-independency of Southern δ-Aquariids can be caused by the equipment used. The same result also hold for Leonids (more details in section 3.5.3), which fulfill apparent mass-independency of the beginning heights, h_B =111 $\pm$ 5 km for the range of photometric masses from 10^{-1} to 10^{3} g, but from video observations we know that Leonids are not mass-independent. This apparent mass-independency is caused by the fact that all Leonids reach at the hight of 111 km an absolute brightness of approximately -2^{m}. Other faster showers have their beginnings by about 10 to 20 km higher and for all studied showers hold a condition that terminal height decreases with increasing initial mass (Figure 3.32).

3.7.3 PE coefficients

According to atmospheric behavior, we can arrange studied streams in order of strenght of material of their meteoroids. On the basis of the PE criterion

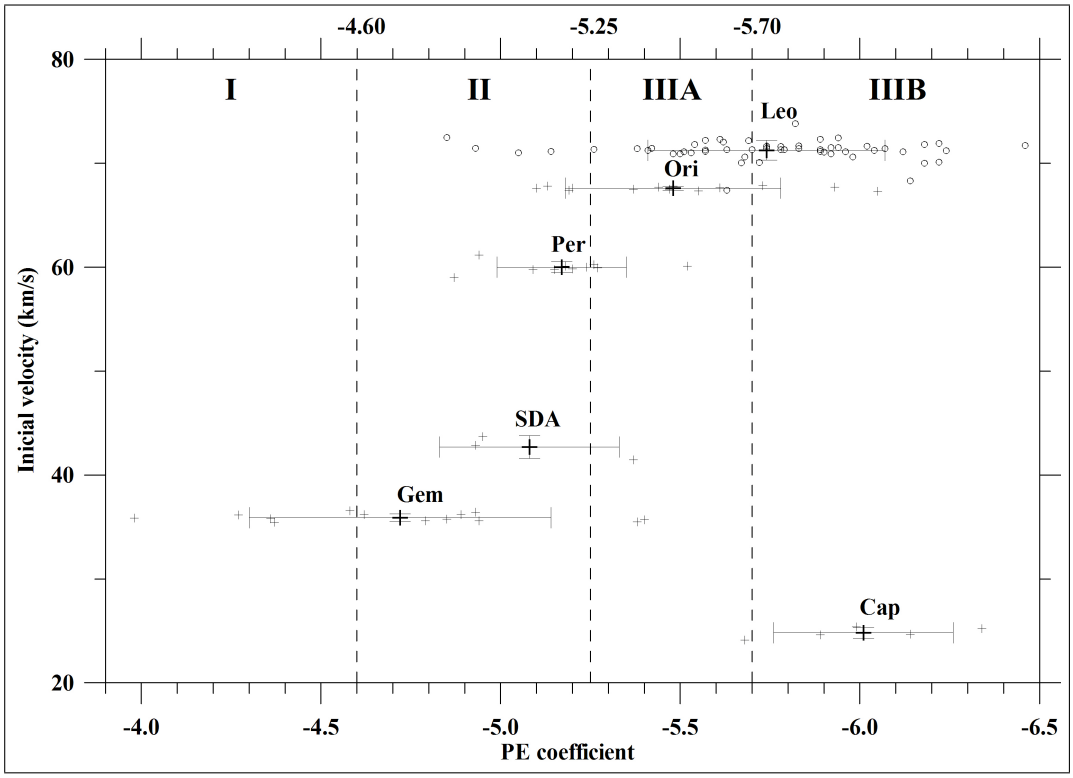

Figure 3.33: Distribution of strenght of material depending on PE coefficients for all the studied showers. To distinguish Leonids and Orionids, positions of Leonids are denoted by small circles. Vertical dashed lines at PE values of -4.60, -5.25 and -5.70 divide the graph into the meteor types I, II, IIIA and IIIB (Ceplecha and McCrosky, 1976). The error bars presented here are standard deviations of individual mean values.

(Figure 3.33) the softest and the most fragile are α-Capricornids, which are the type IIIB with mean value of PE beeing -6.01 $\pm$ 0.25. Leonids follow, which have, together with Geminids, the biggest dispersion in PE coefficients (PE = -5.70 $\pm$ 0.35). Therefore the parent comet of Leonids is likely the most heterogenous one among studied showers. Next shower are Orionids, with mean PE = -5.48 $\pm$ 0.30 followed by Perseids and Southern δ-Aquariids, which both have similar mean value of PE. Perseids have PE = -5.17 $\pm$ 0.18, which is the smallest spread and corresponds to the suggestion that the parent comet is very uniform. Southern δ-Aquariids have a bit higher PE compared to Perseids (PE = -5.08 $\pm$ 0.25), but it has to be mentioned that the value is based on three fireballs only. The most solid are Geminids (between types I and II) with the biggest dispersion in PE coefficients (PE = -4.76 $\pm$ 0.45), but in this case we can not be certain if the parent comet is heterogenous or this spread is caused by changes of physical properties during the close approaches to the Sun in the perihelion.

Table 3.28: Values of mean PE coefficients and dynamic pressures, p, for all the studied meteor showers. p is in MPa, v_∞ is the initial velocity in km/s and n is the number of meteors used. Gray color text denotes less probable type of fireball. Standard deviations for each entry are shown below.

	GEM	SDA	PER	ORI	LEO	CAP
v_∞	35.90	42.7	59.99	67.59	71.3	24.80
	36	1.1	53	18	9	51
PE	-4.72	-5.08	-5.17	-5.48	-5.70	-6.01
	42	25	18	30	32	25
p	0.186	0.075	0.027	0.021	0.016	0.013
Type	I/II	II/IIIA	II/IIIA	IIIA	IIIA/IIIB	IIIB
n	13	3	10	13	54	5

3.7.4 Dynamic pressures

Tensile strength of the material of the studied meteorids can be estimated from the dynamic pressures determined in specific positions of their atmospheric trajectories. These positions are either fragmentations or sudden outbursts or terminal flares or terminal points (for single-body meteor without fragmentation or with smooth light curve without outbursts). On the basis of mean values of the dynamic pressures (Table 3.28) we can arrange studied streams as follows (the ranges of the dynamic pressures are shown in Figure 3.34): the softest and the most fragile are α-Capricornids, with dynamic pressures in fragmentation points in the range from 0.004 to 0.032 MPa and the mean value of 0.013 MPa. Leonids follow, which have very similar values of the mean dynamic pressures in all studied years. In 1999, the mean value is 0.009 MPa and corresponds to either sudden outbursts or to terminal points. In 2001, 2002 and 2006, majority of the Leonids disintegrated in the Earth's atmosphere in terminal flare and the mean values of the corresponding dynamic pressures are in chronological sequence 0.023, 0.014 and 0.017 MPa. The mean value for all the 54 studied Leonids is 0.016 MPa and appropriate pressures range from 0.002 to 0.050 MPa. Next shower are Orionids with the mean value of 0.021 MPa. ORI11 was not taken into account as an outlier (0.074 MPa). Determined pressures are in the range from 0.007 to 0.074 MPa. Perseids have the mean dynamic pressure of 0.027 MPa and determined pressures are in the range from 0.004 to 0.055 MPa. The pressures for Orionids and Perseids were determined either from the sudden outbursts or from the terminal flares. Next shower are Southern δ-Aquariids. Unfortunately, only three fireballs were studied and the mean determined dynamic pressure is 0.075 MPa. The dynamic pressures in fragmentation points (according to observed heights of trails) range from 0.040 to 0.110 MPa. The most solid are Geminids, the mean dynamic pressure is 0.186 MPa. Geminids have, similarly to their PE coefficient dispersion, the biggest dispersion in observed dynamic pressures ranges from 0.011 to 0.535 MPa.

Studied showers are arranged in the same order as according to PE criterion. PE criterion describes meteors according to behaviour at the very

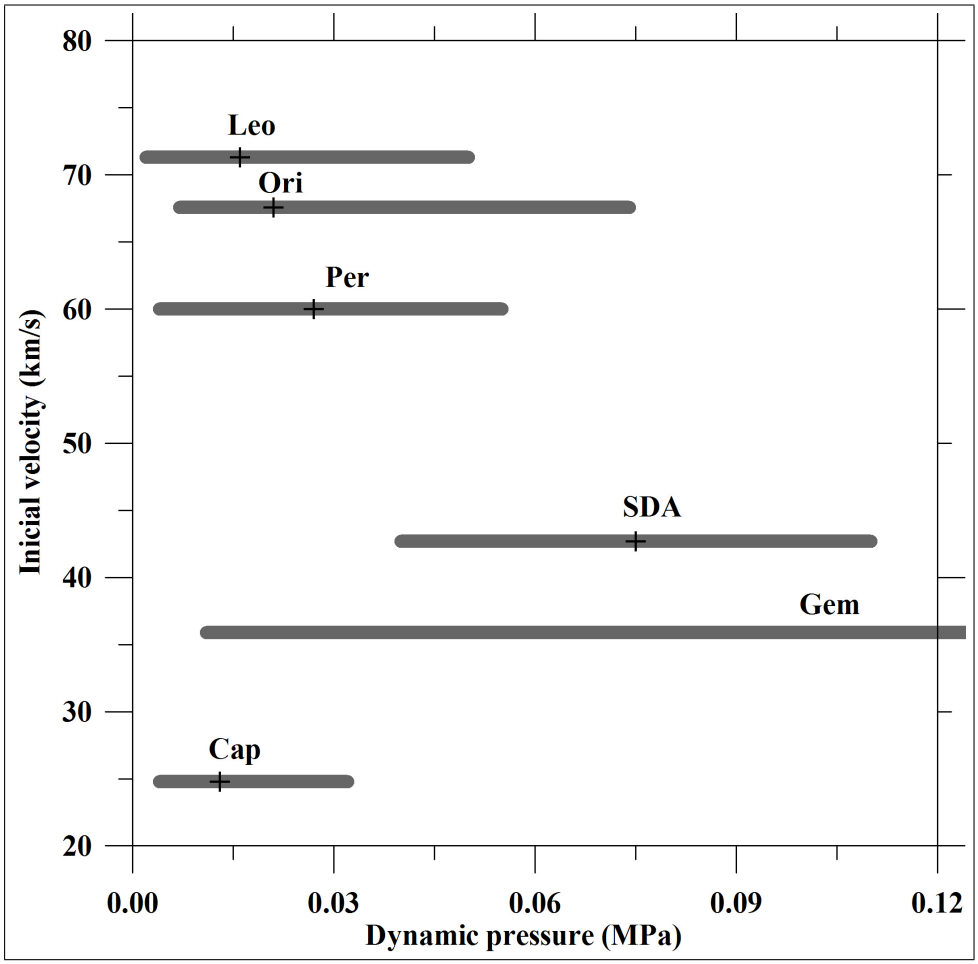

Figure 3.34: The ranges of dynamic pressures observed for Leonid, Orionid, Perseid, Southern δ-Aquariid, Geminid, and α-Capricornid fireballs. The mean values of the dynamic pressures are denoted by black crosses and are plotted for the mean initial velocities (Table 3.28). The mean value for the Geminids is 0.186 MPa and lies out of the graph's defined area. The maximum observed dynamic pressure for Geminids have the value of 0.535 MPa.

beginning and at the terminal point, while dynamic pressure is a value derived from only one point "somewhere" along the trajectory. The fact, that these two approaches leads to the same result means, that the point "somewhere" also (as PE coefficient) depends on more parameters and not only on the material tensile strength. Very probable dependant variable is initial photometric mass. In Figure 3.35 we can see approximate increasing dependancy of dynamic pressure on initial photometric mass and similar dependency for individual PE types in Figure 3.36. The dashed lines plotted in Figure 3.35 are only approximate border lines and the linear dependencies in Figure 3.36 correspond to exponential increas of p with increasing m_{inf}, $p \approx m_{inf}^{A}$, where the exponent A has similar values for different PE types. From the type I fireballs to the type IIIB fireballs the values are 0.22, 0.29, 0.24 and 0.30.

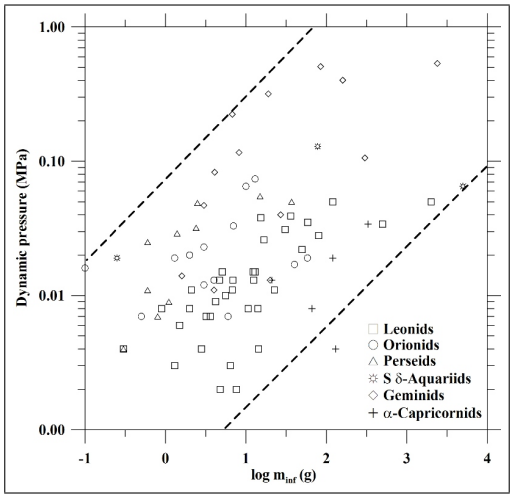

Figure 3.35: Dependency of dynamic pressure, p, on initial photometric mass, m_{inf}, for all the studied fireballs. The dashed lines plotted are only approximate border lines.

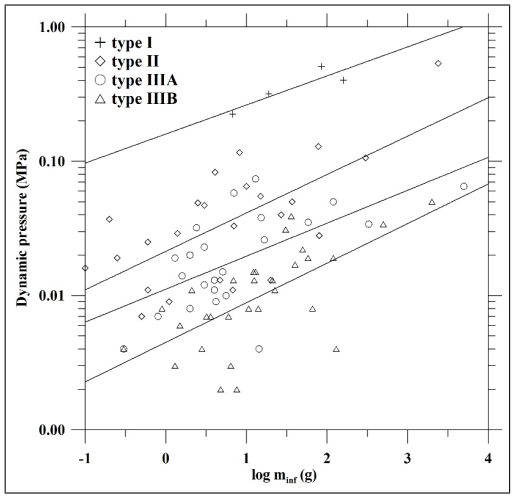

Figure 3.36: Dependency of dynamic pressure, p, on initial photometric mass, m_{inf}, for individual PE types of all the studied fireballs. The linear dependencies plotted have similar values of the slopes. From the type I fireballs to the type IIIB fireballs the slopes are 0.22, 0.29, 0.24 and 0.30.

3.7.5 Orbital elements

A confirmation of selection effect, laid on meteoroids intersecting the Earth's orbit, is given by the gray-denoted curve in Figure 3.37, which was taken from Steel (1996). Observed dependencies of arguments of perihelion on perihelion distances correspond to this. The upper branch in the graph consists of meteoroids that met the Earth in their ascending nodes, which corresponds to Geminids, α-Capricornids, Leonids and Perseids. The lower branch consists of meteoroids, which are observed in their descending nodes, Southern δ-Aquariids and Orionids belong to this group. Dependencies ω-q are linear for all showers in the scale of Figure 3.37, but if we plot this dependency for individual showers, linear dependency holds only for Leonids, Orionids, best for Perseids and maybe also for Southern δ-Aquariids (three orbits only), i.e., for showers with high inclination of orbit to the ecliptic plane, where the selection effect is more evident.

Another dependencies were observed and recognized among studied showers. For Geminids and Southern δ-Aquariids the dependency of geocentric velocity on eccentricity was recognized (Figure 3.38). The dependency arises from the law of conservation of energy. Both these showers have substantially lower perihelion distance in comparison to the other showers, where the dependency is remarkable not at all. Likely higher gravitational action of the Sun in the perihelion area is the reason for the dependency. Next dependencies observed are inclination on declination of geocentric radiant for Orionids

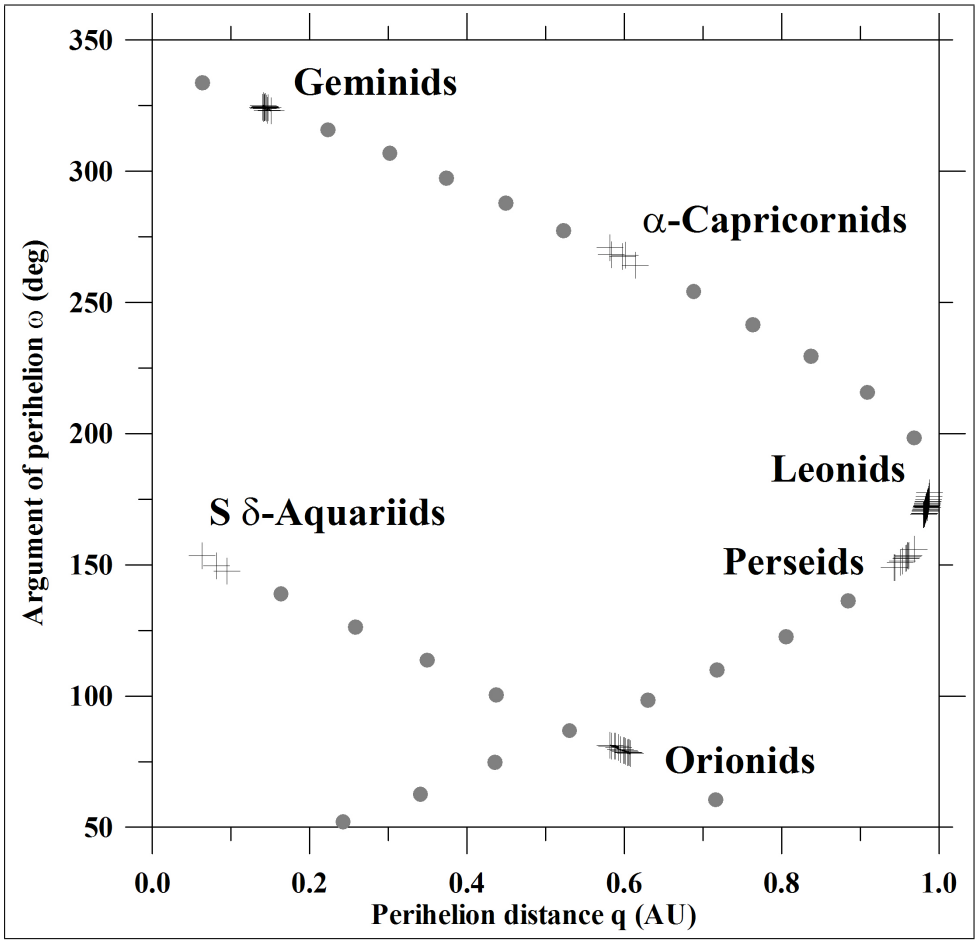

Figure 3.37: Dependency of argument of perihelion on perihelion distance as a result of selection effect. Gray dots represent the requirement that the meteoroids have to have node near 1 AU and were taken from Steel (1996).

(Figure 3.2 on page 35), geocentric velocity on right ascension of geocentric radiant for Southern δ-Aquariids (Figure 3.14 on page 56), and temporal dependencies of orbital elements of the 2006 Southern δ-Aquariids on longitude of the ascending node (equations on page 58).

3.7.6 Comparison with meteorite dropping fireballs

During decades long operation of all-sky photographic observation of fireballs in the Czech part of the EN approximately twenty meteors with predicted terminal mass were recorded (Table 3.29). Even if meteorites were recovered only in one case, the probability of meteorite fall of weight in the range from hundreds of grams to tens of kilograms was high. In contrast to the meteorite dropping fireballs, which belong to a sporadic backgroung with unknown parent bodies, meteors of major streams have the parent object known – comet or asteroid – and obtaining of their samples would help to better understanding

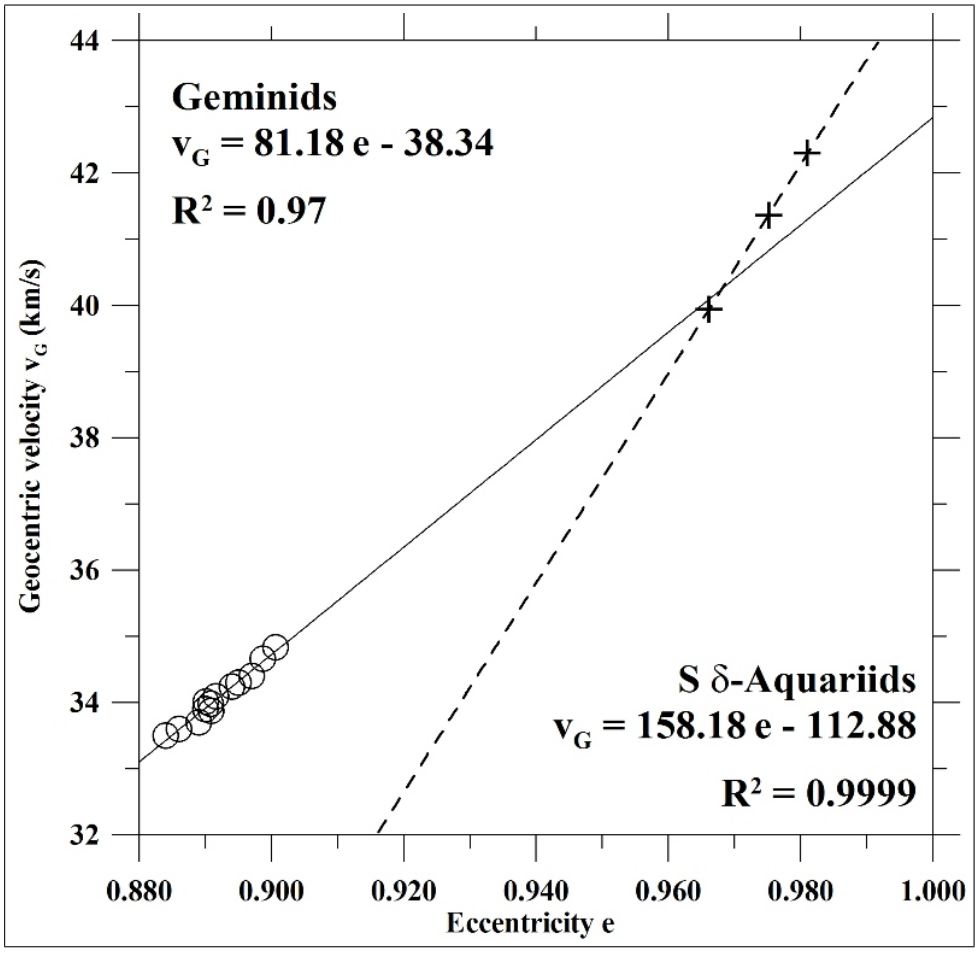

Figure 3.38: Dependency of geocentric velocity on eccentricity for the Geminid and Southern δ-Aquariid stream, which have substantially lower perihelion distance in comparison to other showers.

of these bodies. Hence I have performed comparison between shower fireballs and meteorite dropping fireballs in order to say if shower fireball can produce meteorite fall and which preatmospheric properties of such meteoroid have to be satisfied.

The comparison was performed on the basis of beginning and terminal heights, PE coefficients, initial velocities, and decelerations. Only fireballs with predicted terminal mass higher than or equal to 1 kg (Table 3.29), and based on all-sky photographic observation within the scope of the EN were used for the comparison.

When we compare beginning heights, PE coefficients, and initial velocities, we can see in Figure (3.39) similarities between beginning heights of Geminids, Southern δ-Aquariids, and α-Capricornids and meteorite dropping fireballs. Similarities between these showers and meteorite dropping fireballs also are visible for PE coefficients and initial velocities (Figure 3.40). Nevertheless,

Table 3.29: Meteorite dropping fireballs with terminal mass larger or equal to 1 kg

Name	Date	h_B (km)	h_E (km)	v_∞ (km/s)	v_E (km/s)	m_∞ (kg)	m_E (kg)	M_{max} (mag)	Type
The Alps	12.6.1977	78	25.7	14.1	8.9	850	30	-12.8	II
Žďár	9.10.1983	83.754	25.17	15.047	4.66	16.1	1.5	-8.3	I
Neuberg	4.12.1983	72.9	29.5	16.8	11.2	42	4	-11.0	I/II
Valeč	3.8.1984	83.82	19.17	12.406	3.085	380	16	-9.9	I
Valmez	13.8.1985	76.7	27.5	15.13	4.8	87	2.1	-10.6	I/II
Koln	16.8.1985	75.9	30.1	24.5	7.3	125	1	-13.0	I/II
Janov	4.10.1987	71.1	19.0	15.834	2.8	500	75	-11.7	I
-	24.12.1987	70.090	23.19	16.79	8.9	424	10	-13.3	I/II
-	14.5.1988	78.71	26.96	12.686	4.9	353	1	-11.6	II
Benešov	7.5.1991	97.723	16.046	21.086	2.0	15000	10	-18.5	II
Neuberg III	9.3.1992	97.8	20.0	18.72	4.2	30	10	-9.9	I
Meuse	22.2.1993	77.3	21.5	26.74	7	3000	2.7	-17.3	I/II
Tisza	25.10.1995	80.54	26.5	29.23	12.1	890	2.6	-16.1	I/II
Jindřichův Hradec	23.11.1995	93.79	20.40	22.200	0.93	3600	2	-16.9	I/II
Vimperk	31.8.2000	81.82	21.46	14.915	6.4	150	5	-13.8	I
Turji-Remety	17.11.2001	81.37	13.5	18.483	4.3	4300	400	-18.0	I
Neuschwanstein	6.4.2002	84.95	16.04	20.95	2.4	300	20	-17.2	I

α-Capricornids have high values of PE (they are very fragile) and Southern δ-Aquariids have high initial velocity. Only Geminids fulfill both dependencies and in adition also the third one and the most important one – dependency of terminal height on initial mass (Figure 3.41). An extrapolation of linear fit of dependency of terminal height on initial mass for the 2006 Geninids inter-

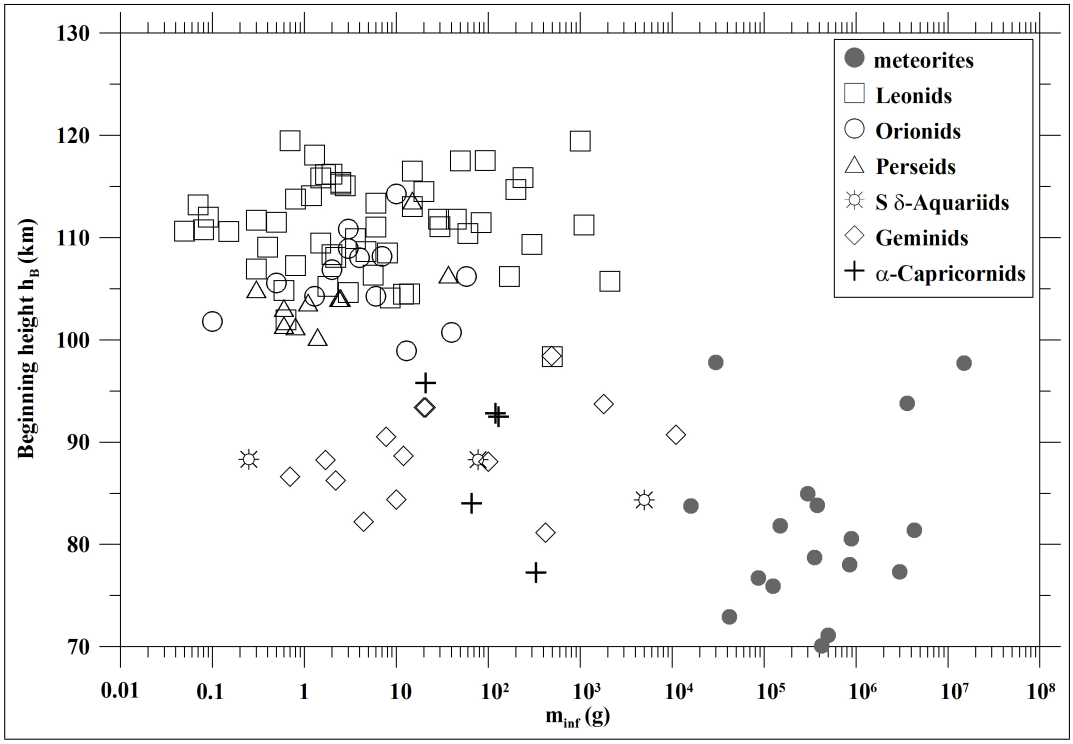

Figure 3.39: Dependency of beginning heights on initial photometric mass. Gray dots mark meteorite dropping fireballs.

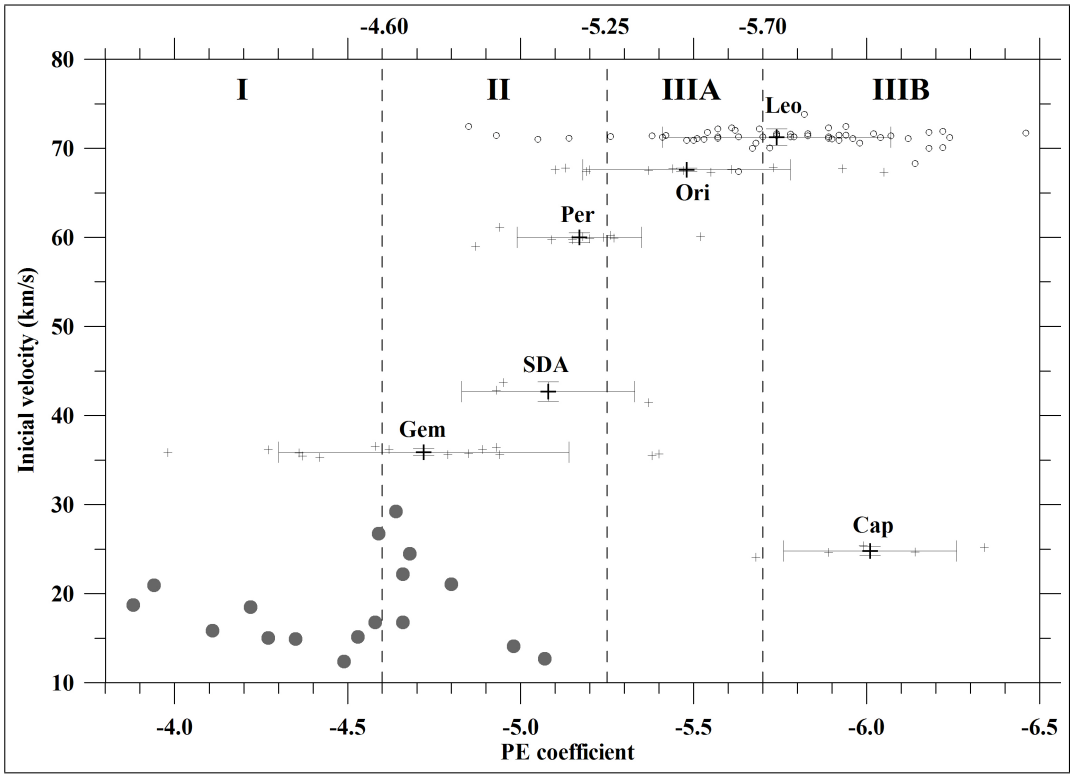

Figure 3.40: Dependency of PE coefficients on initial velocity. Gray dots mark meteorite dropping fireballs.

sects the area of meteorite dropping fireballs (gray dots in Figure 3.41), thus Geminid meteoroid with specific physical properties could probably produce meteorite dropping fireball. I have simulated Geminids with different initial properties to determine these specific physical properties.

The model is based on differential equations for single non-fragmenting body above sphere (Equations 2.1 – 2.4) with atmospheric pressure and temperature for individual height and geographical latitude taken from CIRA86 atmosphere (to determine atmospheric density), and luminous efficiency, τ, from ReVelle and Ceplecha (2001). Meteor beginning is taken for absolute brightness of -4 mag and terminal point either for absolute brightness of -4 mag or for velocity of 3 km/s or for zero mass. Geminids were simulated for northern latitude 50° and with initial slope to the vertical of 45°. Input parameters are initial velocity, $v_\infty = 35.90$ km/s (Table 3.28), initial mass, m_∞, ablation coefficient, σ, zenith distance of radiant, $z_R = 45°$, and meteoroid bulk density, $\rho_d = 3500\,\mathrm{kg/m^3}$ (mean value taken from Wetherill (1986) and Ceplecha and McCrosky (1992)).

The only one parameter, remaining to estimate, is ablation coefficient. Only 7 Geminids with known ablation coefficient are presented in this thesis. I have found it like insufficient statistical set, so I have combined them together with 42 photographic Geminids published by Spurný (1993, 1994). Histogram of

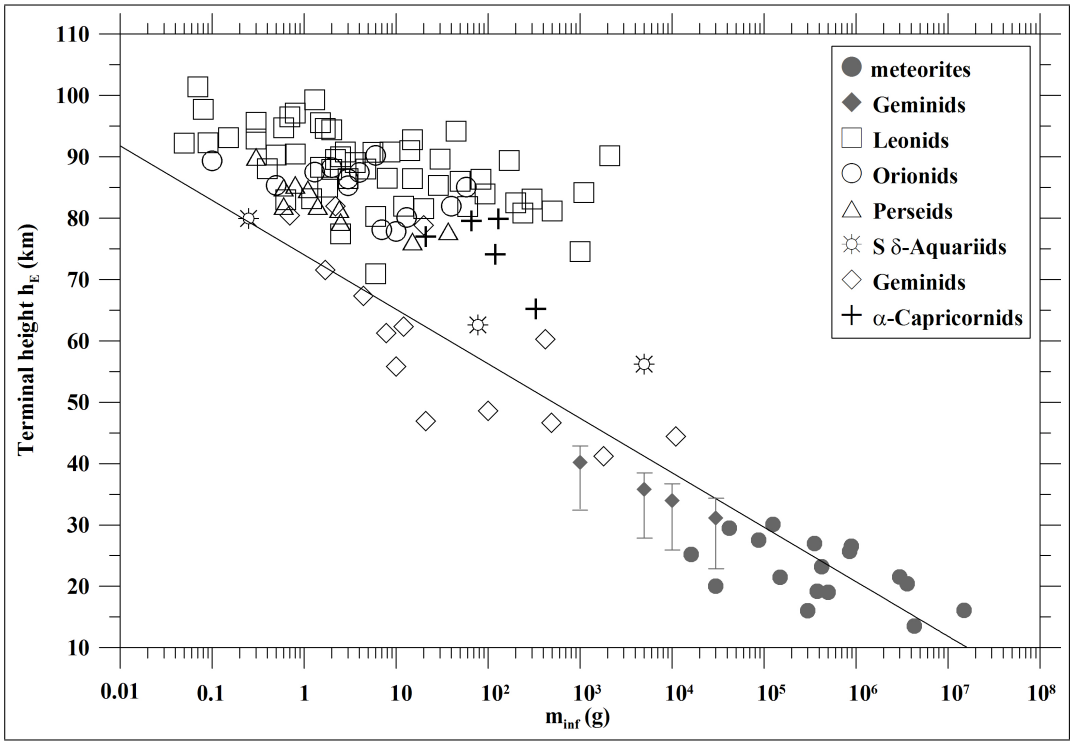

Figure 3.41: Dependency of terminal heights on initial mass. Gray dots mark meteorite dropping fireballs and gray diamonds simulated Geminids of 1, 5, 10, and 30 kg and $\sigma = 0.014\,\mathrm{s^2/km^2}$ (error bars correspond to σ from 0.006 to $0.018\,\mathrm{s^2/km^2}$). The linear dependency is the least square fit for the terminal heights of the 2006 Geminids.

relative frequency of these ablation coefficients is in Figure 3.42. Mean value is $0.014\,\mathrm{s^2/km^2}$ but the most frequent ablation coefficients have values less than or equal to $0.010\,\mathrm{s^2/km^2}$ - favourable for deep penetration. I have simulated Geminids with different initial masses and ablation coefficients and have found, that limit ablation coefficient for nonzero terminal mass was $0.018\,\mathrm{s^2/km^2}$ for initial velocity of 35.90 km/s. It means that Geminid meteoroids with higher ablation coefficients ablate their entire mass. The dependency of terminal height on terminal velocity for simulated Geminids and observed meteorite dropping fireballs is in Figure 3.43. Geminids with initial masses 1, 5, 10 and 30 kg for ablation coefficients from 0.006 to $0.018\,\mathrm{s^2/km^2}$ were simulated.

Table 3.30: Specific physical properties of Geminid meteoroids for probable meteorite fall. σ is the apparent ablation coefficient, m_∞ the initial mass, h_E the terminal height, and m_E the terminal mass. Details about the model used are in the text on page 93.

σ (s^2km^{-2})	m_∞ (kg)	h_E (km)	m_E (g)	σ (s^2km^{-2})	m_∞ (kg)	h_E (km)	m_E (g)
0.006	1	32.6	24	0.014	1	40.2	0.5
	5	28.0	109		5	35.8	1.1
	10	26.0	211		10	34.0	1.6
	30	23.0	608		30	31.2	3.6

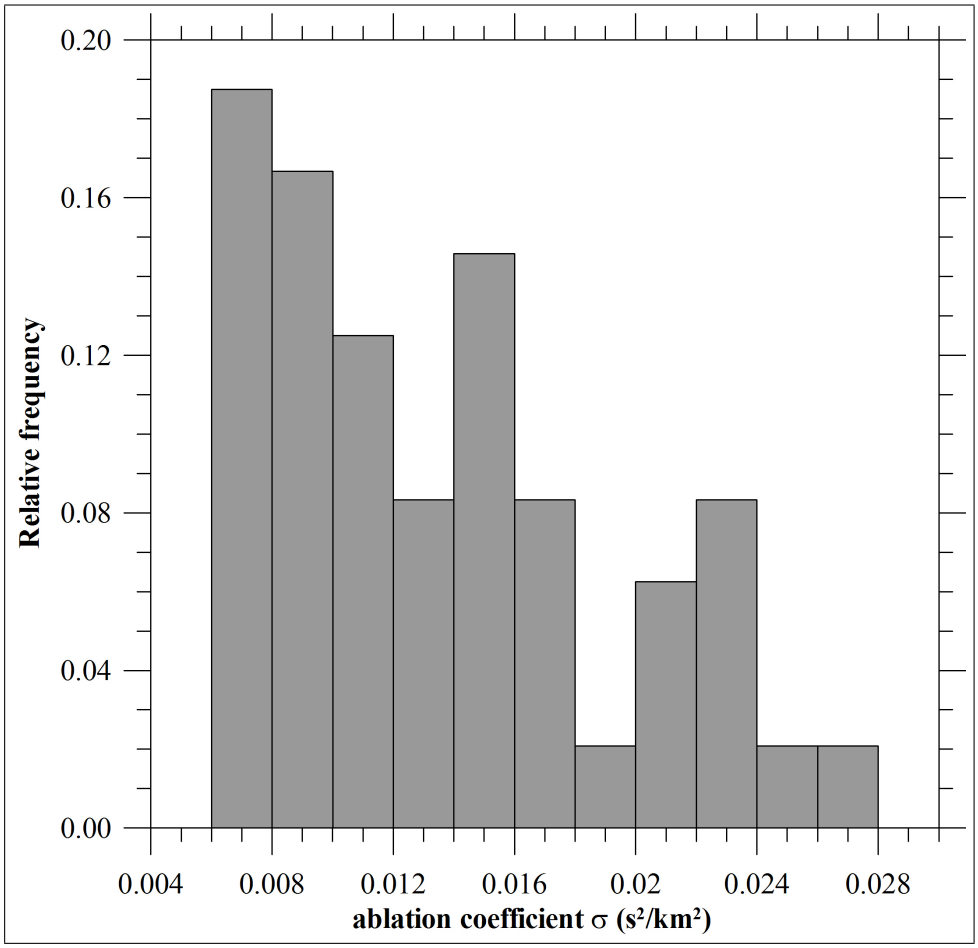

Figure 3.42: Histogram of relative frequency of ablation coefficients for 48 photographic Geminids (Spurný, 1993, 1994).

The result is, that Geminids with ablation coefficient less than approximately $0.010\,\mathrm{s}^2/\mathrm{km}^2$ and with initial mass higher than 5 kg fulfill terminal properties of meteorite dropping fireballs.

Observed Geminids with high initial mass have often high value of ablation coefficient and are type II fireballs, while type I Geminids with $\sigma \approx 0.010\,\mathrm{s}^2/\mathrm{km}^2$ use to be with $\mathrm{m}_\infty \leq 1\,\mathrm{kg}$. When we combine these two types of Geminids we obtain ideal meteoroid for deep penetration and probable meteorite fall (Table 3.30). A 5 kg-Geminid meteoroid with $\sigma = 0.006\,\mathrm{s}^2/\mathrm{km}^2$ is required for significant terminal mass higher than 100 g. 200 g of terminal mass results from 10 kg meteoroid and 600 g from 30 kg meteoroid. Remember, that this holds for non-fragmenting meteoroid, and thus real terminal masses would be probably even smaller.

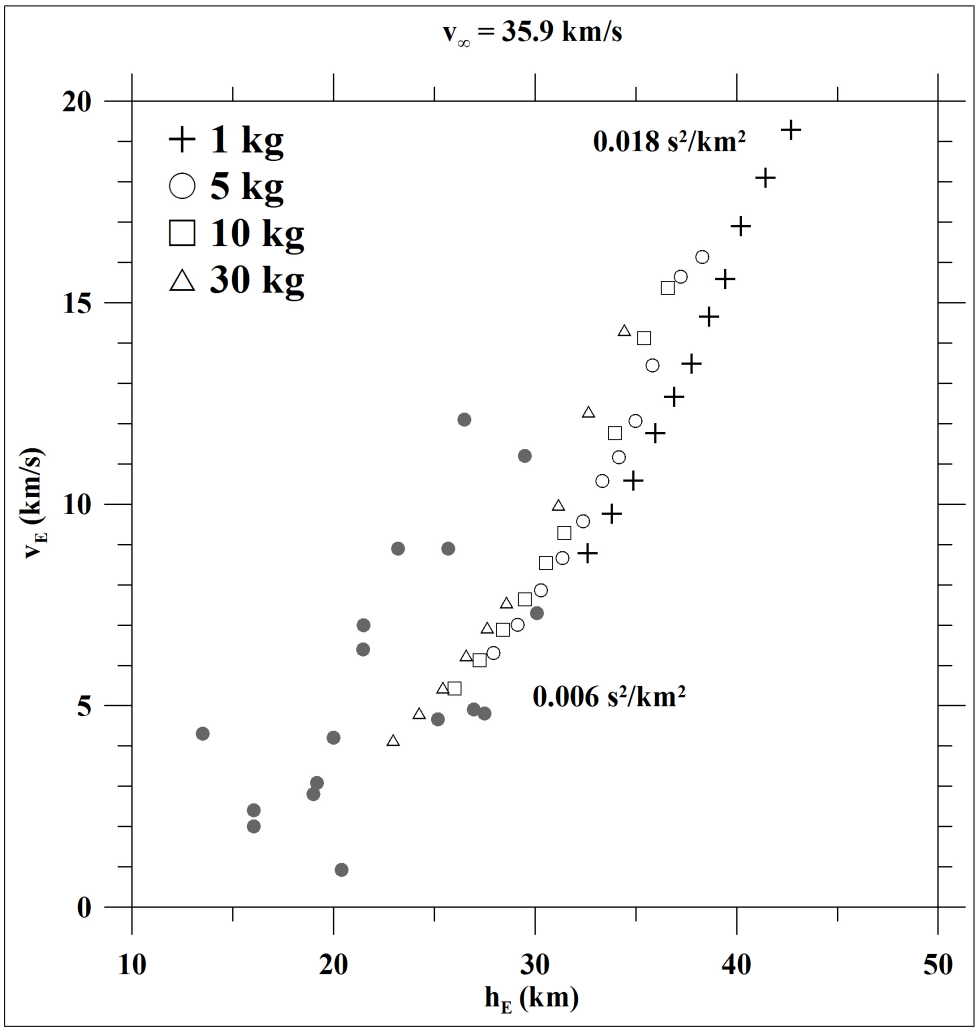

Figure 3.43: The dependency of terminal heights on terminal velocities for simulated Geminids. Gray dots mark meteorite dropping fireballs.

Chapter 4

Conclusions

Main results on the 98 fireballs are summarized in this chapter. Further details are presented in individual sections for each shower.

4.1 Orionids

Results of atmospheric trajectories, orbits, light curves and physical properties of 13 Orionid fireballs recorded by cameras of the Czech Fireball Network are presented. The fireballs were recorded during high Orionid activity on three nights of October 2006 and one night of October 2007. The main conclusions are as follows:

- Unusually high activity of bright Orionids over relatively long period during four consecutive nights from October 20-24, 2006 and similarly in 2007 was observed on the basis of single station photographic data and radiometric records. The lack of multi-station photographic data from second, third and fourth observing nights in 2006 and from almost all four nights in 2007 was partly caused by bad weather conditions over the Czech Republic and partly also by decreasing number of bright meteors. Only 6 fireballs were recorded from more than one station in second and third night in 2006 and in 2007 and their orbital characteristics slightly differ from the filament (Table 3.5). They rather better correspond to the background values (Lindblad and Porubčan, 1999).

- According to analysis of light curves and atmospheric penetration ability, defined by PE coefficient, was found that all recorded Orionid meteors do not significantly differ from each other and belong to a weak and fragile component of interplanetary matter, as expected since the Orionids are associated with comet 1P/Halley. On the basis of heights of terminal flares the material of Orionid meteoroids is beeing destroyed under pressure ranges from 0.02 to 0.11 MPa.

- Precise mean radiant position and orbital elements of the very distinct filament that produced the observed outburst of Orionid activity in morn-

ing hours of 21^{st} of October 2006 were determined. This filament only slightly differs from mean shower characteristics determined from IAU MDC photographic data by Lindblad and Porubčan (1999) or from DMS video data (de Lignie and Betlem, 1999).

- From very consistent mean values of orbital elements of fireballs belonging to the conspicuous filament of the 2006 Orionid outburst was found that this high activity could be caused by meteoroids trapped in 1:5 resonance.

4.2 Geminids

Results of atmospheric trajectories, orbits, light curves and physical properties of 13 Geminid fireballs recorded by cameras of the Czech Fireball Network are presented. The fireballs were recorded during two nights of December 2006. The main conclusions are as follows:

- No expressive terminal flares were observed in the light curves, only three fireballs have small outburst at the end of the trajectory, which corresponds to asteroidal atmospheric behavior rather than cometary. This is partly confirmed on the basis of atmospheric results because seven meteors belonged to type II – generally connected with hard or solid cometary material, and four meteors to type I – asteroidal material.

- Periodic changes of brightness were presented in the first half of the meteors by three light curves from AFO's radiometers (from six applicable). Frequency of cyclic changes ranges from about 10 to 100 Hz in observed heights from about 90 to 70 km. Two these fireballs show exponentialy increasing frequency of change of brightness with rates similar to rate of exponential increase of air density during the atmospheric penetration. This resulted in the fact that these changes of brightness could be described by rotation of the body and its spin-up in the atmosphere. Approximate ages 2400 and 650 years of the two meteoroids were calculated from derived initial rotation.

- No high-frequency (up to several hundred Hz) pulsation of brightness of Geminids that start suddenly, approximately in the middle of a meteor trajectory, was observed, as mentioned by several authors (Astapovich, 1958; Halliday, 1988).

- Type I Geminid fireballs are effectively decelerated in the atmosphere. Using gross-fragmentation model (Ceplecha et al., 1993) mean value of apparent ablation coefficient for the type I meteors was determined, $\sigma_{type\,I} = 0.018 \pm 0.005\,\mathrm{s^2/km^2}$. Two type II fireballs with sufficient deceleration led to similar value, another one type II Geminid with smaller deceleration led to $\sigma = 0.042 \pm 0.002\,\mathrm{s^2/km^2}$.

- The 2006 Geminid fireballs in the range of initial masses 10^0 to 10^3 g have approximately constant beginning height of 89 km, and thus are mass-independent. Terminal heights then decrease with increasing initial masses.
- Values of radiant position and also geocentric velocity well correspond to long-term annual values given by IAU MDC web pages. Also the mean orbit agree with the mean orbit based on 38 photographic orbits from IAU MDC published by Gajdoš and Porubčan (2004).

4.3 α-Capricornids

Results of atmospheric trajectories, orbits, light curves and physical properties of 5 α-Capricornid fireballs recorded by cameras of the Desert Fireball Network are presented. The fireballs were recorded during two nights in July and one night in August 2006. These fireballs are probably the first five photographic α-Capricornids recorded from the southern hemisphere. The main conclusions are as follows:

- According to atmospheric behavior and the end height PE criterion these meteors belong to the weakest component of interplanetary matter (type IIIB). It means that parent comet 169P/NEAT is likely composed of the most fragile material.
- Strenght of the material of IIIB α-Capricornids corresponds to the range of dynamic pressures from 0.012 to 0.025 MPa. This values are derived from terminal flares for IIIB meteors, which occured between 76 and 80 km (meteoroids with masses from 20 to 120 g). The range of dynamic pressures from 0.004 to 0.032 MPa corresponds to the first flares observed, and thus probably to the fragmentation points. The IIIA/B fireball had the first flare at 73 km (0.032 MPa), terminal at 65 km (0.11 MPa). All noted meteoroids are very similar to each other in their composition and course of ablation, and thus we can assume approximately homogenous composition of the parent comet.
- Despite of low value of initial velocity these soft and fragile α-Capricornid meteoroids are not sufficiently decelerated in the Earth's atmosphere. This is likely caused by properties of the material, which reaches its strenght befor deceleration become measurable.
- The 2006 α-Capricornids radiated from not very compact area of geocentric radiants, whose mean value agrees with radiant position published by Jenniskens (2006). Also the heliocentric orbits agree with mean photographic orbit of 27 IAU MDC meteors (Gajdoš and Porubčan, 2004), only inclination of the 2006 α-Capricornid mean orbit is a bit smaller and corresponds rather to inclination of the parent comet than to long-term photographicaly observed value given by the authors.

4.4 Southern δ-Aquariids

Results of atmospheric trajectories, orbits, light curves and physical properties of 3 Southern δ-Aquariid fireballs recorded by cameras of the Desert Fireball Network are presented. The fireballs were recorded during one night in July and two night in August 2006. These fireballs are probably the first three photographic Southern δ-Aquariids recorded from the southern hemisphere. The main conclusions are as follows:

- According to atmospheric behavior, the 2006 Southern δ-Aquariid meteoroids consist of solid cometary material (PE types II to IIIA). Beginning height for both type II fireballs was the same (88.3 km) and all three, in the range of initial masses 10^{-1} to 10^{3} g, have approximately constant beginning height 87 km, and thus may be mass-independent. This results from three observed meteors only, and thus it is evident that it will need further study to confirm this.
- On the basis of light curves the course of radiation differs between type II and IIIA Southern δ-Aquariids. Type II has gradual increase of brightness, about maximum some short flares occure and fades towards the end. Maximum lies approximately in 3/4 of the trajectory, which corresponds to a single-body meteor without deceleration. Completely different is the light curve of type IIIA. Its course of the light curve is something like mirrored single-body profile. Directly at the beginning of the trajectory rapid increase of brightness takes place and after reaching the maximum in 1/3 of the trajectory fades out very slowly.
- Decrease of brightness of persistent train was observed in the light curve of SDA03. The decrease can be described as an exponential dependency of intensity on time, I $\approx$ e^{At} with A = -9.07. The train had, after the meteor disappearance, absolute brightness -4 to -5 mag, its total observed duration was 0.8 s and maximum absolute brightness about -10.7 mag.
- The mean geocentric radiant is shifted by about 3° in right ascension and 1° in declination in comparison with values published on the IAU MDC web pages. New formula for radiant motion in right ascension was proposed for these three meteors.
- Orbital elements of Southern δ-Aquariids are time dependent. Except the inclination, where the decrease with increasing node is not well corelated, all the other elements are linear functions of the ascending node.

4.5 Leonids

Results of atmospheric trajectories, light curves and physical properties of 54 Leonid fireballs and orbits of 34 of them are presented. The fireballs were recorded within the Czech Fireball Network and during the Dutch-Czech

Leonid expedition in Spain. The fireballs were recorded during three nights in November 1999, two nights in 2001, one night in 2002, and three nights in 2006. The main conclusions are as follows:

- Five individual dust trails (released from the comet in 1800, 1833, 1866, 1899, 1932) were identified as probable sources of some of the observed Leonid fireballs, and the next trail (1767) as a less probable source. In each year, fireballs from the Filament were also photographed (except for 2002).

- An apparent non-dependence of beginning heights on initial photometric mass was observed and recognized as a result of the use of all-sky cameras. Nevertheless, this non-dependence suggests the existence of a height h_{lim} (equal to 111 $\pm$ 5 km) which is the height where all Leonids reach an absolute magnitude of about -2^m.

- Most of the observed Leonids did not survive dynamic pressures higher than 0.02 MPa. The highest dynamic pressure of 0.19 MPa was observed in the terminal flare of LEO25, which was the deepest penetrating Leonid fireball among those studied.

- According to atmospheric behavior and the PE criterion we can conclude that the parent comet 55P/Tempel-Tuttle is not homogeneous. Three different fireball types were observed among the presented Leonids: II, IIIA, and IIIB. The most numerous is type IIIB, which was derived for more than one half of the fireballs.

- Two main types of light curves were recognized for the Leonids. The first type shows only one dominant flare near the end of a visual trajectory, after which the final fading portion of the light curve is very steep. This sudden end of the luminous trajectory is typical for bright fireballs of the PE type IIIB. The second type shows a symmetric shape, smooth course of brightness without flares, and looks like the light curve of a single-body model of a meteor. This light curve is typical for faint Leonid meteors.

- Three fireballs left persistent train bright enough beeing detectable by radiometers. Decrease of the brightness of these trains are exponential functions of time, $I \approx e^{At}$ with different values of A. Even if these three trains were not observed by the same detector, course of their brightness is similar. The first detection after the meteor disappearance having -8 mag, the last one on the sensitivity limit -5 mag. Nevertheless, no dependency among the rate of decrease of brightness (decay coefficient A), meteoroid initial mass or duration of the train was found out. The decay is due to decrease of temperature, not density (Borovička and Jenniskens, 2000), and thus we can say that there were different courses of temperature in the trains of these three fireballs.

- The mean geocentric radiant (here normalized to solar longitude 235.1°) agrees with the position of the geocentric radiant for Leonids from the 1998 Fireball Night, and a halo-like structure of radiants was recognized for meteors from the 1899 dust trail in 1999.
- A significant spread in orbital elements among meteoroids belonging to one dust trail was observed.

4.6 Perseids

Results of atmospheric trajectories, orbits, light curves and physical properties of 10 Perseid fireballs recorded by cameras of the Czech Fireball Network are presented. The fireballs were recorded during two nights in August 2007. The main conclusions are as follows:

- All the light curves of the 2007 Perseids are similar to each other. Slow increase of brightness accompanied by several short bursts takes place and an intensive flare (maximum brightness of the meteor) appears before the end, in 7/8 of the trajectory. After that also an inexpressive or faint terminal flare occurs very often.
- According to atmospheric behavior and the PE criterion we can conclude that parent comet 109P/Swift-Tuttle consists of material of similar composition and strenght. The scatter of the PE values is less than 0.2 with the mean value of -5.2, which corresponds to border type II/IIIA and presumption that the comet is composed rather of hard cometary material.
- The 3 meteors have orbits, which resemble 2 of 17 Perseid filaments proposed by Kaňuchová et al. (2005).
- Geocentric radiants have high dispersion in right ascension and declination even if errors of individual radiant positions are small. High dispersion of values of orbital elements, positions of geocentric radiants and geocentric velocities of the 2007 Perseids indicate big age and spatial dimension of dust cloud of the shower.

4.7 Comparison

Results of atmospheric trajectories, orbits and physical properties of the 98 fireballs from 6 different showers are presented. The main conclusions are as follows:

- Beginning heights for studied Orionids and Perseids increase slowly with increasing initial mass. On the other hand, photographic Geminids (initial mass from 10^0 to 10^3 g) and Southern δ-Aquariids (10^{-1} to 10^3 g) were observed in approximately constant beginning heights of around 88 km.

Both of these showers have substantially lower perihelion distance in comparison to the other showers, which can be related to this. Also beginnings of the α-Capricornids occured around the height of 88 km but with higher dispersion, and thus it is difficult to say if the beginning heights are also mass-independent. Possible mass-independency of the Southern δ-Aquariids can be caused by the equipment used. The same result also hold for the Leonids, which fulfill apparent mass-independency of the beginning heights, h_B =111 $\pm$ 5 km, for the range of photometric masses from 10^{-1} to 10^3 g, but from video observations we know that Leonids are not mass-independent. This apparent mass-independency is caused by the fact that all Leonids reach at the hight of 111 km an absolute brightness of approximately -2^m.

- For all studied showers hold a condition that terminal height decreases with increasing initial mass.
- According to atmospheric behavior we can arrange studied streams in order of strenght of material of their meteoroids. On the basis of the PE criterion the softest and the most fragile are α-Capricornids, which are the type IIIB. Follow Leonids, Orionids, Perseids, Southern δ-Aquariids and the most solid are Geminids (between types I and II). The most heterogenous parent body is 3200 Phaeton of Geminids, the most uniform is 109P/Swift-Tuttle of Perseids.
- On the basis of the mean values of dynamic pressures we can arrange studied streams in the same order. According to the spread of dynamic pressures, Geminids have the most heterogenous parent body and the most homogenous one have α-Capricornids and Perseids.
- The height of the fragmentation point (based on the flares in the light curves) does not depend only on the tensile strenght of the material (based on the dynamic pressure at this point) but also on the initial photometric mass of the meteoroid. The dynamic pressures, observed at the point of fragmentation, increase with increasing initial photometric masses.
- The dependency, ariseing from the low of conservation of energy, between geocentric velocity and eccentricity was observed only for streams with the lowest perihelion distance – Geminids and Southern δ-Aquariids.
- Comparison with meteorite dropping fireballs results in probable meteorite fall of Geminid meteoroid with ideal initial preatmospheric properties. Non-fragmenting body with initial mass of 5 kg, initial velocity of 35.9 km/s, and ablation coefficient of 0.006 s^2/km^2 results in 100 grams of terminal mass.

Bibliography

Asher, D. J., Bailey, M. E., Emelyanenko, V. V. (1999) MNRAS 304:53-56

Astapovich, I. S. (1958) Meteornye yavleniya v atmosfere Zemli (Meteoric Phenomena in the Earth's Atmosphere). Moscow: Fizmatgiz, 640

Ayers, W. G., McCrosky, R. E., Shao, C. -Y. (1970) Photographic Observations of 10 Artificial Meteors. SAO Special Report #317

Babadzhanov, P. B., Konovalova, N. A. (1987) On the light pulsation of bright Geminids according to photographic data. Publications of the Astronomical Institute of the Czechoslovak Academy of Sciences, Volume 67, 189–191

Babadzhanov, P. B. (2002) Fragmentation and densities of meteoroids. A&A 384:317–321

Babadzhanov, P. B., Konovalova, N. A. (2004) Some features of Geminid meteoroid disintegration in the Earth's atmosphere. A&A 428:241–246

Beech, M. (2001) Meteoroid rotation and fireball flickering: A case study of the Innisfree fireball. MNRAS 326:937–942

Beech, M. (2002) The age of the Geminids: a constraint from the spin-up time-scale. MNRAS 336:559–563

Beech, M., Illingworth, A., Murray, I. S. (2003) Analysis of a "flickering" Geminid fireball. Meteoritics and Planetary Science 38:1045–1051

Betlem, H., Jenniskens, P., van't Leven, J., Ter Kuile, C., Johannink, C., Zhao, H., Lei, C., Li, G., Zhu, J., Evans, S., Spurný, P. (1999) Very precise orbits of 1998 Leonid meteors. Meteoritics and Planetary Science 34:979–986

Betlem, H., Jenniskens, P., Spurný, P., Docters van Leeuwen, G., Miskotte, K., Ter Kuile, C., Zarubin, P., Angelos, C. (2000) Precise Trajectories and Orbits of Meteoroids from the 1999 Leonid Meteor Storm. EM&P 82/83:277-284

Bland, P. A., Spurný, P., Shrbený, L., Borovička, J., Bevan, A. W. R., Towner, M. C., McClafferty, T., Vaughan, D., Deacon, G. (2008) The Desert Fireball Network: First results from two years of systematic monitoring of fireballs over the Nullarbor Desert of Western Australia. Poster at the 2008 ACM Conference

Borovička, J., Spurný, P., Keclíková, J. (1996) A new positional astrometric method for all-sky cameras. A&A 112:173–178

Borovička, J., Jenniskens, P. (2000) Time Resolved Spectroscopy of a Leonid Fireball Afterglow. EM&P 82/83:399–428

Borovička, J. (2006) Meteor Trains – Terminology and Physical Interpretation. JRAS 100:194–198

Čapek, D. (2008) Thermal Effects in Physics and Dynamics of Small Bodies of the Solar System (Thesis)

Ceplecha, Z., McCrosky, R. E. (1976) Fireball end heights - A diagnostic for the structure of meteoric material. JGR 81:6257–6275

Ceplecha, Z. (1987) Geometric, dynamic, orbital and photometric data on meteoroids from photographic fireball networks. Bulletin of the Astronomical Institute of Czechoslovakia 38:222–234

Ceplecha, Z., McCrosky, R. E. (1992) Gross-fragmentation of meteoroids and bulk density of Geminids from photographic fireball records. In Lunar and Planetary Inst., Asteroids, Comets, Meteors 1991, 109–112

Ceplecha, Z., Spurný, P., Borovička, J., Keclíková, J. (1993) Atmospheric fragmentation of meteoroids. A&A 279:615–626

Ceplecha, Z., Borovička, J., Elford, W. G., Revelle, D. O., Hawkes, R. L., Porubčan, V., Šimek, M. (1998) Meteor Phenomena and Bodies. Space Science Reviews 84:327–471

Ceplecha, Z., Revelle, D. O. (2005) Fragmentation model of meteoroid motion, mass loss, and radiation in the atmosphere. M&PS 40:35–54

Cimrman, J. (1899) Results of photographic multiple meteorite fall of Liptákov. Publications of the Tashkent Astronomical Observatory 1:1–2

Cook, A. F. (1973) A Working List of Meteor Streams. Proceedings of the IAU Colloquium No. 13, p.183–192

de la Peña, S., Avery, S. A., Avery, J. P.(2008) Observations of the 2001 Leonid meteor shower using VHF meteor radar. Icarus 196:164–170

de Lignie, M., Betlem, H. (1999) A double-station video look on the October meteor showers. WGN, Journal of the IMO 27:195–201

Dubietis, A. and Arlt, R. (2004) Observational characteristics of meteor showers associated with the Aquarid-Capricornid complex. WGN, Journal of the IMO 32:69–76

Emel'Yanenko, V. V. (2001) Resonance structure of meteoroid streams. In: Warmbein, B. Proceedings of the Meteoroids 2001 Conference, p.43–45

Fox, K., Williams, I. P., Hughes, D. W. (1984) The 'Geminid' asteroid (1983 TB) and its orbital evolution. MNRAS 208:11P–15P

Gajdoš, Š., Porubčan, V. (2004) Bolide Meteor Streams. Proceedings of the IAU Colloquium No. 197, p.393–398

Gural, P. S., Jenniskens, P., Koop, M., Jones, M., Houston-Jones, J., Holman, D., Richardson, J. (2004) The relative activity of the 2001 Leonid storm peaks and implications for the 2002 return. Advances in Space Research 33:1501–1506

Hajduk, A (1970) Structure of the meteor stream associated with comet Halley. Bulletin of the Astronomical Institute of Czechoslovakia 21:37

Halliday, I. (1988) Geminid fireballs and the peculiar asteroid 3200 Phaethon. Icarus 76:279–294

Hasegawa, I. (2001) Parent objects of α Capricornid meteor stream. Proceedings of the Meteoroids 2001 Conference, p.55–62

Hughes, D. W. (1987) P/Halley dust characteristics - A comparison between Orionid and Eta Aquarid meteor observations and those from the flyby spacecraft. A&A 187:879–888

Hughes, D. W. (1990) The mass distribution of comets and meteoroid streams and the shower/sporadic ratio in the incident visual meteoroid flux. MNRAS 245:198-203

Hunt, J., Williams, I. P., Fox, K. (1985) Planetary perturbations on the Geminid meteor stream. MNRAS 217:533–538

IAU MDC web pages: www.astro.amu.edu.pl/˜jopek/MDC2007

Jacchia, L., Verniani, F., Briggs, R. E. (1967) An Analysis of the Atmospheric Trajectories of 413 Precisely Reduced Photographic Meteors. Smithsonian Contributions to Astrophysics 10:1–139

Jenniskens, P. (1995) Meteor stream activity. 2: Meteor outbursts. A&A 295:206–235

Jenniskens, P., Betlem, H., de Lignie, M., Ter Kuile, C., van Vliet, M. C. A., van 't Leven, J., Koop, M., Morales, E., Rice, T. (1998) On the unusual activity of the Perseid meteor shower (1989-96) and the dust trail of comet 109P/Swift-Tuttle. MNRAS 301:941–954

Jenniskens, P., Betlem, H. (2000) Massive Remnant of Evolved Cometary Dust Trail Detected in the Orbit of Halley-Type Comet 55P/Tempel-Tuttle. Astrophys. J. 531:1161-1167

Jenniskens, P. (2006) Meteor Showers and their Parent Comets. Cambridge University Press, Cambridge, pp 790

Jenniskens, P., de Kleer, K., Vaubaillon, J., Trigo-Rodríguez, J. M., Madiedoe, J. M., Haas, R., ter Kuile, C. R., Miskotte, K., Vandeputte, M., Johannink, C., Busf, P., van 't Levenf, J., Jobsef, K., Koop, M. (2008) Leonids 2006 observations of the tail of trails: Where is the comet fluff? Icarus 196:171–183

Jopek, T. J., Valsecchi, G. B., Froeschle, C. (1999) Meteoroid stream identification: a new approach - II. Application to 865 photographic meteor orbits. MNRAS 304:751–758

Kaňuchová, Z., Svoreň, J., Neslušan, L. (2005) The observed structures in the meteoroid stream of Perseids in the range of photographic meteors. Contributions of the Astronomical Observatory Skalnaté Pleso 35:135–162

Koten, P., Borovička, J., Spurný, P., Betlem, H., Evans, S. (2004) Atmospheric trajectories and light curves of shower meteors. A&A 428:683-690

Kronk G. W. (1987) Meteor Showers: A Descriptive Catalogue. (Hillside, NJ:Enslow)

Lindblad, B. A., Porubčan, V. (1994) The activity and orbit of the Perseid meteor stream. Planetary and Space Science 42:117–122

Lindblad, B. A., Porubčan, V. (1999) Orionid meteor stream. Contributions of the Astronomical Observatory Skalnaté Pleso 29:77

McBeath, A. (2005) SPA Meteor Section results: October-December 2002. WGN, Journal of the IMO 33:81–86

McIntosh, B. A., Hajduk, A. (1983) Comet Halley meteor stream - A new model. MNRAS 205:931–943

McIntosh, B. A., Jones, J. (1988) The Halley comet meteor stream - Numerical modelling of its dynamic evolution. MNRAS 235:673–693

McNaught, R. H., Asher, D. J. (1999) Leonid Dust Trails and Meteor Storms. WGN, Journal of the IMO 27:85–102

Misconi, N., Y. (1993) The spin of cosmic dust: Rotational bursting of circumsolar dust in the F corona. JGR, 98 (A11):18,951–18,961

Neslušan, L. (1999) Comets 14P/Wolf and D/1892 T1 as parent bodies of a common, alpha -Capricornids related, meteor stream. A&A 351:752–758

Neslušan, L., Welch, P. G. (2001) Comparison among the Keplerian-orbit-diversity criteria in major-meteor-shower separation. Proceedings of the Meteoroids 2001 Conference, p.113–118

Olsson-Steel, D. (1987) The dispersal of the Geminid meteoroid stream by radiative effects. MNRAS 226:1–17

online database: http://meteor.asu.cas.cz/db/report

Paddack, S., J. (1969) Rotational Bursting of Small Celestial Bodies: Effect of Radiation Pressure. JGR, 74:4379–4381

Plavec, M. (1956) Meteorické roje. Nakladatelství československé akademie věd, Praha, str. 136–161

Porubčan, V., Hajduk, A., McIntosh, B. A. (1991) Visual meteor results from the International Halley Watch. Bulletin of the Astronomical Institute of Czechoslovakia 42:199–204

Rendtel, J., Betlem, H. (1993) Orionid meteor activity on October 18, 1993. WGN, Journal of the IMO 21:264–268

Rendtel, J. (2004) Almost 50 years of visual Geminid observations. WGN, Journal of the IMO 32:57–59

Rendtel, J. (2007) Three days of enhanced Orionid activity in 2006 - Meteoroids from a resonance region? WGN, Journal of the IMO 35:41–45

ReVelle, D., O., Ceplecha, Z. (2001) Bolide physical theory with application to PN and EN fireballs. Proceedings of the Meteoroids 2001 Conference, p.507–512

Sato, M., Watanabe, J. (2007) Origin of the 2006 Orionid Outburst. Publ. Astron. Soc. Japan 59, L21–L24

Shrbený, L., Spurný, P. (2009) Precise data on Leonid fireballs from all-sky photographic records. A&A (accepted by Chief Editor on 3^{rd} July, 2009)

Spurný, P., Borovička, J. (2001) EN310800 Vimperk fireball: probable meteorite fall of Aten type meteoroid. Proceedings of the Meteoroids 2001 Conference, p.519–524

Spurný, P. (1993) Geminids from photographic records. Proceedings of the International Astronomical Symposium held at Smolenice, Slovakia, p.193–196

Spurný, P. (1994) Recent fireballs photographed in central Europe. Planetary and Space Science 42:157–162

Spurný, P., Betlem, H., van't Leven, J., Jenniskens, P. (2000) Atmospheric behaviour and extreme beginning heights of the thirteen brightest photographic Leonid meteors from the ground-based expedition to China. M&PS 35:243–249

Spurný, P., Spalding, R. E., Jacobs, C. (2001) Common ground-based optical and radiometric detections within Czech Fireball Network. In: Warmbein, B. Proceedings of the Meteoroids 2001 Conference, ESA SP-495, p.135–140

Spurný, P., Borovička, J., Shrbený, L. (2007) Automation of the Czech Part of the European Fireball Network: Equipment, methods and first results. Proceedings of the IAU Symposium 236, 121–130

Spurný, P., Shrbený, L. (2008) Exceptional Fireball Activity of Orionids in 2006. EM&P 102:141–150

Steel, D. (1996) Meteoroid Orbits. Space Science Reviews 78:507–553

Svoreň, J., Kaňuchová, Z. (2005) Perseids – the list of photographic orbits. Contributions of the Astronomical Observatory Skalnaté Pleso 35:199–220

Trigo-Rodríguez, J. M., Llorca, J., Fabregat, J. (2002) Photographic observations of the 1999 Leonid storm from Spain. Proceedings of ACM 2002 in Berlin, p.217–220

Trigo-Rodríguez, J. M., Madiedo, J. M., Llorca, J., Gural, P.S., Pujols, P., Tezel, T. (2007) The 2006 Orionid outburst imaged by all-sky CCD cameras from Spain: meteoroid spatial flux and orbital elements. MNRAS 380:126–132

Tupman, G. L. (1873) Catalogue of radiant points of meteors. MNRAS 33:300

Wetherill, G. W. (1986) Sun-Approaching Bodies: Neither Cometary Nor Asteroidal? Meteoritics 21:537

Whipple, F. (1983) 1983 TB and the Geminid Meteors. IAU Circular 3881, Edited by Marsden, B. G.

Wright, F. and Jacchia, L. G. and Whipple, F. (1956) Photographic a-Capricornid meteors. Astronomical Journal 61:61

Wu, Z., Williams, I. P. (1993) Comet P/Halley and its associated meteoroid streams. Proceedings of the International Astronomical Symposium, Smolenice, Slovakia, July 6 - 12, 1992, 77

Yamamoto, M., Y., Toda, M., Higa, Y., Maeda, K., Watanabe, J., I. (2004) Altitudal Distribution Of 20 Persistent Trains: Estimates Derived From Metro Campaign Archives. EM&P 95:279–287

Zvolánková, J. (1992) Activity of the Delta Aquarids meteor shower in the years 1944 – 1952. Contributions of the Astronomical Observatory Skalnaté Pleso 22:193–204

List of publications and conference contributions related to this thesis

- Bland, P. A., Spurný, P., **Shrbený, L.**, Borovička, J., Bevan, A. W. R., Towner, M. C., McClafferty, T., Vaughan, D., Deacon, G. (2008) The Desert Fireball Network: First results from two years of systematic monitoring of fireballs over the Nullarbor Desert of Western Australia. Poster at the 2008 ACM Conference
- **Shrbený, L.**, Spurný, P. (2009) Meteor shower fireballs. Contribution at the 2009 Nessi Workshop.
- **Shrbený, L.**, Spurný, P. (2009) Precise data on Leonid fireballs from all-sky photographic records. A&A (accepted by Chief Editor on 3^{rd} July, 2009)
- **Shrbený, L.**, Spurný, P. (2009) Differences between shower fireballs and meteorite dropping ones. Contribution at the 2009 Bolides and Meteorite Falls Conference
- Spurný, P., Borovička, J., **Shrbený, L.** (2007) Automation of the Czech Part of the European Fireball Network: Equipment, methods and first results.
- Spurný, P., **Shrbený, L.** (2007) Exceptional Fireball Activity of Orionids in 2006. Poster at the Meteoroids 2007 Conference
- Spurný, P., **Shrbený, L.** (2008) Exceptional Fireball Activity of Orionids in 2006. EM&P 102:141–150